Aus dem Institut für Molekularbiologie und Tumorforschung
Geschäftsführender Direktor: Prof. Dr. Rolf Müller
des Fachbereichs Medizin der Philipps-Universität Marburg

Functional characterisation of cancer-associated mutations in the chromatin remodeler CHD4/dMi-2

Inaugural-Dissertation
zur Erlangung des Doktorgrades der Naturwissenschaften
(Dr. rer. nat.)
dem Fachbereich Medizin der Philipps-Universität Marburg
vorgelegt von

Kristina Kovač

aus Zagreb, Kroatien

Marburg, 2018

Angenommen vom Fachbereich Medizin der Philipps-Universität Marburg am:

24.04.2018

Gedruckt mit Genehmigung des Fachbereichs.

Dekan: Prof. Dr. Helmut Schäfer

Referent: Prof. Dr. Alexander Brehm

1. Korreferent: Prof. Dr. Sandra Hake

“I may not have gone where I intended to go,
but I think I have ended up where I needed to be.”

— Douglas Adams

Table of contents

1. Summary

1.1. Abstract

CHD4/Mi-2 is a highly conserved ATP-dependent chromatin remodeller. It is essential in processes like transcription regulation, DNA damage response, cell cycle progression, as well as differentiation and development in eukaryotes. It is one of the catalytic components of the NuRD (nucleosome remodelling and deacetlyation) complex. ATP-dependent chromatin remodellers, including CHD4, are frequently mutated in human cancers. In this study, the effects of several missense mutations derived from endometrial cancer patients were analysed using dMi-2, a *Drosophila melanogaster* homologue of human CHD4, as a model.

Selected point mutants, covering key domains and regions in dMi-2, were biochemically analysed. It was demonstrated through enzymatic and non-enzymatic assays that these mutations can have a wide variety of effects on nucleosome binding, ATP hydrolysis and nucleosome remodelling. Interestingly, this analysis uncovered that these mutations can impact dMi-2 in opposite manners, by lowering or increasing the protein's remodelling ability. Some mutations caused changes in the coupling of ATP hydrolysis with nucleosome remodelling, revealing new roles of certain residues and regions in modulating protein activity. Additionally, a new regulatory region was identified in the C-terminal part of the protein, which is comparable to previously identified regulatory regions in CHD1, ISWI and Snf2. On the N-terminal side, analysis of chromodomain mutants allowed identification of a structural element in dMi-2, similar to one identified in CHD1, that likely contacts nucleosomal DNA during remodelling.

Furthermore, *in vivo* genetic experiments in *Drosophila melanogaster* demonstrated that expression of selected dMi-2 point mutants can cause misregulation in development of epithelial wing structures. These phenotypes

correlated with the nucleosome remodelling characteristics of dMi-2 point mutants. Together, the findings of this thesis give new insight into the consequences of mutations of chromatin remodellers in cancer and provide a basis for understanding molecular mechanisms used by the Mi-2 mutants to contribute to carcinogenesis.

1.2. Zusammenfassung

CHD4/Mi-2 ist ein hoch konservierter ATP-abhängiger Chromatinremodeller. Er ist essentiell für Prozesse der Transkriptionsregulation, der DNA-Schadensantwort, der Zellzyklusprogression sowie der Differenzierung und Entwicklung in Eukaryonten. CHD4 ist eine der katalytischen Untereinheiten des NuRD (*nucleosome remodelling and deacetylation*)-Komplexes. ATP-abhängige Chromatinremodeller, einschließlich CHD4, sind in humanen Karzinomen häufig mutiert. In dieser Studie wurden mehrere *Missense*-Mutationen analysiert, die in Patienten mit Endometrialkarzinomen gefunden wurden. Hierzu wurde dMi-2 verwendet, ein *Drosophila melanogaster* Homolog des humanen CHD4.

In dieser Arbeit wurden ausgewählte Punktmutationen biochemisch analysiert, welche in wichtigen Domänen und Regionen in dMi-2 liegen. Durch enzymatische und nicht-enzymatische Assays wurde gezeigt, dass diese Mutationen breit gefächerte Effekte bezüglich der Nukleosomen-Bindung, der ATP-Hydrolyse und der Remodellierung von Nukleosomen haben können. Die vorliegende Analyse konnte offenlegen, dass diese Mutationen dMi-2 auf entgegengesetzte weise beeinflussen, seine Remodelling-Aktivität entweder senken oder steigern können. Einige Mutationen verursachten Veränderungen der Kopplung von ATP-Hydrolyse mit Nukleosomen-Remodelling. Dies offenbart neue Funktionen bestimmter Aminosäurenreste und Regionen und ihren Einfluss auf die Aktivität des Proteins. Außerdem wurde eine neue regulatorische Region im C-terminalen Teil des Proteins identifiziert, die vergleichbar mit bereits bekannten Regionen in CHD1, ISWI und Snf2 ist. Mutationen der Chromodomänen führten zur Identifikation eines Strukturelements im N-Terminus von dMi-2. Dieses ähnelt einem Motif in CHD1, welches nukleosomale DNA während des Remodelling-Prozesses kontaktiert.

Des Weiteren zeigten genetische *in vivo*-Experimente in *Drosophila melanogaster*, dass die Expression ausgewählter dMi-2-Punktmutanten zur

Fehlregulation der Entwicklung von epithelialen Flügelstrukturen führen kann. Diese Phänotypen korrelierten mit den Remodelling-Eigenschaften der dMi-2-Punktmutanten. Zusammenfassend geben die Ergebnisse dieser Arbeit neue Einblicke in die Folge von Mutation von Chromatinremodellern in Tumorerkrankungen und schaffen eine Grundlage, um die molekularen Mechanismen zu verstehen, mit denen Mi-2-Mutanten zur Karzinogenese beitragen.

2. Introduction

2.1. Building chromatin

The function of DNA is to carry the genetic information of an organism, information that codes for proteins that make up all living organisms. In order to organise 2m long DNA molecules in an eukaryotic nucleus that is on average 10μm in diameter, DNA is organised in chromosomes. Each chromosome is built out of a single negatively charged double-stranded DNA molecule wrapped around small basic histone proteins that function primarily as the scaffold for organising DNA. Together with other nonhistone chromosomal proteins that bind to DNA, they form a DNA-protein complex known as chromatin. The elementary repeating unit of chromatin is the nucleosome. Nucleosomes form long arrays or “beads on a string” that are coiled into higher order structures which allow packing of the DNA.

2.1.1. Chromatin structure and organisation

The nucleosome is a fundamental repeating unit of chromatin, whose high resolution structure was solved in 1997 in a seminal paper from Timothy J. Richmond’s lab (Luger et al. 1997). It was revealed that 147 bp of DNA are tightly wrapped around a histone octamer core in 1.65 turns in a left-handed coil. Histones are 14-18 kDa proteins, basic in nature, that come in five different forms - four core histones (H2A, H2B, H3 and H4) that form the core histone octamer and histone H1, also known as the linker histone. H1 is involved in binding the DNA in between two nucleosomes, the linker DNA. H1 interacts with linker DNA at the entry and exit points of nucleosomal DNA, facilitating the formation of higher order structures. Histones are among the most conserved proteins in eukaryotes indicating the functional importance of each amino acid. Core histones share a common structural motif known as the histone fold, that is formed out of three α helices connected with two loops. During nucleosome assembly, each histone fold binds with a corresponding histone fold. H2A binds

H2B forming the H2A-H2B heterodimer, while H3 binds H4 forming the H3-H4 heterodimer. Histone folds bind each other in an antiparallel arrangement creating a “handshake motif” (Arents et al. 1991, McGinty and Tan, 2014). H3-H4 heterodimers form tetramers which then combine with two H2A-H2B heterodimers and give rise to the histone octamer. Histone core proteins are abundant in arginines and lysines with positive charges that counteract the negative charge of DNA and allow DNA of nearly any sequence to assemble around the histone octamer core. The interaction between DNA and histones is formed between the amino acids of the histone fold and the phosphodiester backbone of DNA. This interaction can come in two different forms; either hydrogen bonds and electrostatic interactions that form salt bridges or hydrogen bonds alone. In addition, each of the core histones has an N-terminal and a C-terminal tail that extends outside of the nucleosome (Luger et al. 1997). These tails can be subjected to diverse forms of covalent modifications by a variety of histone modifying enzymes, through which many aspects of chromatin structure are being controlled. During replication-dependent chromatin assembly, histones are imported into the cell nucleus with help of a wide variety of histone chaperones (Burgess and Zhang, 2013). H2A-H2B are imported with the help of histone chaperone Nap1. Importing H3-H4 tetramers involves an array of histone modifications, primarily histone acetylation and histone chaperones like HSP90, NASP, and Asf1. In the cell nucleus, H3-H4 tetramers are deposited on the newly replicated DNA strand and form a tetrasome with DNA wrapped once around the tetrasome. After that, two H2A-H2B dimers are deposited, the rest of the DNA is wrapped around the histone octamer and the nucleosome is formed (Dennehey and Tyler, 2014) (Figure 2.1).

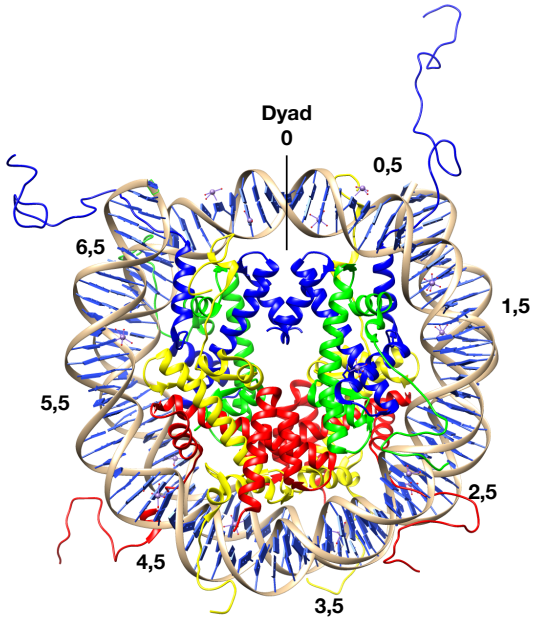

Figure 2.1. Nucleosome crystal structure

Nucleosome crystal structure at 1.9 Å resolution. Eight histone core proteins depicted in different colours; H3 in blue, H4 in green, H2A in yellow and H2B in red. 147 bp DNA is wrapped aroung core histones. DNA numbers are marking super helical locations (SHL), which represent super helical turns where the DNA minor grove faces the histone octamer. Figure was adapted from Davey et al. 2002 using Chimera software, PDB accession code 1KX5.

2.2. Regulation of chromatin structure

Controlling chromatin structure is crucial for processes such as transcription, DNA replication, and DNA repair. Packing of DNA into chromatin hinders access of DNA binding factors, so in order for this molecular machinery to access DNA, chromatin states need to be highly dynamic. The switching between these different states, from tightly packed nucleosomes to a more loosely open chromatin state, is highly regulated. This regulation can involve DNA modifications, such as methylation, RNA regulation mediated through RNA interference (RNAi) or long non-coding RNAs, a wide variety of histone variants, covalent modification of histones by histone modifying enzymes and structural changes introduced by chromatin remodelling enzymes. In next few chapters, I

will focus on regulation by histone variants, posttranslational modifications and chromatin remodelling.

2.2.1. Histone variants

During evolution a diverse array of histone variants has emerged from canonical histones to perform specific functions. They differ from core histones in sequence, function, and genomic localisation. They are incorporated into chromatin in a DNA replication independent manner in a process called histone exchange. Different histone variants can have distinct effects on nucleosome structure, stability, and binding of different proteins to the nucleosome (Talbert and Henikoff, 2010 and 2017).

Histone H3 has two distinct variants; histone H3.3 and CenH3.3 (also known as CENP-A). H3.3 has a difference of 5 amino acids to canonical histone H3, and it forms more structurally unstable nucleosomes (Jin and Felsenfeld 2007, Tachiwana et al. 2011). It is incorporated into chromatin near the body of transcribed genes, more specifically at the promoters of transcriptionally active genes (Chow et al. 2005, Mito and Henikoff. 2005). H3.3 serine 31 (not present in canonical H3) is phosphorylated during mitosis in centromeres and telomeres (Hake et al. 2005; Wong et al. 2010). Post-translational modifications, such as acetylation of lysine 9, 18 and 23, as well as trimethylation of lysine 4 are common for active chromatin regions and found on H3.3, indicating its role in active transcription. The other histone H3 variant, CenH3 or CENP-A, is found in centromeric nucleosomes. An important difference between the canonical histone H3 and the centromeric CenH3 maps to the CATD domain contained in CenH3 which contributes to a more solid and compact structure and interacts with histone chaperones specific for the centromere region (Black et al. 2004).

Histone H2A has four different variants, H2A.Z, H2A.X, H2AB, and macroH2A. Histone H2A.Z is highly conserved across different species and is expressed together with H2A in different organisms (Talbert and Henikoff, 2010). H2A.Z

builds nucleosomes structurally similar to H2A-containing canonical nucleosomes, but discrete changes in the amino acid sequence of H2A.Z give rise to less stable nucleosomes. H2A.Z incorporated in the nucleosome affects the connection of H2A.Z-H2B dimers and H3-H4 tetramers (Suto and Luger, 2000. Venkatesh and Workman, 2015). Given the mentioned properties, H2A.Z nucleosomes are less stable which contributes to their role in transcriptional activation, DNA repair, and chromosome segregation (Venkatesh and Workman, 2015). Histone H2A.X is best known for its role in the DNA damage response (DDR). Upon the generation of DNA double strand breaks, H2A.X is phosphorylated (giving rise to γ-H2A.X) on serine 139 by DDR kinases. This is one of the earliest events in the DDR pathway (Rogakou et al, 1998). γ-H2A.X serves as the main coordinator of DDR, but it is not actively involved in repair itself. In mammals, γ-H2A.X serves as a recruiter of MDC1 (Mediator of DNA damage Checkpoint 1), which is crucial for recruitment of other important repair factors like the tumour suppressor p53 and BRCA1 (breast cancer type 1 susceptibility protein). In addition to phosphorylation, acetylation and ubiquitylation were found as important modifications of H2A.X. These modifications are also relevant for the recruitment of the DDR repair machinery to DNA damage sites (Yuan et al, 2010). The largest and most unusual H2A variant is macroH2A, found only in vertebrates. This variant is defined by its long additional 30kDa domain in the C-terminal region, which extends out of the nucleosome and serves as an interacting region with various chromatin factors (Gamble and Kraus, 2010). Three isoforms of macroH2A exist in mammals; macroH2A1.1 and macroH2A1.2 are splice variants of a single gene, while macroH2A2 is encoded by a separate gene. Structurally, the macroH2A containing nucleosome is similar to the canonical nucleosome and they organise the same amount of DNA (Changolkar and Pehrson, 2002). MacroH2A is enriched in the inactive X chromosome in female mammals, where it is involved in transcriptional repression that leads to X inactivation (Costanzi and Pehrson, 1998). It is noteworthy that macroH2A is equally expressed in females and males, although X inactivation is restricted only to females (Rasmussen et al. 1999). This indicates a general role of macroH2A as a factor in repression of

transcription. Another vertebrate-specific H2A variant is H2ABbd (Bar-body deficient). H2ABbd localisation is strongly correlated with transcriptionally active regions and is mutually exclusive with macroH2A. It was shown that H2AB organises less nucleosomal DNA and builds less stable nucleosomes than canonical H2A (Gautier et al. 2004, Bao et al. 2004)

Histone H4, unlike H2A and H3, has no known variants. It is the most highly conserved histone, having only few amino acid changes when the H4 amino acid sequence is compared between different organisms. This level of conservation is somewhat expected since H4 makes protein-protein contacts with all other three core histones (Malik and Henikoff, 2003.). Histone H2B has few variants which are highly specific for certain developmental stages and their function remains mostly unknown.

2.2.2. Post-translational histone modifications

Another mechanism of controlling different chromatin states is by modification of unstructured N-terminal tails of histones. An array of different modifications has been found on histones, including acetylation, methylation, and phosphorylation which are the most prevalent histone modifications. Less abundant modifications include ubiquitylation, sumoylation, ADP ribosylation, deimination and proline isomerization (Kouzarides, 2007). A variety of enzymes that act on chromatin function as epigenetic regulators. Epigenetic "writers" can modify DNA or histones by placing different marks. This function can be performed by DNA methyltranferases, HAT's (histone acetyltransferases), HMT's (histone methyltransferases), PRMT's (protein arginine methyltransferases) and kinases that can modify histone tails. Epigenetic "readers" recognise the marks placed by these writers. They can alter chromatin state or recruit other proteins to change chromatin structure. This includes proteins that contain methyl binding domains, such as PHD (plant homeodomain) fingers, WD40 repeats (40 amino acid repeat terminating with tryptophan-aspartic acid dipeptide) and CW (cysteine and tryptophan) domains. They also include proteins of the Royal

superfamily that encompasses proteins with chromodomains, chromobarrels, Tudor domains and MBT (malignant brain tumour) repeats. Finally, epigenetic "erasers" remove these marks from histones. They are enzymes such as HDAC's (histone deacetylases), KDM's (lysine demethylases) and phosphatases. Adding and removing these marks can have an effect on addition and removal of other histone marks. Different histone marks can affect gene expression by recruiting different chromatin remodelers. Together, they can modulate a variety of processes, such as DNA transcription, replication and repair (Kouzarides, 2007, Greer and Shi, 2012, Falkenberg and Johnstone 2014, Hoppman et al. 2011).

Histone methylation can occur on basic residues like arginines and lysines. Lysines can be mono-, di- or trimethylated, while arginines can be monomethylated, symmetrically dimethylated (me2s), or asymmetrically dimethylated (me2a). Methylation of different residues can have different outcomes and lead to repression or activation of transcription. For example, H3K9me3 binds HP1 (heterochromatin protein 1, protein involved in gene repression by formation of heterochromatin) in heterochromatin and leads to more compacted chromatin that is inaccessible to the transcription maschinery. Another repressive mark is H3K27me3, that is generated and bound by PRC2 (Polycomb repressive complex 2). On the other hand H3K4me3 is an active mark, that was shown to be associated with transcriptional start sites of active genes (Barski et al. 2007). Arginine methylation is also implicated in transcriptional regulation. For example, H4R3me2a, H3R2me2s and H3R26me2a mark active chromatin, while H3R2me2a and H4R3me2s are repressive marks (Blanc and Richard, 2017).

Numerous histone methyltransferases and demethylases have been identified that mediate addition or removal of methylation marks (Greer and Shi, 2012). Three different enzyme families catalyse addition of methyl groups on histone tails. SET-domain (Su(var)3-9, Enhancer-of-zeste and Trithorax) containing proteins and DOT1-like proteins methylate lysine residues, while PRMT family proteins methylate arginines (Bannister and Kouzarides, 2011). Removal of

methyl groups is performed by histone demethylases. One group comprises amino oxidases, like LSD1 (Lysine-specific histone demethylase 1A) that demethylates H3K4, an active mark, by which it functions as a transcriptional repressor (Shi et al. 2004). Another group of histone demethylases are the Jumonji C (JmjC) domain-containing proteins, for example JHDM1 that demethylates H3K36 (Tsukada et al. 2006). All taken together, histone methylation has a wide role in transcription control, from organising global chromatin architecture to the regulation of specific loci (Greer and Shi, 2012).

Histone acetylation is involved in the opening of chromatin structure. Addition of an acetyl group to lysine residues removes positive charge from lysine which in turn destabilises the interaction between DNA and histones, leading to a more open chromatin state. Acetylation can also have an effect on nucleosome/ nucleosome interactions. Specifically, H4K16 acetylation can destabilise the interaction between the H4 tail and an "acidic patch" on the neighbouring nucleosome, affecting higher order chromatin folding (Kalashnikova et al. 2013). Acetylation of histones is catalysed by histone acetyltransferases (HATs), which transfer acetyl to the ε-amino group on a lysine residue. The reverse reaction of histone deacetylation is catalysed by histone deacetylases (HDACs) (Shahbazian and Grunstein, 2007). Acetylation has an important role in nucleosome assembly; newly synthesised histones are transiently acetylated on H4K5 and H4K12 in all eukaryotes, while the acetylation of newly synthesized H3 is more variable: K9 and K14 are acetylated in *Tetrahymena*, while K14 and K23 are acetylated in *Drosophila.* These acetylations might have a role in the recognition of new histones by histone chaperones (Sobel et al. 1995, Shahbazian and Grunstein, 2007). The most prominent role of acetylation is to promote transcriptional activation. Histone acetylation strongly correlates with active gene transcription by creating a more open chromatin state that facilitates binding of the transcriptional machinery (Reid et al. 2000, Shahbazian and Grunstein, 2007).

Histone phosphorylation was discovered on serine, threonine and tyrosine histone residues. These residues can be phosphorylated by numerous kinases and dephosphorylated by phosphatases (Rossetto et al. 2012). Histone phosphorylation is best known for its role in DNA damage repair. As mentioned above, H2AX is phosphorylated upon DNA damage (Rogakou et al. 1998). Histone H3 tail phosphorylation is highly conserved throughout eukaryotes, it has been found on T3, S10, T11, and S28. The most thoroughly investigated H3 phosphorylation is S10P, generated by the Aurora B kinase, which is important in chromatin condensation during mitosis and meiosis (Wei et al. 1998, Rossetto et al. 2012). This phosphorylation is important for ejection of HP1 from chromosomes during M phase, shifting the equilibrium to the HP1 unbound state. This indicated a role of H3S10 in mediating the release of HP1 from the mitotic chromosome (Fischle et al. 2005, Banerjee and Chakravarti, 2011). Dephosporylation of H3S10 is performed by PP1 (protein phosphatase 1) which is important for proper chromosome segregation (Rossetto et al. 2012).

Histone ubiquitination is most abundant on histone H2A and H2B in its monoubiquitinated form. They can be monoubiquitinated on H2AK119 and H2B K123 (Goldknopf et al. 1975, West and Bonner, 1980). Ubiquitinated histones play a significant role in transcription, where H2Aub is associated with gene silencing, while H2Bub is linked with transcriptional activation. Besides transcriptional control, ubiquitination has an important role during the DNA damage response, when H2A, H2AX, and H2B can be ubiquitinated at the sites of DNA damage (Cao and Yan, 2012, Uckelmann and Sixma, 2017).

2.2.3. Chromatin remodelling enzymes

A plethora of ATP dependent chromatin remodelers are modulating gene expression by making chromatin more closed and compact or more open and accessible for the transcription machinery. Unlike histone/DNA modifying enzymes, they are not covalently changing chromatin, but use energy derived from ATP hydrolysis to change chromatin structure. Besides transcriptional

regulation, they have a role in DNA repair, recombination, and chromatin assembly.

2.2.3.1. Common ATPase motors

ATP-dependent chromatin remodelers belong to the helicase superfamily 2 (SF2) of ATPases. Within the SF2 superfamily, they form their own Snf2 subfamily, named after the first discovered chromatin remodeler. Their central feature is an ATPase motor consisting of two copies of RecA-like lobes. These lobes are derived from the ancestral bacterial RecA protein that performs ATP-dependent strand exchange between single stranded DNA (ssDNA) and double stranded (dsDNA). RecA oligomerises on ssDNA, binds ATP and forms a helical filament which then binds to dsDNA and catalyses the exchange of complementary strands (Chen et al. 2008, Cox, 2007). During the reaction one RecA monomer provides ATP binding and hydrolysis motifs, while the neighbouring monomer brings in two lysine residues that stabilise the transition state and stimulate ATP hydrolysis, which leads to DNA release. This lysines are analogous to arginine finger motif in many GTPases and ATPases. In the SF2 family, duplication of the RecA lobe has transfered these enzymatic functions onto a single protein. Thus, the ATPase domain consists of the first lobe, also known as DExx, that retains ATP binding and hydrolysis and the second lobe, also known as HELICc, that provides the arginine finger motif (formed out of two arginines, separated with 2 other amino acids) for ATP hydrolysis and stabilisation of the transition state (Chen et al. 2008, Zhou et al. 2016).

When an ATP-dependent chromatin remodeler is bound to DNA in its resting state, the two lobes are in an open conformation. Upon binding of ATP, the two lobes go through conformational changes that result in their closure. It was shown that ATPase motors bind to the DNA on the nucleosome at the SHL2 (superhelical location 2) position and then translocate along the DNA, by pulling the DNA from the proximal side of the nucleosome (DNA entry site), towards the distal side of the nucleosome (DNA exit side). This translocation is propagated

in a wave-like manner and it leads to DNA translocation by one base pair. After hydrolysis and release of ADP, conformational changes reopen the two lobes and return them to the resting state. In that manner, ATP binding and hydrolysis are facilitating a series of structural changes that enables remodelers to move along the DNA substrate (Zhou et al. 2016, Wigley and Bowman, 2017, Farnung et al. 2017, Nodelman et al. 2017, Clapier et al. 2017). Highly conserved motifs and blocks within the ATPase motor act in concert to perform the remodeler's enzymatic function. The ATPase motor of chromatin remodelers contains seven helicase-related motifs that cooperate in ATP binding, hydrolysis and translocation: Motifs I, Ia, II, III, IV, V and VI are scattered between the two lobes (Figure 2.2). Motif I, Ia, II and III are located in the first DExx lobe, while

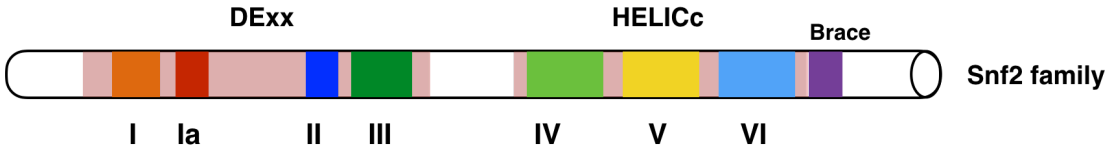

Figure 2.2. Conserved motifs of the Snf2 family of ATP-dependent chromatin remodelers

Diagram showing relative positions of conserved helicase motifs (shown in orange, red, dark blue, dark green, light green, yellow and light blue) in relation to two RecA-like lobes (shown in light red). Motifs I, Ia, II and III are located in the first DExx lobe. Motifs IV, V and VI are located in the second HELICc lobe. Brace domain in purple. Modified according to Flaus et al. 2006.

IV, V and VI are in the second HELICc lobe (Flaus et al. 2006). Motifs I, II and VI are equivalent to the Walker A and B boxes found in many ATPases and they are involved in ATP binding and hydrolysis. Highly conserved arginine fingers, which are part of motif VI, are interacting with the ATP binding motifs of the DExx lobe upon nucleosome binding (Zhou et al. 2016, Liu et al. 2017). Motif III is involved in the coupling of ATP hydrolysis with translocation. Motifs Ia, IV and V are involved in nucleic acid binding and translocation. Additionally, the Snf2 family of enzymes contains conserved blocks that represent structural features

that are unique to the Snf2 family. These blocks are located throughout the ATPase domain, but also on the C terminal side following the second HELICc lobe where the alpha helical brace domain is located (Pyle, 2008, Dürr et al. 2005, Flaus et al. 2006, Singleton et al. 2007).

Throughout the years it became clear that mechanism of nucleosome remodelling is a shared feature of all remodelers. During evolution, an ancestral protein that moved along the DNA aquired histone anchoring ability, which enabled interaction with the nucleosome and translocation of DNA along the surface of the octamer. Later, mechanisms for regulating the ATPase domain evolved: such regulation is provided by domains, insertions or accessory proteins that modulate the activity of the ATPase domain. For example, autoinhibition of the ATPase domain is a common mechanism of keeping the remodeler in its resting state. This inhibition is released when the remodeler contacts certain epitopes on the nucleosome (Clapier et al. 2017). This fine

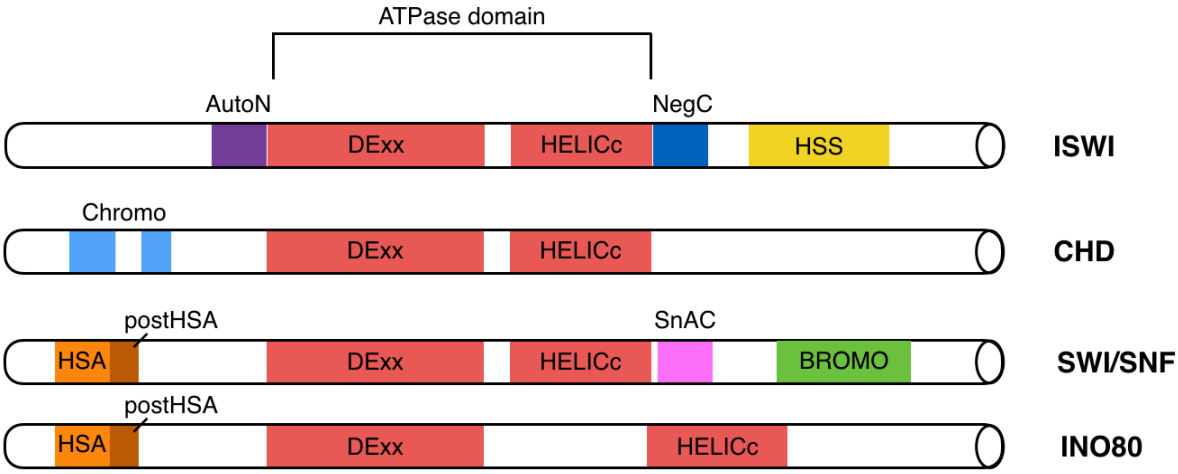

Figure 2.3. ATP dependent chromatin remodeler families

Simplified representation of the domain structure of ATP-dependent remodelers. The two lobes of the ATPase domain - Dexx and HELICc - are depicted in red, Chromodomains in blue, HSA (helicase SANT domain) in orange, postHSA in dark orange, bromodomain in green. AutoN in purple, Neg C in dark blue, HSS (Hand-Sant-Slide domain) in yellow and SnAC in pink (Modified after Workman and Abmayr, 2014).

tuning led to the specialisation of different remodellers. They are divided into 4 main families according to similarities in their ATPase domain and associated domains: ISWI, SWI/SNF, INO80 and CHD. These remodelers are often part of multisubunit complexes that act on chromatin and perform diverse functions.

2.2.3.2. SWI/SNF family

SWI/SNF enzymes encompass a large family of multisubunit complexes. *Snf* (sucrose non fermenting) and *swi* (switch) genes were first found in genetic screens in yeast. These studies were aiming to find genes that regulate expression of (a) homothalic switching endonuclease (HO) that controls mating type switching (SWI) and (b) transforming enzyme sucrose invertase (SUC2) necessary for sucrose non-fermentation (SNF). Later, it became apparent that these studies identified genes that encode for the same large protein complex with important roles in the regulation of transcription through chromatin remodelling (Neigeborn and Carlson, 1984. Stern et al. 1984, Masliah-Planchon et al. 2015, Tang et al. 2017). This was named SWI/SNF complex according to the two phenotypes that led to its discovery (Masliah-Planchon et al. 2015). Further studies found that the SWI/SNF complex is a large multisubunit complex consisting of 11 proteins, with the Swi2/Snf2 ATPase being the catalytic subunit (Workman and Kingston, 1998). Another related SWI/SNF family complex is RSC (Remodelling the Structure of Chromatin), also found in yeast. These two complexes differ in their ATPase subunit, the SWI/SNF complex has Swi2/Snf2p, while RSC contains Sth1 (Cairns et al. 1994. Tang et al. 2010). Although, RSC ans SWI/SNF complexes contain several homologous subunits and share two identical subunits, these two complexes have important functional differences. Genome-wide gene expression studies have found that they control different sets of target genes. RSC is 10x more abundant than SWI/SNF in yeast and is essential for growth and normal cell cycle progression. Both complexes can function as transcriptional activators and repressors (Muchardt and Yaniv, 2001, Mohrmann et al. 2004, Martens and Winston, 2003).

SWI2/SNF2-containing complexes exist in other organisms, including *Drosophila*, human, and mouse. In *Drosophila*, the Swi2/Snf2-homolog brahma (BRM), which was discovered in the Tamkun lab in 1994, is a component of two different complexes - BAF and PBAF (Elfring et al. 1994). Human cells contain the homologous complexes hBAF, that can contain hBRM or BRG1 as its ATPase subunit, and hPBAF that contains only BRG1 (Tang et al. 2010). Interestingly, hPBAF is related to yeast RSC and has a functionally similar role in cell growth (Xue et al. 2000).

These ATPase motors have a central SF2 like ATPase domain which is flanked by additional functional domains (Figure 2.3). An N-terminal HSA (helicase-SANT-associated) domain is important for the interaction with ARPs (actin related proteins) like Arp7 and Arp9 that are part of the both RSC and SWI/SNF complexes (Cairns et al. 1998). In Sth1, loss of the HSA domain causes loss of actin proteins and reduction of ATPase activity. An additional domain adjacent to the HSA, the postHSA domain, was also identified in Sth1 and is also present in other remodelers that contain ARPs (Szerlong et al. 2008). Subsequently, it was found that the postHSA domain has a role in downregulating ATPase activity and the rate of DNA translocation (Clapier et al. 2016). SWI/SNF remodelers have a bromodomain on the C-terminal side of the ATPase domain. First identified by the Kennison lab in the *Drosophila* brahma protein, it exists in many other proteins (Tamkun et al. 1992). Bromodomains have a role in recognising acetylated lysines in histone tails, by which they can contribute to targeting of the complex and modulate chromatin remodelling (Syntichaki et al., 2000, Marmorstein and Berger, 2001). The most recently identified domain of SWI/SNF remodelers was found by the Bartholomew lab and named SnAC (Snf2 ATP coupling). Located in the C-terminal part of the protein, located immediately after ATPase domain, this domain has a role in pairing the energetically favourable ATP hydrolysis with the energetically unfavourable translocation reaction. Mutation or deletion of this domain severely affected ATPase and remodelling functions of SWI/SNF. The SnAC domain positively regulates the catalytic activity of SWI/SNF (Sen et al. 2011). This regulation

comes from the interaction between SnAC and histones, where SnAC is acting as an histone anchor. This interaction is a prerequisite for SWI/SNF remodeler to efficiently couple ATP hydrolysis to DNA translocation (Sen et al. 2013).
SWI/SNF chromatin activities include nucleosome sliding that mobilises mononucleosomes from the center to the end of a DNA fragment *in vitro* (Fan et al. 2003). Apart from sliding, SWI/SNF can also eject histones. Regulation between sliding and ejection is mediated by the HSA, postHSA and protrusion 1 domains (located between the two ATPase cores), as well as by two ARPs that bind to the HSA domain. In this way translocation efficiency can be modulated from a lower activity that leads to sliding to a higher activity that results in histone ejection (Yanf et al. 2007, Clapier et al. 2017). Additionally, the RSC complex catalyses the transfer of the H2A/H2B dimer or the entire octamer from one DNA template to another (Rowe and Narlikar 2010).

2.2.3.3. ISWI family

After identification of the first ATP-dependent chromatin remodeller, the yeast SWI2/SNF2 complex, the search for similar proteins continued. John Tamkun's lab identified ISWI (imitation switch), a protein with high sequence similarity to the human SNF2L remodeller (Elfring et al. 1994). Carl Wu's, James Kadonaga's and Peter Becker's labs went on to identify three ISWI containing complexes in *Drosophila* - NURF, ACF, and CHRAC, respectively (Tsukiyama et al. 1995, Ito et al. 1999, Varga-Weisz et al. 1997). Afterwards, homologous complexes were purified from other organisms like *Xenopus*, yeast, and human (Oppikofer et al. 2017).

ISWI containing complexes encompass many roles within the cell. This includes transcriptional activation and repression. The NURF complex can facilitate GAL-4 mediated transcription *in vitro*, which was the first hint that ISWI containing complexes can facilitate gene activation (Mizuguchi et al. 1997). Afterwards, a role in transcriptional activation was demonstrated for other ISWI complexes, like ACF (Levenstein and Kadonaga, 2002). On the other hand, transcriptional repression has been indicated for *Drosophila* ISWI - in polytene

chromosomes, ISWI associated with euchromatin regions that do not colocalize with RNA Pol II, suggesting that it could play a part in repression. The same study emphasised the importance of ISWI in organising chromatin higher order structures since ISWI null mutants showed X chromosome defects in male flies (Deuring et al. 2000. Corona and Tamkun, 2004). The wide variety of functions that ISWI containing complexes perform within a cell, posed the question of their mechanism of action.

In vitro experiments showed that ISWI complexes perform two different actions on chromatin - nucleosome sliding and nucleosome assembly. (Hamiche et al. 1999, Längst et al. 1999, Ito et. al. 1997). By sliding the ISWI remodelers are able to regulate gene expression. The ISWI ATPase moves nucleosomes on its own, but the precise outcome of this sliding activity often depends on other subunits of ISWI complexes, that modulate its activity. For example, ACF1, the noncatalytic subunit of the human ACF complex, modulates the activity of SNF2h *in vitro* by sensing linker DNA lengths, by which it can regulate nucleosome spacing (Yang et al. 2006). Another activity of ISWI ATPases is nucleosome assembly (Ito et al. 1997). ISWI complexes can turn “nascent” pre-nucleosome particles (containing all histones, but in non-canonical conformations) that are formed immediately after passage of DNA replication forks into more canonical mature nucleosomes, as characterised by nuclease digestion and sedimentation properties (Torigoe et al. 2011, Zhou et al. 2016).

More insight into the workings of ISWI ATPase motors was obtained from many structural studies that have elucidated domain structures and have shed some light on nucleosome-remodeler interactions. ISWI ATPases contain a C-terminal HSS domain, which consists of a SANT domain that is structurally similar to c-MyB DNA binding domains (DBD) (Clapier and Cairns, 2009). Unlike the DBD of c-MyB, the SANT domain of ISWI lacks amino acid residues, that interact with DNA in c-MyB. (Grüne et al. 2003). Instead, the SANT domain interacts with unmodified histone tails (Boyer et al. 2002 and 2004). A DNA binding role of ISWI is contained in its SLIDE domain, that interacts with linker DNA at the

entry to the nucleosome. The HAND domain binds to extranucleosomal DNA near the entry site of the nucleosome, similarly to the SLIDE domain (Dang and Bartholomew, 2007). Together these domains help to regulate nucleosome recognition and stimulate ATPase activity (Clapier and Cairns, 2009). Two additional small domains of ISWI ATPases were recently identified - AutoN and NegC, which are flanking core 1 and core 2 of the ATPase domain, respectively, and are functioning as negative regulators of ISWI activity (Figure 2.2). AutoN negatively influences ATP hydrolysis. Mutations in or deletions of AutoN increase ATPase activity and nucleosome sliding and decrease the dependency on H4 tails for ATP hydrolysis. Nevertheless, reliance on the H4 tail to couple ATP hydrolysis with remodelling is still retained. This supports a model in which AutoN holds the ATPase domain in an inactive conformation. This conformation is changed upon binding to the H4 tail, that dislodges AutoN enabling conformational changes that activate the ATPase motor (Clapier and Cairns, 2012). More insight into the structural workings of AutoN inhibition was obtained by recent studies from the Chen lab: AutoN keeps the two core domains 'glued' together, by bridging over core 1 and binding to the core 2 domain (Yan et al. 2016). Another small negative regulator domain is NegC - identified as a negative regulator of coupling the ATP hydrolysis to remodelling (Clapier and Cairns, 2012). Further studies showed NegC plays a role in preventing translocation in the DNA length sensing state by controling the motor from transitioning to a translocation competent state (Leonard and Narlikar, 2015). Again, a study from the Chen lab showed that NegC - core2 interactions are necessary for regulation of this DNA length sensing (Yan et al. 2016). Results from these studies can likely be extended to related ATPases.

2.2.3.4. INO80 family

The INO80 family of chromatin remodelers consists of two different types of enzymes - INO80 and Swr1. Characterised in yeast, *Drosophila,* and mammals, INO80 family of remodelers are defined by their split ATPase domain, with a large insertion between motifs III and IV. The length of this insertion can range

from around 200 amino acids in yeast INO80 and Swr1, to >1000 amino acids in mammalian SCRAP (Watanabe and Peterson, 2010). This large insertion is important for interaction with other subunits like ARPs (Szerlong et al. 2008). This suggests that the subunit composition could be dictated by the amino acid content of this insertion, that in turn could regulate activities of Swr1 and INO80 (Zhou et al. 2016). INO80 remodelers also contain an HSA (helicase SANT) domain that interacts with ARP (see SWI/SNF remodelers) (Szerlong et al. 2008).

These remodelers perform many different functions within the cell, from DNA repair, replication, chromosome segregation to telomere maintenance (Morrison and Shen, 2009). INO80 and Swr1 use distinct mechanisms to regulate chromatin. Swr1 catalyse the exchange of H2A/H2B dimers with H2A.Z/H2B dimers (Mizuguchi et al. 2004). It is proposed that Swr1-Z, a small N-terminal region of Swr1, and Swc2, a subunit of the SWR complex, regulate the ability of Swr1 to exchange the H2A/H2B dimer with the H2A.Z/H2B variant (Luk et al. 2010, Zhou et al. 2016). On the other side, INO80 slides nucleosomes to the center of a DNA fragment and evenly spaces di- and trinucleosomes (Udugama et al. 2010).

It has been proposed that Swr1 and INO80 might produce a common nucleosome intermediate that is unwrapped from one side. This nucleosome then could be used by Swr1 to mediate histone exchange to H2A.Z/H2B, while INO80 could use it to slide the histone octamer (Zhou et al. 2016). INO80 remodelers could also have a role in reversing the Swr1 reaction; exchanging H2A.Z/H2B with canonical dimer H2A/H2B (Watanabe and Peterson, 2010).

2.2.3.5. CHD family

The CHD family of chromatin remodelers is characterised by its N-terminal chromodomains and the central SNF2-like ATPase domain. This family encompasses a large group of chromatin remodelers divided into 3 subfamilies

according to the presence of additional domains. The first family member was identified in mouse and named CHD1 - chromodomain helicase DNA binding protein 1 (Delmas et al. 1993). Afterwards, many CHD family proteins were identified in *Drosophila*, yeast, human and many other organisms.

2.2.3.5.1. Chromodomains as distinct domains of the CHD family

In CHD proteins the chromodomain region is located in the N-terminal part of the protein as tandem chromodomains. This domain was originally identified as a conserved 37 amino acid region in HP1 and Pc (Polycomb). The name chromodomain (chromatin organizer domain) signifies that both of these proteins are involved in chromatin organisation (Paro and Hogness, 1991, Marfella and Imbalzano, 2007). Today, the chromodomain is defined as a region of approximately 50 amino acids that is present in a growing number of proteins (Jones et. al. 2000). Many chromodomains bind methylated lysines of histone tails, for example, Pc binds H3K27me3 and HP1 binds H3K9me3 (Jacobs et al. 2001, Schwartz and Pirrotta, 2007). In the CHD family, chromodomains have somewhat different characteristics: human CHD1 binds H3K4me2/3, but the chromodomains of dMi-2, the *Drosophila* homolog of human CHD4, act as a DNA binding module, and they do not interact with methylated histone H3 tails (Flanagan et. al 2005, Bouazoune et al. 2002). In addition, deletion of the dMi-2 chromodomains impairs nucleosome-stimulated ATP hydrolysis and nucleosome remodelling (Bouazoune et al. 2002). In humans, the CHD4 chromodomains stimulate ATPase activity. In cross-linking experiments, it was shown that human CHD4 interacts with the ATPase domain, indicating a regulatory role of the chromodomains in human CHD4 (Watson et al. 2012). The crystal structure of yeast CHD1 was solved in the Bowman lab and revealed that chromodomains act as negative regulators of the ATPase motor that interact with both ATP lobes and keep the motor in an inactive open conformation. They identified two helices that connect the two chromodomains and named them the chromo-wedge. The chromo-wedge contacts the ATPase domain at its DNA binding surface. These interactions interfere with the binding of naked DNA to CHD1. Upon binding to the nucleosome, structural changes in

CHD1 release the chromodomains from the ATPase motor and bring them into an “ungated” position, enabling the ATPase motor to switch to the closed and active conformation ready for hydrolysis (Hauk et al. 2010). This model, in which chromodomains act as negative regulators of the ATPase motor and as modules for the distinction between DNA and nucleosomes, could apply to other members of the CHD family.

2.2.3.5.2. Members of CHD family

As mentioned previously, the CHD family consists of 3 subfamilies, where CHD proteins are divided according to their respective domains. Since CHD4/Mi-2 is a protein of interest in this thesis, it will be discussed in a separate chapter.

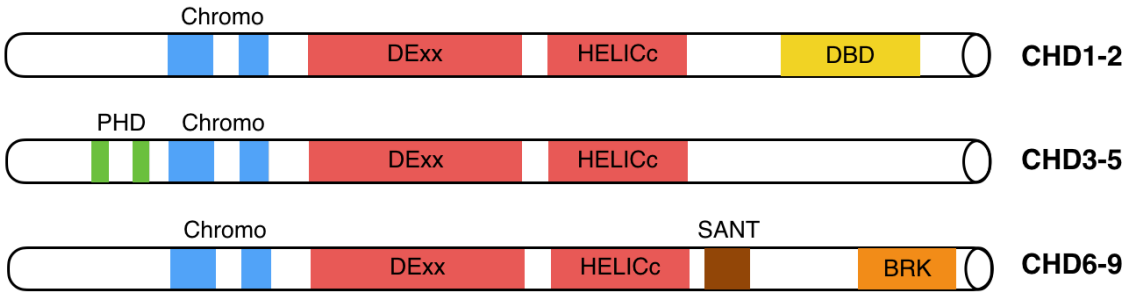

Figure 2.4. CHD subfamilies

CHD proteins are divided in 3 subfamilies - CHD1-2, CHD3-5 and CHD6-9. Chromodomains in blue, ATPase lobes in red, DBD (DNA binding domain in yellow), PHD fingers in green, SANT domain in brown, BRK domain in orange.

CHD1-2 subfamily

The first CHD subfamily consists of CHD1 and CHD2, that are highly homologous to each other. Both proteins contain a DNA binding domain. This domain preferentially binds to AT-rich DNA via minor-groove interactions (Stokes and Perry, 1995). *Drosophila* CHD1 localises to regions of extended chromatin on polytene chromosomes (interbands) and regions with high transcriptional activity (puffs). This strongly suggests that CHD1 is helping to

maintain open chromatin structures and facilitates transcription (Stokes et al. 1996). Studies in *Drosophila* showed that CHD1 could be involved in nucleosome assembly - CHD1 can assemble histone H1-deficient chromatin, but not histone H1-containing chromatin, indicating a role in assembly of transcriptionally active DNA into chromatin (Marfella and Imbalzano, 2007, Lusser et al. 2005).

CHD6-9 subfamily

Members of the third CHD subfamily are characterised by additional domains not present in other CHD family members - the SANT domain and the BRK domain. The BRK domain is also found in many SWI/SNF proteins like *Drosophila* BRM, human BRM and human BRG1. This domain is not present in yeast chromatin remodelers related to BRM. This suggests that this domain could play a role in functions specific to higher eukaryotes, or interact with chromatin features that are unique to higher eukaryotes. There is also a DNA binding domain that can be found in first CHD subfamily, as well as in third subfamily (Marfella and Imbalzano, 2007). The DNA domains of CHD6-9 likely also bind AT-rich DNA, as was demonstrated for CHD9 (Shur and Benayahu, 2005). CHD7 has been established as a regulator of vertebrate development. Mutations in this protein can cause developmental disorders like CHARGE syndrome (Bouazoune and Kingston, 2012). In vitro, CHD6, CHD7, and CHD8 exhibited significant differences in nucleosome binding and mobilisation, indicating distinct roles in their action on chromatin (Manning and Yusufzai, 2017).

CHD3-5 subfamily

Members of the second subfamily share a double PHD finger domain. An N-terminal domain present in CHD3-5 is the double PHD (plant homeo domain) finger. Discovered in 1993 in *Arabidopsis thaliana,* it was identified as a Cys_4-His_1-Cys_3 evolutionary conserved motif (Schindler et al. 1993). This small domain encompasses 50-80 amino acid residues and contains a zinc binding

motif that is present in many chromatin proteins (Aasland et al. 1995). In the NURF complex, the NURF301 subunit contains this zinc finger structural fold that is able to 'read' histones, more specifically histone H3K4me3 (Wysocka et al. 2006). In human CHD4, the PHD fingers bind histone H3, more specifically the PHD finger 2 binds H3K9me3, H3K9ac as well as unmodified H3K4 (Mansfield et al. 2011, Musselman et al. 2009). In addition, both PHD fingers, through interaction with histone H3, are essential for the transcriptional repressive activity of CHD4 (Musselman et al. 2011). In a further study from the Laue lab, it was demonstrated that the PHD fingers of human CHD4 are relevant for efficient nucleosome remodelling; a mutant lacking the PHD finger domain has diminished sliding activity compared to a construct with PHD fingers (Watson et al. 2012).

CHD3 and CHD4, also known as Mi-2α and Mi-2β, respectively, and CHD5 are catalytic subunits of the NuRD (nucleosome remodelling and deacetylation) complex. Depending on the cell type, the NuRD complex can contain CHD3 or CHD4 and exhibit different nuclear localisation patterns (Hoffmeister et al. 2017). CHD5 has been identified as a tumour suppressor gene involved in proliferation, apoptosis, and senescence. Inactivation of CHD5 has been found in wide array of human cancers, including neuroblastoma (Bagchi et al. 2007; Potts et al., 2011). It was first identified in the brain, where it is a component of the NuRD complex. CHD5 is also expressed at high levels in testis and required for male fertility (Bergs et al. 2014).

CHD4/Mi-2

CHD4 (chromodomain helicase DNA binding protein 4) was first identified in humans as an autoantigen in dermatomyositis, an inflammatory disease characterised by inflamed muscles and skin. The protein was named Mi-2, after a patient called Mitchell in whose serum Mi-2 antibodies were found. Patients diagnosed with dermatomyositis are more susceptible to developing cancer (Seelig et al. 1995 and 1996). Later, Danny Reinberg's lab identified human

Mi-2 together with histone deacetylase HDAC1/2 and MTA2/3 (metastasis-associated protein) to be part of a complex with deacetylation and nucleosome remodelling activities. It was named the NuRD complex, a complex with two distinct enzymatic activities (Zhang et al. 1998). Jürg Müller's lab identified the *Drosophila* CHD4 homolog dMi-2 as a factor that interacts with the Hunchback protein and is important in Polycomb-mediated repression of HOX genes, the first indication of dMi-2's involvement in repression *in vivo* (Kehle et al. 1998). dMi-2 is a chromatin stimulated ATPase, with distinct nucleosome remodelling properties compared to other remodelers (Brehm et al. 2000). In *Drosophila*, dMi-2 is also part of the dNuRD complex, a homologue to the human NuRD complex. However, it was shown that the bulk of dMi-2 in *Drosophila* is part of the dMec complex (*Drosophila* MEP-1-containing complex). This complex is composed of dMi-2 and dMEP-1, and represses proneural genes (Kunert et al. 2009).

CHD4 complexes are devoid of any subunits that could bind to DNA in a sequence specific manner, therefore, CHD4's recruitment to chromatin must be mediated through other mechanisms. The NuRD complex subunit MBD2 (methylated DNA binding domains 2) can recruit NuRD to methylated DNA and in that way promote transcriptional repression (Feng and Zhang, 2001). Further on, dMi-2 was shown to be recruited to heat shock genes in a PARP dependent manner. dMi-2 was shown to bind PARylated heat shock loci in respones to the heat shock in Drosophila (Murawska et al. 2011). Recently, dMi-2 was shown to be recruited by EcR (ecdysone receptor) to repress transcription of hormone regulated genes. This interaction results in stimulation of dMi-2-mediated chromatin remodelling, revealing new molecular mechanisms of chromatin remodeller regulation by a nuclear hormone receptor (Kreher et al. 2017).

Human CHD4, also acts as an ATP-dependent chromatin remodeller; recombinant CHD4, as well as the NuRD complex, disrupt histone-DNA contacts in an ATP-dependent manner. Unlike dMi-2, CHD4 is also activated by naked DNA (Wang and Zhang, 2001). As a part of the NuRD complex, CHD4 is

involved in a wide range of cellular processes, with transcriptional repression the most extensively studied (Deslow and Wade, 2007). NuRD was shown to interact with the protein kinase ATR (ataxia telangiectasia and Rad3 related), that has a prominent role in the DNA damage response (DDR). The NuRD components CHD4 and HDAC2 were shown to co-purify with ATR, suggesting a potential role of those two proteins or the NuRD complex in DDR (Schmidt and Schreiber, 1999). Another indication of CHD4 as a potential factor in DDR was provided by experiments that showed increased CHD4 protein levels upon UV exposure (Burd et al. 2008). NuRD is recruited to DNA damage sites in a poly(ADP-ribose) dependent manner. Upon CHD4 knockdown, DNA repair is impaired, establishing CHD4 as an important factor in the repair of DNA double-strand breaks. In addition, a potential novel role of CHD4 in cell cycle control was suggested by the finding that NuRD deacetylates p53, thereby regulating G1/S cell cycle transition (Luo et al. 2000, Polo et al. 2010). Some studies identified CHD4 as a potential tumour suppressor in certain cancers: CHD4 expression is reduced in gastric and colorectal cancers with microsatellite instability, as is often the case for tumour suppressor genes (O'Shaughnessy and Hendrich, 2013, Kim et al. 2011). Recent exome sequencing studies showed CHD4 to be mutated in 17% of endometrial cancers of the serous type. Most of the mutations identified map to the ATPase motor. Other mutations also map to its PHD fingers and chromodomains (LeGallo et al. 2012, Zhao et al. 2013). CHD4 is also mutated in other cancers like thyroid, ovarian, malignant lymphoma, gastric, skin, and bladder cancer (Längst and Manelyte, 2015). Besides mutations in cancer, CHD4 mutations were identified in patients with intellectual disability syndromes (Weiss et al. 2016), congenital heart defects (Sifrim et al. 2016) and developmental disorders (Deciphering Developmental Disorders Study, 2017).

Collectively, these results link CHD4 to a variety of diseases. However, the molecular consequences of CHD4 mutations have not been defined.

2.3. Objectives

Several independent studies have identified human CHD4 as a highly mutated gene in several different human malignancies, especially serous endometrial carcinoma where CHD4 mutations reach the high percentage of 17-19 % (Le Gallo et al. 2012, Zhao et al. 2013.). Recently, de novo mutations in CHD4 were also reported in patients with an intellectual disability syndrome (Weiss et al. 2016.). Additionally, CHD4 mutations were reported in cancers like thyroid, ovarian, gastric, skin, bladder and malignant lymphoma, where numerous single somatic mutations were identified (Längst and Manelyete, 2015.). Many mutations affect highly conserved residues within functional domains of the protein, like the ATPase domain, chromodomains and PHD fingers (Figure 2.5).

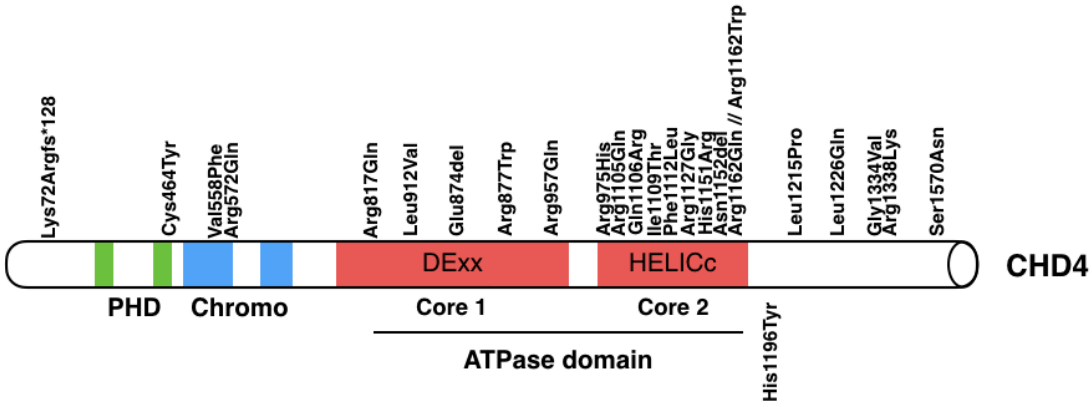

Figure 2.5. Schematic overview of CHD4 amino acid residues affected by point mutations in endometrial cancer, an ovarian cancer line and intellectual disability syndrome Two PHD fingers depicted in green, chromodomains in blue and two ATPase domain cores in red (Le Gallo et. al. 2012., Zhao et al. 2013., Weiss et al. 2016., R. Müller, pers. comm.)

This study aims to determine consequences of selected cancer relevant point mutations on dMi-2, the *Drosophila* homolog of human CHD4. High conservation levels between these two proteins allows dMi-2 to be used as a paradigm for charachterisation of the enzymatic properities of CHD proteins *in vitro* (Bouazoune et al. 2002, Kreher et al. 2017, Murawska et al. 2008, Brehm

et al. 2000.). Previously, dMi-2 was used in our lab as a model to study its role in development and differentiation (Murawska et al. 2011, Mathieu et al. 2012, Fasulo et al. 2012, Kim et al. 2017). Therefore, selected point mutations were introduced into dMi-2 and analysed *in vitro* to determine the effects on ATP binding and hydrolysis, nucleosome remodelling, DNA and nucleosome binding. Furthermore, this study investigates the *in vivo* effects of expression of selected mutants in the developing wing of *Drosophila.*

3. Material and Methods

3.1 Material

3.1.1. Material sources

All common chemicals, reagents, instruments, and materials in this study were purchased from the following companies: Abcam, Alexis Biochemicals, AppliChem, Beckmann, BioRad, Calbiochem, Eppendorf, Fermentas, Fisher Scientific, Fujifilm, Gibco, Gilson, GE Healthcare, Greiner, Heraeus, Hartmann Analytic GmbH, Invitrogen, Kobe, Leica, Millipore, Merc, PAA, MWG Biotech, New England Biolabs, PeqLab, Polysciences, Promega, Qiagen, Roche, Roth, Santa Cruz Biotechnology, Sarstedt AG, Sigma, Stratagene, Thermo Scientific Inc., Whatman, Zeiss.

3.1.1.1. Enzymes

Fast AP Thermosensitive alkaline phosphatase	Thermo Scientific
Restriction endonucleases	Thermo Scientific, NEB
Micrococcal Nuclease (Nuclease S7)	Roche
Taq DNA Polymerase	Thermo Scientific
T4 DNA ligase	Thermo Scientific
RNAse A	Qiagen
Proteinase K	Roth
RedTaq DNA polymerase	Sigma
Phusion polymerase HT II	Thermo Scientific

3.1.1.2. Enzyme inhibitors

Aprotinin	Roth
Leupeptin	Roth

Pepstatin	Roth
PMSF (phenyl-methane-sulfonyl-fluoride)	Roth

3.1.1.3. Chromatographic material

Hydroxyl apatite resin	Biorad
Chromatography system (ÄKTA, HPLC, FPLC)	Amersham
Econ-Pac Chromatography columns	Bio-Rad
TLC PEI Cellulose F	Millipore

3.1.1.4. Affinity purification material

M2 Agarose (FLAG beads)

3.1.1.5. Dialysis and filtration material

Dialysis membranes	Spectra/Por
Sterile syringe filters	VWR
Cellulose nitrate filter	Sartorius
Filtropur bottle top filters	Sarstedt
Slide-A-Lyzer Dialysis Cassettes	Thermo Scientific
Amicon Ultra-15 Centrifugal filter units	Milipore
Amicon Ultra-0,5mL Centrifugal filter units	Milipore

3.1.1.6. Consumable material

APS (ammonium persulfate)	Merck
6x DNA Loading Dye	Thermo Scientific
GeneRuller 1kb DNA Ladder Plus	Thermo Scietific
GeneRuller 100 bp DNA Ladder	Thermo Scientific
TEMED (tetramethyl-ethylene diamine)	Roth
PageRuler Prestained Protein Ladder	Thermo Scientific
Rotiphorese Gel 30	Roth
Rotiphorese Gel 40	Roth

Ethidium Bromide	Roth
SyBr Gold	Thermo Scientific
Protein Assay (Bradford solution)	Bio-Rad
Whatman 3MM paper	Whatman
Safety-Multifly-Needle	Sarstedt
Ultracentrifuge tube	Nalgene
PVDF membrane	Roth
SuperRX Fuji Medical X-ray films	Fuji

3.1.1.7. Radioactive material

(γ-^{32}P)-ATP	Hartmann Analytic
(α-^{32}P)-dCTP	Hartmann Analytic

3.1.1.8. Kits

Table 3.1: List of kits used in this study, their corresponding application and company

Kit	Application	Company
QuikChange II Site-Directed Mutagenesis Kit	Site-directed mutagenesis	Agilent Technologies
Bac-to-Bac Baculovirus Expression system	Transfection of Sf9 cell for production of baculoviruses	Life Technologies
QIAquick PCR purification kit	DNA purification after PCR	Qiagen
QIAquick Gel Extraction kit	DNA purification from agarose gels	Qiagen
Maxiprep kit	Purification of large scale plasmid preps	Qiagen
Gateway LR Clonase II Enzyme mix	Cloning	Invitrogen
pENTR Directional Topo cloning kit	Cloning	Invitrogen

Kit	Application	Company
Immobilon Western Chemiluminescent HRP Substrate Kit	Detection of proteins on PVDF membrane using chemiluminescence	Millipore

3.1.2. Standard solutions and buffers

Buffers and stock solutions were prepared according to standard protocols. Additional buffers are described in Methods section.

Phosphate Buffered Saline (PBS)	140mM NaCl 2,7mM KCl 8,1mM Na2HPO4 1,5mMKH2PO4 pH adjusted to 7,4 with HCl
Tris-EDTA (TE)	10mM Tris-HCl, pH8 1mM EDTA
TBE buffer	90mM Tris 90mM Boric Acid 2mM EDTA
SDS-running buffer	192mM Glycin 25mM Tris 0,1% (w/v) SDS

3.1.3. Plasmids

Table 3.2. Plasmids used for baculovirus generation and protein expression in Sf9 cells.

Numbers in plasmid name indicate position of mutated amino acid residue.

Construct name	Description	Source
pFastBacDual-dMi-2_WT-FLAG	Full length wild type dMi-2 with C-terminal FLAG tag for generation of recombinant baculovirus	Ulla Kopiniak
pFastBacDual-dMi-2_C452Y-FLAG	Full length dMi-2 with cytosine at position 452 mutated to tyrosine with C-terminal FLAG tag for generation of recombinant baculovirus	This study
pFastBacDual-dMi-2_V538F-FLAG	Full length dMi-2 with valine at position 538 mutated to phenylalanine with C-terminal FLAG tag for generation of recombinant baculovirus	This study
pFastBacDual-dMi-2_R552Q-FLAG	Full length dMi-2 with arginine at position 552 mutated to glutamine with C-terminal FLAG tag for generation of recombinant baculovirus	This study
pFastBacDual-dMi-2_L914V-FLAG	Full length dMi-2 with leucine at position 914 mutated to valine with C-terminal FLAG tag for generation of recombinant baculovirus	This study
pFastBacDual-dMi-2_R1164Q-FLAG	Full length dMi-2 with arginine at position 1164 mutated to glutamine with C-terminal FLAG tag for generation of recombinant baculovirus	This study
pFastBacDual-dMi-2_H1153R-FLAG	Full length dMi-2 with histidine at position 1153 mutated to arginine with C-terminal FLAG tag for generation of recombinant baculovirus	This study
pFastBacDual-dMi-2_H1198Y-FLAG	Full length dMi-2 with histidine at position 1198 mutated to tyrosine with C-terminal FLAG tag for generation of recombinant baculovirus	This study
pFastBacDual-dMi-2_L1217P-FLAG	Full length dMi-2 with leucine at position 1217 mutated to proline with C-terminal FLAG tag for generation of recombinant baculovirus	This study

Table 3.3. Plasmids used for generation of transgenic flies

Numbers in plasmid name indicate position in mutated amino acid residue

Plasmid	Description	Source
pUASt-attB-dMi-2_WT-FLAG	Full length wild type dMi-2 with C-terminal FLAG tag for generation of UAS transgenic flies	This study
pUASt-attB-dMi-2_C452Y-FLAG	Full length dMi-2 with cytosine at position 452 mutated to tyrosine with C-terminal FLAG tag for generation of UAS transgenic flies	This study
pUASt-attB-dMi-2_R1164Q-FLAG	Full length dMi-2 with arginine at position 1164 mutated to glutamine with C-terminal FLAG tag for generation of UAS transgenic flies	This study
pUASt-attB-dMi-2_H1153R-FLAG	Full length dMi-2 with histidine at position 1153 mutated to arginine with C-terminal FLAG tag for generation of UAS transgenic flies	This study
pUASt-attB-dMi-2_H1198Y-FLAG	Full length dMi-2 with histidine at position 1198 mutated to tyrosine with C-terminal FLAG tag for generation of UAS transgenic flies	This study
pUASt-attB-dMi-2_L1217P-FLAG	Full length dMi-2 with leucine at position 1217 mutated to proline with C-terminal FLAG tag for generation of UAS transgenic flies	This study

Table 3.4 Other plasmids used in this study

Plasmid	Description	Source
pUC12x601	Contains 12 nucleosome positioning sequences (601). Used for assembly of nucleosome arrays.	G. Längst

Plasmid	Description	Source
pUC1x601	Contains 1 nucleosome positioning sequence (601). Used for assembly of mononucleosomes.	G. Längst
pFastBacDual	Baculovirus transfer vector used for generation of recombinant baculoviruses	Life Technologies
pUASt-attB	Integration vector for Gal4/UAS mediated expression of transgenes. Attachment *attB* site in the plasmid is recognised by ϕC31 integrase, that integrates construct into the *attP* site in transgenic fly genome. It carries *lacZ* reporter and white^{+} marker gene and ampicilin resistance	H. Jäckle, Generated by Basler lab (Bischof et al. 2007)

3.1.4. Oligonucleotides

Oligonucleotides used in this study were purchased from Eurofins MWG Operon and diluted to final concentration of 100μM with nuclease-free water.

3.1.4.1. Oligonucleotides for site-directed mutagenesis

Table 3.5. Oligonucleotides used for site-directed mutagenesis. Mutated bases are indicated in bold, numbers in oligonucleotide name indicate the position of mutated amino acid position.

Oligo name	Sequence (5'>3')
dMi-2_C452Y_fwd	TTGCTGTGCTACGACTCATGTCCCTCC
dMi-2_C452Y_rev	GGAGGGACATGAGTCGTAGCACAGCAA
dMi-2_V538F_fwd	TGCGAATGGTTCCCCGAAGTGCAACTGGAC
dMi-2_V538F_rev	GTCCAGTTGCACTTCGGGGAACCATTCGCA
dMi-2_R552Q_fwd	CTCATGATTCAGTCGTTCCAGCGCAAG
dMi-2_R552Q_rev	CTTGCGCTGGAACGACTGAATCATGAG
dMi-2_L914V_fwd	CTCGAGGAGGTGTTCCATCTGCTCAACTTC
dMi-2_L914V_rev	GAAGTTGAGCAGATGGAACACCTCCTCGAG
dMi-2_H1153R_fwd	AATCCCCGAAACGATATTCAGGCC

Oligo name	Sequence (5'>3')
dMi-2_H1153R_rev	GGCCTGAATATCGTTTCGGGGATT
dMi-2_R1164Q_fwd	CTTCTCCCGAGCCCATCAGATTGGCCAGGCT AACAA
dMi-2_R1164Q_rev	TTGTTAGCCTGGCCAATCTGATGGGCTCGGG AGAAG
dMi-2_H1198Y_fwd	CGTAAGATGATGTTGACTTATCTTGTGGTCC
dMi-2_H1198Y_rev	GGACCACAAGATAAGTCAACATCATCTTACG
dMi-2_L1217P_fwd	TTT ACA AAG CAA GAA CCG GAC GAT ATC CTT CGT
dMi-2_L1217P_rev	ACG AAG GAT ATC GTC CGG TTC TTG CTT TGT AAA

3.1.4.2. Oligonucleotides for sequencing

Table 3.6. Oligonucleotides used for sequencing of dMi-2 and dMi-2 mutants.

Oligo name	Sequence (5'>3')
fwd1_dMi-2	TGGCATCGGAGGAAGAGAAT
fwd2_dMi-2	CAGTGTGACAGGCGATGAG
fwd3_dMi-2	AGAGGGCAAGTGGTCGTG
fwd4_dMi-2	CGACACAAGGACAAGGTTGG
fwd5_dMi-2	GCATTAACTGGTTGCGCTAC
fwd6_dMi-2	GCTGCAACCATCCGTATCTC
fwd7_dMi-2	CTCATCTTGTGGTCCGTCC
fwd8_dMi-2	CCTCAATGCCATTATGCGGT
fwd9_dMi-2	GCGAGGTGAAGCAAGAACAA
fwd10_dMi-2	GCATCTGAGCAAGGAATCGC
rev1_dMi-2	CTAGCTTTGGTGCCGCAATC
rev2_dMi-2	CTCCGGGAAGTTCTTCGTTT
rev3_dMi-2	CCGCCACATCCTGTTTCAG

3.1.4.3. Oligonucleotides for mononucleosome assembly DNA fragment

Table 3.7. Oligonucleotides used to generate DNA fragments for mononucleosome assembly.

Oligo name	Sequence (5'>3')
601_147_fwd	ctggagaatcccggtgcc
+80_601rev	tcggtacccggggatcc
0-77fwd	gat cca gaa tcc tgg tgc tga g
0-77rev	gta cag aga ggg aga gtc aca aaa c
77-77fwd	atc ttt tga ggt ccg gtt ctt t
77-77rev	gta cag aga ggg aga gtc aca aaa c

3.1.4.3. Other oligonucleotides

Table 3.8. Other oligonucleotides used in this study

Oligo name	Sequence (5'>3')
attB1-dMi-2-fwd	caccatggcatcggaggaagagaatg
attB2-dMi-2-rev	ctacttgtcatcgtcgtccttgtagtcgacg

3.1.5. Baculoviruses

Table 3.9. Baculoviruses used for protein expression in Sf9 cells

dMi-2_WT-FLAG	Full length wild type dMi-2 with C-terminal FLAG tag
dMi-2_C452Y-FLAG	Full length dMi-2 with cytosine at position 452 mutated to tyrosine with C-terminal FLAG tag
dMi-2_V538F-FLAG	Full length dMi-2 with valine at position 538 mutated to phenylalanine with C-terminal FLAG tag
dMi-2_R552Q-FLAG	Full length dMi-2 with arginine at position 552 mutated to glutamine with C-terminal FLAG tag

dMi-2_L914V-FLAG	Full length dMi-2 with leucine at position 914 mutated to valine with C-terminal FLAG tag
dMi-2_R1164Q-FLAG	Full length dMi-2 with arginine at position 1164 mutated to glutamine with C-terminal FLAG tag
dMi-2_H1153R-FLAG	Full length dMi-2 with histidine at position 1153 mutated to arginine with C-terminal FLAG tag
dMi-2_H1198Y-FLAG	Full length dMi-2 with histidine at position 1198 mutated to tyrosine with C-terminal FLAG tag
dMi-2_L1217P-FLAG	Full length dMi-2 with leucine at position 1217 mutated to proline with C-terminal FLAG tag

3.1.6. Cell lines and tissue culture

Sf9 - cell line established from *Spodoptera frugiperda* ovaries used for recombinant protein expression in Baculovirus system (Vaughn et al. 1977). Sf9 cells were cultured in Sf-900 II SFM media (Life Technologies), supplemented with 10% (v/v) FBS (Hyclone) and 1% of Penicillin/Streptomycin (10mg/mL) (PAA). Cells were kept in the incubator at 26°C.

3.1.7. Bacteria strains and culture media

Escherichia coli strain **XL1-Blue** was used for cloning and plasmid DNA amplification. Genotype: recA1 endA1 gyrA96 thi-1 hsdR17 supE44 relA1 lac [F´ proAB lacIqZΔM15 Tn10 (Tetr)]

Escherichia coli strain **DH10 Bac** was used for recombination of FastBac plasmid DNA to bacmid. Genotype: F– mcrA Δ(mrr-hsdRMS-mcrBC) ϕ80lacZΔM15 ΔlacX74 recA1 endA1 araD139 Δ(ara, leu)7697galUgalKλ– rpsLnupG/bMON14272/pMON7124

Escherichia coli strain **XL-Gold** was used for transformation of plasmids generated by site-directed mutagenesis. Genotype: Tet^{r}Δ(mcrA)183 Δ(mcrCB-hsdSMR-mrr)173 endA1 supE44 thi-1 recA1 gyrA96 relA1 lac Hte [F´ proAB lacI^{q}ZΔM15 Tn10 (Tet^r) Amy Cam^r]

Escherichia coli strain **One shot TOP 10** was used for production of entry vector for Gateway system. Genotype: F- mcrA Δ(mrr-hsdRMS-mcrBC) ϕ80lacZΔM15 ΔlacX74 recA1 araD139 Δ(ara- leu)7697 galU galK rpsL (Str^R) endA1 nupG

Escherichia coli strain **NEB 5**α was used to transforamtion of LR recombination reaction for production of pUAST_attB_rf destination vectors. Genotype: fhuA2 (argF-lacZ)U169 phoA glnV44 80 (lacZ)M15 gyrA96 recA1 relA1 endA1 thi-1 hsdR17

3.1.7.1. Culture media

LB Medium (Luria Bertani)	1% (w/v) Tryptone 0,5% (w/v) Yeast extract 1% NaCl
Agar plates	1,5% (w/v) Agar LB medium

3.1.7.2. Antibiotics, selection markers, and inducers

Table 3.10. Antibiotics used for selection, X-gal in blue/white screening and IPTG as the inducer in LB agar plates and/or LB media in indicated concentrations.

Antibiotic/selection markers/reagent	Concentration (μg/mL)
Ampicilin	100
Gentamycin	7
Kanamycin	50
Tetracyclin	10
X-gal (5-bromo-4-chloro-3-indolyl-β-D-galactopyranoside)	100
IPTG (Isopropylthio-β-galactoside)	40

3.1.8. Fly strains

Fly stocks were maintained at room temperature and all crosses were kept at 26°C in a fly incubator. Fly stocks were sustained on standard food as described in Kunert and Brehm, (2008).

Table 3.11. Fly strains used in this study

Name	Description and genotype	Source
UAS_dMi-2_WT-FLAG	Transgenic fly line carrying UAS_dMi-2_WT, inserted at 3rd chromosome. w(-);;dMi-2_WT/ dMi-2_WT	This study
UAS_dMi-2_C452Y-FLAG	Transgenic fly line carrying UAS_dMi-2_C452Y, inserted at 3rd chromosome. w(-);;dMi-2_C452Y/ dMi-2_C452Y	This study
UAS_dMi-2_H1153R-FLAG	Transgenic fly line carrying UAS_dMi-2_H1153R, inserted at 3rd chromosome. w(-);;dMi-2_H1153R/ dMi-2_H1153R	This study
UAS_dMi-2_R1164Q-FLAG	Transgenic fly line carrying UAS_dMi-2_R1164Q, inserted at 3rd chromosome. w(-);;dMi-2_R1164Q/ dMi-2_R1164Q	This study
UAS_dMi-2_H1198Y-FLAG	Transgenic fly line carrying UAS_dMi-2_H1198Y, inserted at 3rd chromosome. w(-);;dMi-2_H1198Y/ dMi-2_H1198Y	This study
UAS_dMi-2_L1217P-FLAG	Transgenic fly line carrying UAS_dMi-2_L1217P, inserted at 3rd chromosome. w(-);;dMi-2_L1217P/ dMi-2_L1217P	This study
GAL4-engrailed	P(engrailed), GAL4 expression in posterior part of fly wing	Bloomington
w^{1118}	Isogenic strain	Bloomington
OrR	Oregon R wild type flies	P. Becker

3.2. Methods

3.2.1. Cell biological methods

3.2.1.1. General tissue culture procedures

Sf9 cells were propagated in T75 flask (Sarstedt/Greiner) at 26°C in Sf-900 II SFM media supplemented with 10% FBS and 1% Penicillin/Streptomycin (see 3.1.6.). Every three to four days cells were removed using cell scraper and split by diluting with fresh media to approx. $2x10^6$ cells/ml. Cell number was determined using hemocytometer. Collection of cells for experiments was done at 1000rpm for 5 minutes (Heraeus Megafuge 1.0).

3.2.1.2. Freezing and thawing the cells

For freezing, cells were collected from a dense flask, spun down and resuspended in 1mL of media containing 80% of supplemented Sf-900 II SFM media, 10% FBS and 10 % DMSO. Cells were transferred to cryovial and frozen in 50 mL Falcon tube which contained 100% isopropanol. Isopropanol ensures freezing rate of approximately -1°C/min and ensures viability of the cells. Cells are stored at -80°C.

For thawing, cells were transferred from -80 to RT. When thawed, cells were transferred to 15 mL Falcon and resuspended in approx. 10 mL fresh media, pelleted with centrifugation, media containing DMSO was removed and 15mL fresh media was added. Cells were seeded in the $75cm^2$ flask. After 24h media was exchanged.

3.2.2. Molecular biological methods

Standard molecular biology techniques such as plasmid DNA transformation into chemically-competent *E.coli*, amplification and purification of plasmid DNA from *E.coli*, digestion of plasmid DNA using restriction endonucleases, dephosphorylation of DNA, ligation of DNA, determination of DNA concentration and analysis of DNA on TBE or TAE agarose gels were carried out according to

standard protocols and manufacturer's instructions (Thermo Scientific, Sambrook and Russell, 2001).

Small-scale plasmid DNA preparation was performed using P1(resuspension), P2 (lysis) and P3 (neutralisation) buffers from QIAGEN. Shortly, bacteria were resuspended in P1 buffer containing RNase. Alkaline lysis was performed with P2 containing SDS and NaOH and P3 containing potassium acetate for neutralisation. DNA was precipitated using isopropanol according to the standard protocol. For large scale plasmid DNA preparation QIAGEN Plasmid Maxi Kit was used and DNA was precipitated using isopropanol according to the standard protocol.

3.2.2.1. PCR for site-directed mutagenesis

To introduce specific changes into a DNA sequence, site-directed mutagenesis was performed using the Quick Change Site-directed Mutagenesis Kit (Agilent Technologies) according to the manufacturer's instructions. A general PCR reaction of 50μL was set up as follows:

5μL	10x Reaction buffer
1μL	dNTP's
1μL	Forward Primer (125ng)
1μL	Reverse Primer (125 ng)
1μL	plasmid DNA (100ng)
1,5μL	Quick solution buffer
0,50μL	PfuUltra HF DNA Polymerase
39μL	H_2O

A general PCR reaction was incubated in a T3000 Thermocycler (Biometra) with the following programme:

Initial Denaturation	95°C	3min 30sec	
Denaturation	95°C	20 sec	18 cycles
Annealing	60°C	10sec	
Elongation	68°C	1min/kb	
Final elongation	68°C	7min	

3.2.2.2. Genomic DNA isolation from flies

Fly genomic DNA was isolated from 30-40 transgenic flies. Flies were ground in 200μL of extraction buffer in 1,5mL Eppendorf tube with an eppi pestle for 1 minute, after which additional 200μL of extraction buffer was added to the solution and flies were ground until well homogenized. Additional 600μL of extraction buffer was added to the solution and incubated at 65°C for 30 minutes. The solution was left to cool down to room temperature and 200μL of 8M potassium acetate was added to the reaction, mixed and left to incubate on ice for 10 minutes. The reaction was pelleted with centrifugation at 13 000 rpm in table-top centrifuge for 15 minutes at room temperature. The supernatant was transferred to the 2mL tube and RNase A was added to digest any residual RNA, incubation was done for 10 minutes on ice. 600μL of isopropanol was added to the solution and mixed by tilting. The solution was centrifuged for 30 minutes at 13000 rpm at 4°C. The supernatant was discarded and the pellet was washed with 70% Ethanol and centrifuged for 20 minutes at 13000 rpm. Supernatant was discarded, the pellet was dried at room temperature and dissolved in 100μL of nuclease-free H_2O.

Extraction buffer	100mM Tris, pH 7,5
	100mM EDTA
	100mM KCl
	0,5% SDS

3.2.3. Protein biochemistry methods

Protein aliquotes were kept on ice in presence of protease inhibitors - Leupeptin, Aprotinin, Pepstatin A (1μg/mL), PMSF (0,2mM) and DTT (1mM) as a reducing agent. All buffers were freshly supplemented with protease inhibitors before the start of the experiment. Critical steps were performed in the cold room at 4°C.

3.2.3.1. Whole cell extract from Sf9 cells

Whole cell extract was prepared 72 hours post baculovirus infection. Cells were collected, centrifuged and washed with cold 1xPBS. The pellet was resuspended in 1mL LyBu200 per 15cm plate. Cells were lysed by three freeze-thaw cycles in liquid nitrogen, after which cell extracts were centrifuged at 13000rpm for 30 minutes at 4°C. Supernatant containing protein extract was transfered to 15mL Falcon tubes, frozen in liquid N_2 and stored at -80°C until purification.

LyBuX buffer	20mM HEPES KOH, pH 7,6
	X mM KCl
	10% Glycerol (v/v)
	0,1% NP-40
	+DTT, protease inhibitors (added freshly)

3.2.3.2. FLAG affinity purification

For FLAG affinity purification of dMi-2_WT-FLAG and dMi-2-FLAG mutants whole cell extract was prepared as described in 3.2.3.1. α-FLAG M2 agarose beads (Sigma Aldrich) were equilibrated by washing three times in LyBu200. 50μL of FLAG beads per 1mL of whole cell extract were used and incubated for 4 hours on a rotating wheel. Beads were collected by centrifugation at 1000rpm for 2 minutes at 4°C. Beads were washed over 10mL Econ-Pac Chromatography columns (Bio-Rad) with LyBu buffers with increasing salt

concentration to remove unbound proteins and then with decreasing salt concentration, in the following order:

2 x 10 mL of LyBu500
2 x 10 mL of LyBu1000
1 x 10 mL of LyBu500
1 x 10 mL of LyBu200
1 x 10 mL Lybu150
1 x 10 ml elution buffer

Proteins were eluted three times with elution buffer (1:1 elution buffer:beads) supplemented with Flag peptide to the final concentration of 250ng/μL after 10 minutes incubation. Eluted proteins were subjected to SDS-PAGE electrophoresis. All washing steps and elutions from the column were performed in the cold room.

Elution buffer	20mM Tris pH 7,6
	150mM KCl
	10% Glycerol (v/v)
	+DTT, protease inhibitors (added freshly)

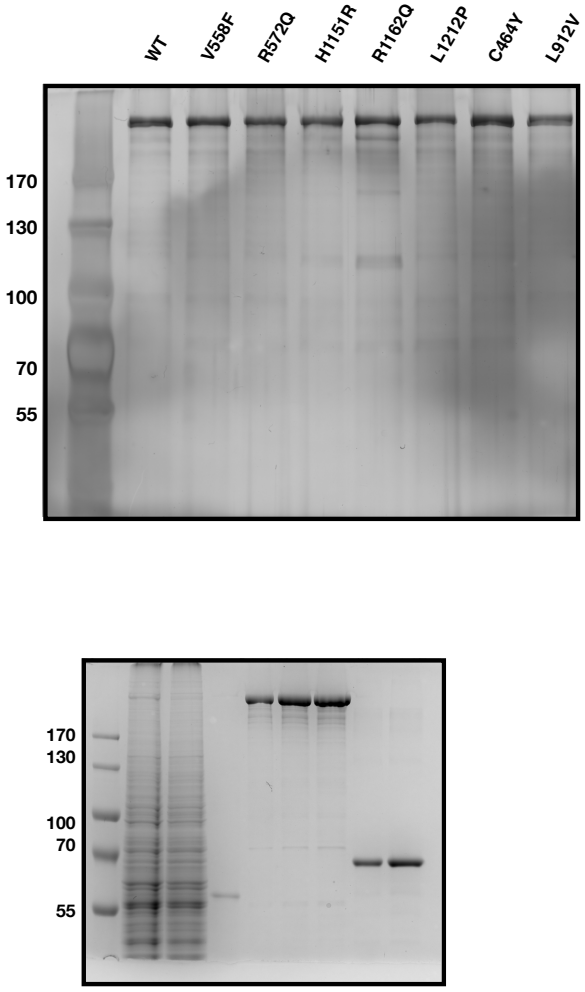

Figure 3.1. Elution profiles of immunopurified mutants and WT dMi-2

Proteins are resolved on 8% SDS PAGE gel. Silver stain gel showing 1μg immunopurified FLAG-tagged *Drosophila melanogaster* WT protein and point mutants(upper panel) and Coomassie Brilliant Blue stained gel showing immunopurified FLAG-tagged H1196Y point mutant (lane 1 - input 1%, lane 2 - flowthrough 1%, lane 3 - beads 1%, lane 4 - 1μL eluate, lane 5 - 2μL eluate, lane 6 - 3μL eluate, lane 7 - 1μg BSA, lane 8 - 2μL BSA) (lower panel)

3.2.3.3. Determination of protein concentration

Protein concentration of purified recombinant dMi-2 proteins was determined using Bio-Rad Protein assay (Bio-Rad) which is based on a colorimetric assay described by Bradford (Bradford, 1976). Protein aliquots were compared to a protein standard of known concentration (BSA) and run on the SDS-PAGE gel, afterwards stained with Coomassie brilliant blue and quantified using ImageJ software (Ferreira and Rasband, 2012).

3.2.3.4. SDS-polyacrylamide gel electrophoresis

SDS-PAGE is a method used to qualitatively analyse proteins and protein mixtures. It can be used to asses purity of purified proteins and, since the method is based on separating proteins by size, it can be applied to assess the apparent molecular mass of the protein. SDS-polyacrylamide gels were prepared using disposable pre-assembled gel cassettes and gels were run in the XCell Sure Lock Mini-Cell Electrophoresis system (Thermo Scientific). Stacking and resolving gels were prepared with a ready-to-use acrylamide-bisacrylamide mix (Rotiphoresegel 30, 37.5:1; Roth) and prepared according to the manufacturer's instructions. The stacking gel contained 4% and resolving gel contained 8%, 15% or 18% polyacrylamide, depending on the analysed protein. Protein samples were mixed with 1xSDS loading buffer, incubated for 5 minutes at 95°C, cooled shortly on ice and loaded onto the gel. Electrophoresis was performed in SDS running buffer at 100V until the dye reached the resolving gel, after which the voltage was increased to 150V and electrophoresis was stopped when the dye reached the end of the gel. To monitor proper separation through the gel, PageRuler Prestained Protein Ladder (Thermo Scientific) was loaded next to the sample of interest. After electrophoresis, the gel was stained with Coomassie Brilliant Blue or subjected to Western blot.

3.2.3.5. Coomassie Brilliant Blue staining of the protein gels

Visualisation of proteins from polyacrylamide gels was done using Coomassie Brilliant Blue staining solution. Gels were incubated on a shaker overnight. Gels were destained using destaining solution, until protein bands were visible.

Coomassie Brilliant Blue staining solution	50% (v/v) Methanol 10% (v/v) Acetic Acid 0,1% (w/v) Coomassie Brilliant Blue R-250
Destaining solution	50% (v/v) Methanol 10% (v/v) Methanol

3.2.3.6. Western blot

Western blot is a method used to transfer proteins from gels and to immobilise them on a membrane, thereby maintaining the high resolution of the protein pattern on the membrane. When on the membrane, proteins are easily probed with antibodies which allows detection of specific proteins.

Proteins were separated using SDS-PAGE (3.2.3.4.) and transferred to polyvinylidene difluoride membrane (PVDF), that was, prior to use, activated in methanol. The membrane was placed over the gel and stacked between 4 Whatman-3M papers soaked in transfer buffer. Proteins were then transferred to PVDF membrane in a Wet Blot Module (Biorad) at 400mA for 1 hour and 15 minutes. The chamber was kept cold with an ice block inside and was surrounded with ice to provide further cooling from the outside. After transfer, the membrane was placed in blocking solution (5% milk powder in PBSt) for 1 hour to reduce non-specific binding of the antibody to the proteins on the membrane. After the blocking stage, the membrane was transferred to the appropriate dilution of the primary antibody and incubated overnight in the cold room or 2 hours at room temperature. Following the incubation with primary antibody, the membrane was washed 3 times in PBSt for 5 minutes at room

temperature and placed for incubation with appropriate HRP-labelled secondary antibody for two hours at room temperature. The membrane was washed again 3 times for 5 minutes in PBSt and antibody-antigen complex was detected by chemiluminescence using Immobilon Western Chemiluminescent HRP Substrate Kit (Millipore) and SuperRX Fuji Medical X-ray films. Exposure time differed for different antibodies.

Transfer buffer	192 mM Glycin
	24 mM Tris
	20% methanol
	0,02% SDS
PBSt	1xPBS
	0,1% Tween 20%

3.2.3.7. Non-denaturating-polyacrylamide gel electrophoresis

In order to analyse interactions between dMi-2 and nucleic acids or nucleosomes, nondenaturating polyacrylamide gels in absence of SDS were used. This way biological activity of proteins is preserved and can be visualised on the gel. In general for 100 mL 5% polyacrylamide native gels the following components were used:

12,5 mL	polyacrylamide mix (Rotiphoresegel 40, 29:1; Roth)
5mL	10xTBE
1mL	10%APS
50μL	TEMED
81,45mL	H_2O

Gels were prerun with 1x GelPilot Loading dye to monitor color separation for at least 30 minutes at 90V. Samples were loaded on the gel and run in 0,5XTBE buffer between 90-120V until the bromphenol blue dye reached 75% of the gel.

Following electrophoresis gels were stained with ethidium bromide or SyBr Gold reagent to visualise DNA or nucleosomes. In case of the radioactively labelled nucleosome, gels were dried and exposed to a Phosphoimager screen.

3.2.3.8. Recombinant protein expression using the Baculovirus Expression system

The Baculovirus expression system is very useful for expression and purification of recombinant eukaryotic proteins of large sizes. Unlike bacterial systems, the baculovirus system has higher size limit and in most cases ensures soluble, properly folded and functionally active protein. The coding sequence of dMi-2-WT was cloned in the FastBacDual vector and used for generation of point mutants by site-directed mutagenesis (3.2.2.1).

3.2.3.8.1. Bac-to-Bac Baculovirus Expression system

pFastBacDual containing dMi-2 WT or an dMi-2 mutant was transformed into DH10 Bac *E.coli* cells. These cells contain a bacmid with the mini-*att*Tn7 site in the sequence of LacZα, that functions as an attachment site for mini Tn7 element from FastBacDual. This transposition results in recombinant bacmid. Successful integration of the mini Tn7 element from plasmid to bacmid is confirmed by blue-white screening and by PCR according to manufacturer's instructions. $1x10^6$ of Sf9 cells were seeded in 6-well plates and left to settle for 20 min at 26°C. Meanwhile, the transfection mix was prepared in the following way: 500-1000ng of bacmid DNA (5μL volume) was diluted in 100μL of unsupplemented Sf-900 II SFM medium. 8μL of Cellfectin reagent (Thermo Scientific) was combined with 100μL of unsupplemented Sf-900 II SFM medium. This mixture was vortexed, then mixed with previously prepared bacmid DNA and incubated for 30 min at room temperature. After incubation, transfection mix (210μL) was added to the cells in a dropwise manner. Cells were left to incubate for 24h at 26°C. On the next day, transfection media was removed and replaced with supplemented (10% FBS, 1% Pen/Strep) Sf-900 II SFM. 6-well plate was wrapped with parafilm to prevent evaporation and

incubated at 26°C for 5 days. The medium was collected, centrifuged for 5 min at 1000rpm and the supernatant (P_1) was transferred to a 15mL Falcon tube, which was stored at 4°C.

3.2.3.8.2. Amplification of baculovirus

Virus amplification was performed by infecting Sf9 cells for two consecutive times. The first viral amplification was carried out by seeding 7,5x10^6 Sf9 cells in 5mL supplemented Sf-900 II SFM medium in a 10 cm cell culture dish. Cells were left to settle for 20 minutes, after which 500μL of viral stock was added to the cells in a dropwise manner. Cells were left to incubate on a shaker for 1 hour. Plates were turned by 90° every 15 minutes to ensure proper mixing. Additional 5 mL of supplemented Sf-900 II SFM medium was added to the cells, the plate was wrapped with parafilm and left to incubate for 6-7 days. The medium was collected, centrifuged and the supernatant (P2) was stored at 4°C. The second viral amplification was carried out by seeding 12,5x10^6 Sf9 cells in 7mL of supplemented Sf-900 II SFM medium in a 15 cm cell culture dish and cells were left to settle for 20 minutes. 500μL of P2 viral amplification was added to the cells in a dropwise manner and incubated on a shaker for 1 hour, rotating plates by 90° every 15 minutes. Additional 8mL of media was added to the cells, the plate was wrapped with parafilm and incubated for 6-7 days at 26°C. Medium was collected, centrifuged and supernatant (P3) was stored at 4°C.

3.2.3.8.3. Infection for protein expression

Supernatant from the second viral amplification (P3) was used to infect Sf9 cells for protein expression. The same procedure as for the second viral amplification was used to infect the cells, with the only difference that the cells were collected 72 hours post infection. For large scale infection, in general 30-35 15-cm cell culture dishes were used. Whole cell extracts were prepared as described in 3.2.3.1. and subsequent protein purification was performed as described in 3.2.3.2.

3.2.3.9. ATP binding assay

To determine effects of mutations on the ability of dMi-2 to bind ATP, a filter binding assay was established and performed in presence of ATP radioactively labelled on its γ phosphate ((γ-^{32}P)-ATP., 3000Ci/mmol, 10mCi/mL). A typical reaction was performed in BC100 buffer, containing 90nM dMi-2, 0,25mM $MgCl_2$ and 0,0375μL of (γ-^{32}P)-ATP. Reactions were preincubated for 5 minutes in a waterbath at 26°C before addition of ATP to the reaction mix. ATP was added in 2μL volume in 20mM HEPES. Total reaction volume was 15μL. Reaction was then further incubated for additional 30 min. 2μL from the reaction was spotted on nitrocellulose membrane under vacuum using a vacuum filtration system and washed with approximately 150mL of BC100 buffer to remove unbound ATP. The membrane was left for 30 minutes to dry at room temperature and exposed to a Phosphoimager screen. Quantification of signals was done using Science Lab Image Gauge (FUJIFILM) software. To establish the specificity of the method and to exclude unspecific binding of ATP to protein, unlabelled GTP and ATP were used in competition with radioactive ATP. Difference in radioactive ATP binding was monitored. Protein was incubated with a constant amount of ATP and increasing amounts of unlabelled GTP or ATP. Unlabelled GTP did not have a major effect on the amount of radioactive ATP binding detected, but adding unlabelled ATP showed a clear reduction in binding of radioactive ATP to dMi-2, showing the specificity of the method. (Figure 3.2.).

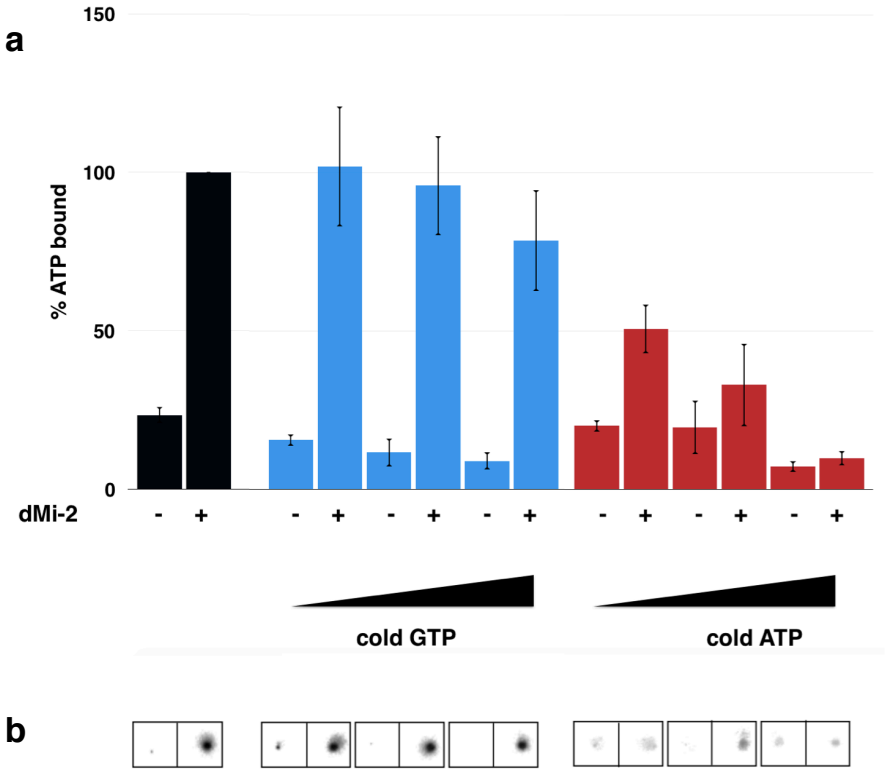

Figure 3.2. Establishing dMi-2 ability to bind ATP using ATP binding assay

(a) Quantification of reactions were performed with (+) or without (-) dMi-2 with only hot ATP (black bars), with hot ATP in competition with increasing amounts of GTP (blue bars) or with hot ATP in competition with cold ATP (red bars). (b) Competition reactions were carried out in presence of (γ-^{32}P)-ATP and exposed to Phosphoimager screen.

3.2.4. Chromatin specific methods

3.2.4.1. Histone octamer isolation from *Drosophila* embryos

In order to provide histones for nucleosome based enzymatic assays, embryos were isolated from *Drosophila* embryos collected 0-12 hours after egg deposition.

3.2.4.1.1. Dechorionation of embryos

Embryos were collected from agar trays and washed with embryo wash buffer (EW - 0.7 % NaCl / 0.04 % Triton -X100) in a measuring cylinder. Depending on the embryo yield up to 100-200 mL of EW buffer was added to the cylinder, usually 1:1 - EW buffer:embryo ratio. In order to dechorionate embryos, 30-60 mL of 12% sodium hypochlorite was added and stirred vigorously for 3 minutes. Embryos were washed with tap water over a fine collection sieve, transferred to a measuring cylinder and washed with EW. Floating chorions were aspirated. Embryos were settled once in EW and once in 0,7% NaCl. The pre-wetted filter paper was set up on the funnel and embryos were poured over the funnel and left to drain, after which they were washed with deionized water. After embryos were nearly dry, they were weighed and transferred to 50mL Falcon tube.

3.2.4.1.2. Histone isolation

All buffers were supplemented with protease inhibitors before use and kept at 4°C or on ice. For histone preparation, 50 g of dechorionated embryos were used. Embryos were resuspended in 40 mL Glycine buffer and homogenised using a Yamamoto homogeniser (1000rpm, 6 strokes, 4°C). After homogenisation, the embryo suspension was filtered through Miracloth filter (Calbiochem) to remove the residual yolk and unhomogenised parts of embryos. The filtered homogenate was then centrifuged for 10 minutes at 8000 rpm at 4°C in a Sorvall RC-5B (HB-4 rotor). The supernatant was discarded and nuclei were resuspended in 50 mL SUC buffer and centrifuged as before. After centrifugation, nuclei were on top of biphasic pellet. They were resuspended again in SUC buffer and spun down as before. Finally, nuclei were resuspended in 60 mL SUC buffer. $CaCl_2$ was added to the solution to a final concentration of 3mM (using a 1M $CaCl_2$ stock) and the entire reaction was warmed up to 26°C in a waterbath for 5 minutes, after which 12500U (166μL) of MNase (50U/μL - Nuclease S7 - Roche) was added for digestion of internucleosomal DNA. Incubation was continued for approximately 20 minutes. During 20 minute period, increase in DNA presence was monitored by Nanodrop, by taking

reaction aliquotes every 5 minutes. The flask was swirled every few minutes to mix the solution. The reaction was stopped with 1200μL of 0,5M EDTA, pH8 and spun down immediately for 10 minutes(8000rpm, 4°C). In order to extract nucleosomal particles, the pellet was resuspended in 12mL 1xTE pH 7,6, 1mM DTT, 0,2mM PMSF and all the protease inhibitors (see 3.1.1.2) and the solution was incubated with rotation for 45 minutes at 4°C. The sample was centrifuged for 30 minutes, at 12000rpm, 4°C. The supernatant which contained nucleosomal particles was kept and salt was adjusted to 0,63M KCl with 2M KCl/100mM K-PO_4 (pH 7,2). Octamer isolation was performed using Chromatography Systems from Amersham (ÄKTA, FPLC, and HPLC) on a hydroxylapatite column which was prepared one day before according to the manufacturer's instructions and let to settle overnight. The column material was washed several times with 0,63M KCl/100mM K-PO_4 (pH 7,2) to remove the fines. Before loading the sample, the column was washed with 3 volumes of 0,63M KCl/100mM K-PO_4 (pH 7,2). The sample was loaded onto the column via a loop (1mL/min), flowthrough (histone H1) was collected and the column was washed overnight with 10 column volumes (300mL) of 0,63M KCl/100mM K-PO_4 (pH 7,2). In the morning, 2M KCl/100mM K-PO_4 (pH 7,2) was used to elute the histones from the column. Elution was monitored at OD 215nm and 1mL fractions were collected. Peak fractions were analysed on an 18% SDS-PAGE gel and stained with Coomassie brilliant blue. Peak fractions containing only histone octamer were pooled together. Chosen peak fractions were concentrated over an Amicon Ultra-15 Centrifugal filter unit (Millipore) according to the manufacturer's instructions. An equal volume of 100% glycerol was added to concentrated fractions and histones were stored at -20°C. Different volumes of histones were loaded on 18% SDS-PAGE gel and analysed by Coomassie blue staining to determine if the pooled histones are in equimolar amounts.

Glycine buffer	15mM HEPES/KOH pH 7,6
	10mM KCl
	5mM $MgCl_2$

	0,05mM EDTA
	0,25mM EGTA
	10% glycerol
Before use add:	1mM DTT
	0,2mM PMSF
	protease inhibitors (see 3.1.1.2)

SUC buffer	15mM HEPES KOH pH 7,6
	10mM KCl
	5mM $MgCl_2$
	0,05mM EDTA
	0,25mM EGTA
	350mM Sucrose
Before use add:	1mM DTT
	0,2mM PMSF
	protease inhibitors (see 3.1.1.2)

100mM K-PO_4	0,2M KH2PO4 and 0,2M K2HPO4 were
	mixed and adjusted to pH 7,2, water
	was added until 100mM

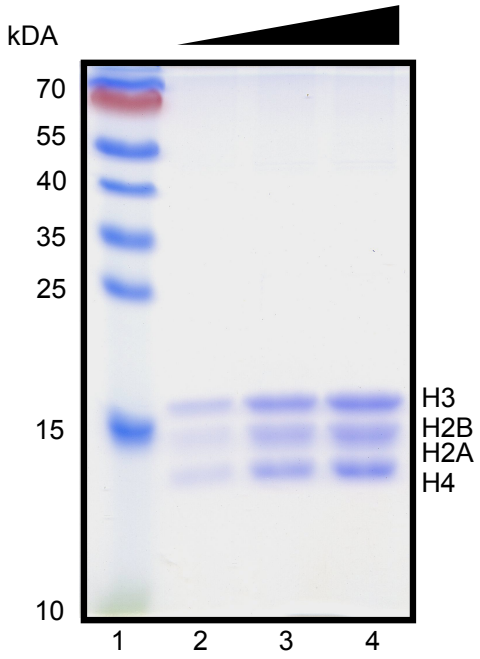

Figure. 3.1. Core histones from Drosophila embryos

Core histones were isolated from Drosophila embryos collected 0-12 hours after egg deposition. Pulled fractions in 50% glycerol were resolved on 18% SDS-PAGE and stained with Coomassie blue. Different volumes were loaded on the gel; Lane 1 - molecular weight marker, lane 2 0,25μL, lane 3 - 0,5μL, lane 4 - 1μL.

3.2.4.2. Nucleosome assembly by salt dialysis

The most common approach for *in vitro* nucleosome assembly is the salt gradient method. This method depends on a tendency of H3-H4 tetramer to bind DNA at higher ionic strength than the H2A-H2B dimer. Core histones are first mixed in 2M salt where ionic strength is too high to form interactions between DNA and histones. By decreasing the salt concentration, and thereby the ionic strength of the mixture, histones are deposited on the DNA in a stepwise manner. First, between 1.2 and 0.85M salt the $(H3\text{-}H4)_2$ tetramer is deposited on the DNA and a tetrasome is formed. H2A-H2B dimers bind progressively as the salt concentration is lowered further and are stably associated in the nucleosome at 0.25M salt. (Wilhelm et al. 1978.). Using this method various kinds on nucleosomes can be assembled, from nucleosomal arrays on a plasmid DNA to single nucleosomes on the linear DNA.

3.2.4.2.1. Polynucleosome assembly by salt dialysis

Polynucleosomes were assembled using plasmid DNA that contains 12 repeats of the 147bp '601' nucleosome positioning sequence. This sequence was identified to have high affinity for histone octamer binding and it gives a stable nucleosome (Lowary and Widom, 1998). In order to generate properly reconstituted nucleosomal arrays, DNA and histones have to be in specific molar ratios, so titration of different DNA:histone ratios was performed. Titration reactions were performed in the lid of a siliconized 1,5mL Eppendorf tube. The bottom of the tube was cut with a hot metal scalpel, the titration reaction was pipetted in the lid and covered with a dialysis membrane that was previously equilibrated in Hi buffer. Tubes were placed in 300mL of Hi buffer in a beaker with a magnetic stirrer and the salt gradient dialysis was performed by continuous addition of Lo Buffer (3L in total) using a peristaltic pump. Dialysis was performed over-night in the cold room. A typical titration assembly reaction contained 5μg of plasmid DNA and varying amounts of histone octamer in a 50μL volume. To estimate the optimal ratio of DNA:histones, increasing amounts of histones were mixed with a constant amount of DNA. Due to the high concentration of histones, a 1:10 dilution of histones was prepared with Hi buffer, to increase pipetting accuracy. After dialysis, polynucleosomes were analysed by Not I digestion. All 12 repeats of '601' sequence have NotI restriction site infront of it. This way it is possible to analyse quality of nucleosome assembly and determine the levels of assembled nucleosomes compared to levels of free DNA and over assembled nucleosomes. For large scale assemblies of approximately 100μg, the estimated histone amount was reduced by 10% to avoid histone precipitation and the DNA concentration was set to 100ng/μL. Large scale assemblies were performed in a dialysis membrane (Spectra/Por) using the same procedure as for a titration. After dialysis, assemblies were centrifuged at 14 000rpm, 2 min, 4°C to remove any precipitate. The concentration was measured using a Nanodrop.

Hi buffer	10mM Tris pH 7,5
	1mM EDTA

	2M KCl
	1mM β-mercaptoethanol
Lo buffer	10mM Tris pH 7,5
	1mM EDTA
	50mM KCl
	1mM β-mercaptoethanol

3.2.4.2.2. Assembly of radioactively labelled mononucleosomes by salt dialysis

Mononucleosomes were assembled on a body labelled ((α-^{32}P)-dCTP), 227bp linear DNA fragment that contained one '601' nucleosome positioning sequence. The 227bp fragment was obtained by PCR from a plasmid cointaining one '601' positioning sequence and an 80bp overhang (+80). A typical PCR reaction of 100μL was set up as follows:

10xTaq Polymerase buffer	10μL
Forward primer (10μM)	2,5μL
Reverse primer (10μM)	2,5μL
dNTP's	2μL
$MgCl_2$ (25mM)	8μL
'601' plasmid (330ng/μL)	0,6μL
(α-^{32}P)-dCTP (>6000Ci/mmol)	0,20μL
Taq DNA Polymerase	0,50μL
H_2O	73,70μL

The PCR reaction was incubated in a T3000 Thermocycler (Biometra) using the following programme:

Initial Denaturation	94°C	3min	
Denaturation	94°C	30 sec	30 cycles
Anneling	51°C	30 sec	
Elongation	72°C	15 sec	
Final elongation	72°C	5min	

Typically, 50 PCRs were performed in parallel to obtain approximately 150μg of DNA. PCR reactions were pooled, purified and concentrated over an Amicon Ultra-15 Centrifugal filter unit (Millipore, 30K MWCO). Approximately 10 unit washes were done with 1xTE to remove residual nucleotides and salts. Finally, DNA was concentrated to a 300μL volume and the DNA concentration was determined by agarose gel electrophoresis (1% agarose) by loading different amounts of DNA and comparing band intensities to a 200bp DNA of known concentration. Quantifications were done using ImageJ software.

In order to estimate the optimal DNA:histone ratio, a titration with a constant DNA amount and varying histone amounts was set up. In general, a titration reaction contained 1μg of radioactively labelled DNA and varying amounts of histones in a 30μL volume. Reactions were pipetted into the lid of a 1,5mL Eppendorf tube as described in 3.2.4.2.1. Step dialysis was performed by placing tubes in 250mL of 2M Hi buffer for 30 minutes, then the salt concentration was reduced to 1M by adding 250mL of 1XTE with β-mercaptoethanol (1mM). Dialysis was continued for 1 hour, after which salt was further reduced to 0,5M by adding 500mL of 1XTE with β-mercaptoethanol (1mM) and dialysis was continued for 1 hour. Finally, salt was reduced to 50mM and dialysis was performed for an additional hour. Samples were collected from the lid of the tube and loaded on a prerun 5% PAA non-denaturating gel. Electrophoresis and analysis of the gel was performed as described in 3.2.3.6. In the example titration shown in Fig. 3.2 the histone:DNA ratio from lane 4 was chosen for the large scale assembly.

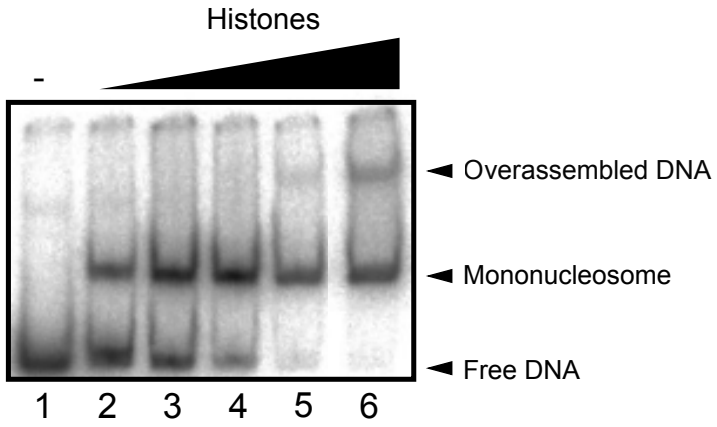

Figure. 3.2. Histone octamer titration for mononucleosome assembly

Increasing amounts of core histones were titrated to a 227bp DNA fragment. 10μL of each titration reaction was separated on a 5% non-denaturating PAA gel and exposed to Phosphoimager screen. Lane 1 - free DNA without histones, lanes 2-6:increasing amounts of histones.

For large mononucleosome assemblies, at least 100μg of DNA was used. The histone amount determined in titration was reduced by 10% to avoid histone precipitation. The reaction was prepared in a 500μL volume, with DNA concentration fixed at 200ng/μL and 2M salt was adjusted using a 2xHi buffer. The reaction was pipetted into a dialysis membrane with 6-8 kDa MWCO (Spectra/Por) or into Slide-A-Lyzer Dialysis Cassettes (Thermo Scientific) with 10kDa MWCO and step dialysis was performed as described for titration assembly. During the last dialysis step, a 10-30% glycerol gradient was generated using an ÄKTA prime (Amersham) and 10% and 30% glycerol gradient buffers (GGB). After dialysis, the assembly was centrifuged at 14 000 rpm, 2 minutes, 4°C to remove any precipitates. The supernatant was then carefully layered on top of the 10-30% glycerol gradient and centrifuged in an ultracentrifuge (Beckman Optima LE-80K (rotor SW40i)) at 35 000 rpm for 18 hours at 4°C to separate mononucleosomes from free DNA and any overassembled nucleosomes.

10/30% Glycerol gradient buffer (GGB)	50mM KCl
	50mM Tris pH 8
	0,1% NP-40
	10/30% glycerol

After centrifugation, fractions of 3-5 drops were collected by puncturing the centrifuge tube using a Safety-Multifly “butterfly” syringe (Sarstedt). Fractions were collected in a 96-well plate. Gradient central fractions are expected to contain mononucleosomes. To determine profile of each fraction and quality of assembly, central fractions were loaded in 3μL volume and resolved over 5% non-denaturating PAA gel. Peak fractions, containing only mononucleosomes, were pooled together and concentrated over Amicon Ultra-0,5mL Centrifugal filter units (Millipore). In order to determine nucleosome concentration, DNA of known concentration and nucleosomes were separated over the 5% PAA gel. Gel was dried, exposed to Phosphoimager and analysed using ImageJ.

3.2.4.2.3. Assembly of non-radioactive mononucleosomes by salt dialysis

In order to analyse possible differences in dMi-2 remodelling, mononucleosomes were assembled using different DNA templates, including a 224bp long DNA fragment with a ‘601’ nucleosome positioning sequence that will give end positioned mononucleosome with a 77bp overhang (0-77) and a 301 bp long DNA fragment with a ‘601’ nucleosome positioning sequence that will give a centrally positioned mononucleosome with 77bp overhang on both sides (77-77). These DNA fragments were a kind gift from G. Längst. In general, DNA and histones were titrated the same way as described in 3.2.4.2.2., Gels were stained with ethidium bromide or Sybr Gold after electrophoresis for 10 minutes and exposed to UV for analysis. Large scale assembly was performed as described in 3.2.4.2.2. except for the ultracentrifugation step, which was omitted in this case. After dialysis, assemblies were centrifuged at 14000rpm for 2 min at 4°C, and the DNA concentration was measured using a Nanodrop.

3.2.4.3. ATPase assay

In order to determine the ATPase activity of dMi-2 WT and mutants thin layer chromatography (TLC) was used. ATPase assays were performed in presence of dMi-2 WT or mutant protein, polynucleosomes and ATP radioactively labelled on its γ phosphate ((γ-^{32}P)-ATP, 3000Ci/mmol, 10mCi/mL). Cold ATP was prepared as 10mM ATP with 30mM $MgCl_2$. A typical reaction was performed in 15μL in BC100 buffer in presence of 200ng polynucleosome array or naked plasmid DNA, varying concentrations of dMi-2, 20μM cold ATP, and 0,075μL (γ-^{32}P)-ATP. Protein dilutions were prepared in BC100 buffer. Reactions were started by pipetting them in previously prepared 2μL of ATP mix (a mixture of hot and cold ATP in 20mM HEPES) that was prewarmed at 26°C for 5 minutes. Reactions were incubated for 30 minutes at 26°C. 1,5μL of each reaction was spotted on a TLC PEI Cellulose plate (Millipore) and dried at room temperature. Hydrolysed phosphate was separated from unhydrolysed ATP in 0,5M LiCl/1M formic acid buffer using thin layer chromatography. Samples were run until the buffer was 1cm from the top of the plate. Plates were dried for 1h at room temperature or 5 minutes at 60°C and exposed to a Phosphoimager screen. Signals for unhydrolysed ATP and hydrolysed phosphate were quantified using Science Lab Image Gauge (FUJIFILM) software. The percentage of hydrolysed ATP was determined using the following calculation:

$$[(\gamma\text{-}^{32}P_{hydrolysed})/(\gamma\text{-}^{32}P_{hydrolysed}+\gamma\text{-}^{32}P_{unhydrolyzed})] \times 100$$

BC100 buffer	20mM HEPES, pH 7,9
	100mM KCl
	0,4mM EDTA
	10% glycerol

3.2.4.4. Restriction enzyme accessibility (REA) assay

The restriction enzyme accessibility assay is a sensitive method of assessing a remodeler's ability to expose a MfeI restriction site at +28bp inside of the '601'

sequence that is revealed upon dMi-2 remodelling. Alternatively, restriction site can also be revealed upon octamer disassembly (Kreher et al. 2017, Narlikar et al. 2001, Bouazoune and Kingston, 2012, Logie and Peterson, 1997). An excess amount of MfeI-HF (MfeI - High Fidelity - New England Biolabs) is used in the assay to ensure that DNA will be cleaved immediately upon remodelling. A typical reaction was performed in 20μL in BC100 buffer, in presence of 20nM of radioactively labelled +80 mononucleosome (3.2.4.2.2.), 114nM of dMi-2, 1,5μL (30U) of MfeI-HF and 2mM/6mM ATP/$MgCl_2$. Protein dilutions were made in BC100 buffer. Reactions containing protein, nucleosomes and MfeI-HF were pippeted and incubated for 5 minutes in a waterbath at 26°C. Reaction was started by transferring entire reaction to 2μL ATP/$MgCl_2$ (from 10mM/30mM ATP/$MgCl_2$ stock). Incubation was continued at 26°C in the waterbath. In order to observe rates of remodelling over time, 4μL aliquots were taken after 5, 10, 20 and 40 minutes. Reactions were stopped by adding the aliquots to 6μL of REA stop mix in separate tubes. Proteinase K was added to an end concentration of 1μg/μL and the entire reaction was incubated at 50°C for 2 hours to digest proteins. After incubation, the reaction was loaded on a 5% non-denaturating PAA gel and subjected to electrophoresis as described in 3.2.3.6. Gels were dried and exposed to a Phosphoimager screen, usually overnight, and quantified using Science Lab Image Gauge (FUJIFILMS) software. The percentage of cut DNA was determined using the following calculation:

[(cut DNA)/(cut DNA+uncut DNA)] x 100

REA stop mix	20mM Tris, pH 7,7
	70mM EDTA
	2%SDS
	10% Glycerol
	1% 6x DNA Loading dye (Thermo Scientific)

3.2.4.5. Nucleosome sliding assay

Nucleosome sliding assays were performed on mononucleosome templates with end-positioned mononucleosome (0-77) and centrally positioned mononucleosome (77-77). A typical reaction was performed in a 10μL volume in BC buffer in presence of varying concentrations of dMi-2, 2mM/6mM ATP/$MgCl_2$ and 150nM of 0-77 or 77-77 nucleosome template. Reactions were preincubated for 5 minutes at 26°C in the waterbath and started by addition of ATP/$MgCl_2$ mix. Reactions were further incubated for 45 minutes, after which they were stopped by addition of competitor plasmid DNA (to compete away the remodeler from the nucleosome) at a final concentration of 180ng/μL and incubated on ice for 10 minutes. 4μL of 50% glycerol was added to the reaction and it was loaded on a 5% non-denaturating PAA gel and run as described in 3.2.3.6. Gels were stained with ethidium bromide or Sybr Gold for 10 minutes and exposed to UV for analysis.

3.2.4.6. Nucleosome or DNA bandshift assay

Nucleosome or DNA bandshift assays were set up and performed under the same conditions as the nucleosome sliding assay, but since the ability of dMi-2 or dMi-2 mutants to bind nucleosomal or free DNA was monitored, ATP and competitor DNA was not added to the reaction. Incubation proceeded at 26°C for 30 minutes and reactions were loaded on a 5% PAA native gel and run at 80V at 4°C. Gels were stained with SyBr Gold or ethidium bromide.

3.2.5. Fly work

3.2.5.1. Generation of dMi-2 WT and mutant transgenic UAS fly lines

Vectors for generation of recombinant UAS flies were generated by pENTR Directional Topo cloning kit (Invitrogen) and Gateway LR Clonase II Enzyme mix (Invitrogen). dMi-2 WT and selected mutants were amplified by PCR from the pFastBacDual vector containing dMi-2 WT or corresponding mutants using attB1 forward and attB2 reverse primers. The attB sequence (bacterial

attachment site) is necessary for successful integration into the attP (phage attachment site) site on the chromosome. Fragments were gel purified and cloned into pENTR d-TOPO vector according to manufacturer's instructions. Successful transformants were cloned into the pUAST-attB-rfa vector using Gateway LR Clonase II Enzyme mix (Invitrogen) according to manufacturer's instructions. For establishing transgenic lines, a ϕ-C31 based integration system was used (Bischof et al. 2007). In this system, bacteriophage ϕ-C31 is ectopically expressed in the germ-line where it mediates site-specific recombination between attB sites on the vector and attP site on the chromosome. Vectors were injected into *Drosophila* strain (y[1] M{vas-int.Dm} ZH-2A w[*]; M{3xP3-RFP.attP}ZH-86Fb) which has an attP site docking site on the 3rd chromosome. The vector contains the *white*$^{+}$ marker gene, that will be expressed upon successful integration of the construct. After injection of vectors into embryos, the F0 generation of flies was crossed with a *w*^{1118} isogenic strain, to make sure the integrase is removed. The F1 generation was screened for orange eyes. Flies with orange eyes were crossed between each other to produce flies with red eyes that are homozygous for the UAS constructs. Successful integration of constructs was confirmed by genomic DNA isolation (3.2.2.2) and sequencing. Injections into embryos were performed in collaboration with Christina Rathke's lab.

3.2.5.2. Ectopic expression of dMi-2 WT and mutants in fly wing

In order to determine potential consequences of selected dMi-2 mutations on cell differentiation, lines carrying UAS constructs were crossed with the *engrailed* driver strain. *Engrailed* (en) encodes a transcription factor that is important for the determination of posterior segments of the *Drosophila* wing (McNeill, 2000). Using this fly strain directs the ectopic expression of dMi-2 WT and mutants to the posterior part of the wing. Virgin female flies were collected from the *engrailed* driver strain and crossed to males from the UAS responder strain. Parental flies were discarded after 3-4 days. About 2 weeks after

crossing, the progeny of the *engrailed*-UAS cross hatched. Changes in the posterior part of the wing were analysed by microscopy.

4. Results

4.1. Biochemical characterisation of cancer derived dMi-2 point mutants

4.1.1. Sequence homology between dMi-2 and hCHD4

In order to investigate the sequence homology levels between dMi-2 and hCHD4 and to determine if cancer affected amino acid residues are conserved between the two proteins, I used the CLUSTAL-Omega protein sequence alignment program. High sequence similarity was found in conserved domains, such as the PHD fingers, chromodomains and the ATPase domain. All affected residues are mostly falling within these highly conserved domains.

A

```
dMi-2      APVSSKADNSAPAAQDDGSGAPVVRKKAKTKIGNKFKKKNKLKKTKNFPEGEDGEHEHQD 378
hCHD4      ASINS-------YSVSDGSTSRSSSRSRK--KLRTT---KKKKKGEEEVTAVDGYETDHQD 371
           * :.*        : .*** :   *.:   *: ..   *:* *  ::.   :. * :***

dMi-2      YCEVCQQGGEIILCDTCPRAYHLVCLEPELDEPPEGKWSCPHCEADGGA----------- 427
hCHD4      YCEVCQQGGEIILCDTCPRAYHMVCLDPDMEKAPEGKWSCPHCEKEGIQWEAKEDNSEGE 431
           **********************:***:*:::: ********** :*
                                              C452Y
dMi-2      --------AEEEDDDEHQEFCRVCKDGGELLCCDSCPSAYHTFCLNPPLDTIPDGDWRCP 479
hCHD4      EILEEVGGDLEEEDDHHMEFCRVCKDGGELLCCDTCPSSYHIHCLNPPLPEIPNGEWLCP 491
                     **:**.* ***************:***:** .******  **:*:* **

dMi-2      RCSCPPLTGKAEKIITWRWAQRSNDD--------GPSTSKGSKNSNSRVREYFIKWHNMS 531
hCHD4      RCTCPALKGKVQKILIWKWGQPPSPTPVPRPPDADPNTPSPKPLEGRPERQFFVKWQGMS 551
           **:** *.**.:**: *:*.*   .          .*.* . .  ..   *::*:**:.**
                 V538F              R552Q
dMi-2      YWHCEWVPEVQLDVHHPLMIRSFQRKYDMEEPPKFEESLDEADTRYKRIQRHKDKVGMKA 591
hCHD4      YWHCSWVSELQLELHCQVMFRNYQRKNDMDEPPSGDFGGDEEKSRKRK----------NK 601
           ****.** *:**::*  :*:*.:*** **:***. : . ** .:* ::          :

dMi-2      NDDAEVLEERFYKNGVKPEWLIVQRVINHRTARDGSTMYLVKWRELPYDKSTWEEEGDDI 651
hCHD4      DPKFAEMEERFYRYGIKPEWMMIHRILNHSVDKKGHVHYLIKWRDLPYDQASWESEDVEI 661
           : .   :*****: *:****:::::*::** . :.* . **:***:****:::**.*. :*

dMi-2      QGLRQAIDYYQDLRAVCTSETTQSRSKKSKKGRKSKLKVEDDEDRPVKHYTPPPEKPTTD 711
hCHD4      QDYDLFKQSYWNHRELMRGEEG-------RPGKKL-------KKVKLRKLERPPETPTVD 707
           *.     : * : * :  .*         : *:*        :.  :::   ***.**.*
```

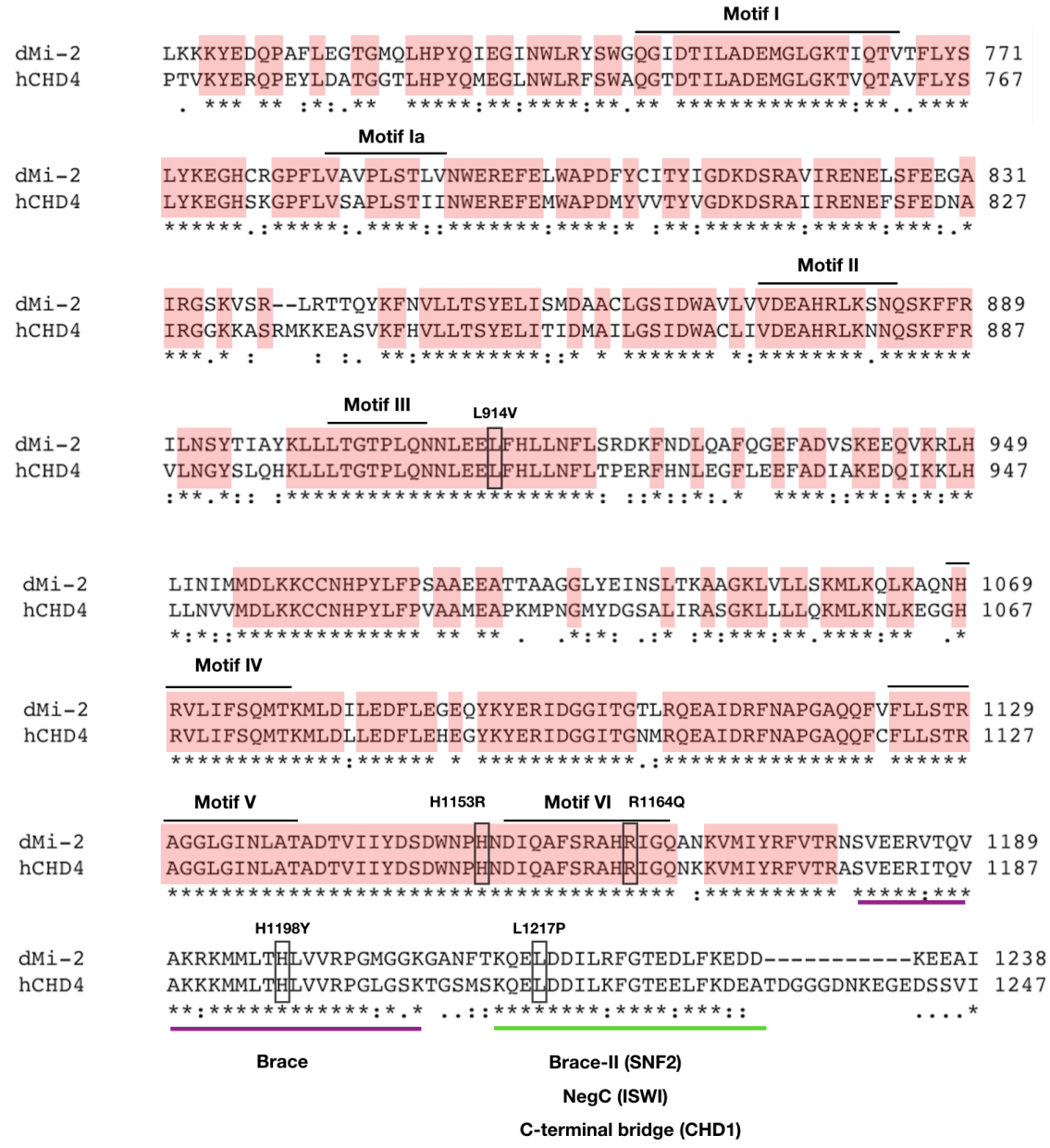
Motif I
dMi-2 LKKKYEDQPAFLEGTGMQLHPYQIEGINWLRYSWGQGIDTILADEMGLGKTIQTVTFLYS 771
hCHD4 PTVKYERQPEYLDATGGTLHPYQMEGLNWLRFSWAQGTDTILADEMGLGKTVQTAVFLYS 767
Motif Ia
dMi-2 LYKEGHCRGPFLVAVPLSTLVNWEREFELWAPDFYCITYIGDKDSRAVIRENELSFEEGA 831
hCHD4 LYKEGHSKGPFLVSAPLSTIINWEREFEMWAPDMYVVTYVGDKDSRAIIRENEFSFEDNA 827
Motif II
dMi-2 IRGSKVSR--LRTTQYKFNVLLTSYELISMDAACLGSIDWAVLVVDEAHRLKSNQSKFFR 889
hCHD4 IRGGKKASRMKKEASVKFHVLLTSYELITIDMAILGSIDWACLIVDEAHRLKNNQSKFFR 887
Motif III
L914V
dMi-2 ILNSYTIAYKLLLTGTPLQNNLEELFHLLNFLSRDKFNDLQAFQGEFADVSKEEQVKRLH 949
hCHD4 VLNGYSLQHKLLLTGTPLQNNLEELFHLLNFLTPERFHNLEGFLEEFADIAKEDQIKKLH 947
dMi-2 LINIMMDLKKCCNHPYLFPSAAEEATTAAGGLYEINSLTKAAGKLVLLSKMLKQLKAQNH 1069
hCHD4 LLNVVMDLKKCCNHPYLFPVAAMEAPKMPNGMYDGSALIRASGKLLLLQKMLKNLKEGGH 1067
Motif IV
dMi-2 RVLIFSQMTKMLDILEDFLEGEQYKYERIDGGITGTLRQEAIDRFNAPGAQQFVFLLSTR 1129
hCHD4 RVLIFSQMTKMLDLLEDFLEHEGYKYERIDGGITGNMRQEAIDRFNAPGAQQFCFLLSTR 1127
Motif V
H1153R
Motif VI
R1164Q
dMi-2 AGGLGINLATADTVIIYDSDWNPHNDIQAFSRAHRIGQANKVMIYRFVTRNSVEERVTQV 1189
hCHD4 AGGLGINLATADTVIIYDSDWNPHNDIQAFSRAHRIGQNKKVMIYRFVTRASVEERITQV 1187
H1198Y
L1217P
dMi-2 AKRKMMLTHLVVRPGMGGKGANFTKQELDDILRFGTEDLFKEDD----------KEEAI 1238
hCHD4 AKKKMMLTHLVVRPGLGSKTGSMSKQELDDILKFGTEELFKDEATDGGGDNKEGEDSSVI 1247
Brace
Brace-II (SNF2)
NegC (ISWI)
C-terminal bridge (CHD1)

B

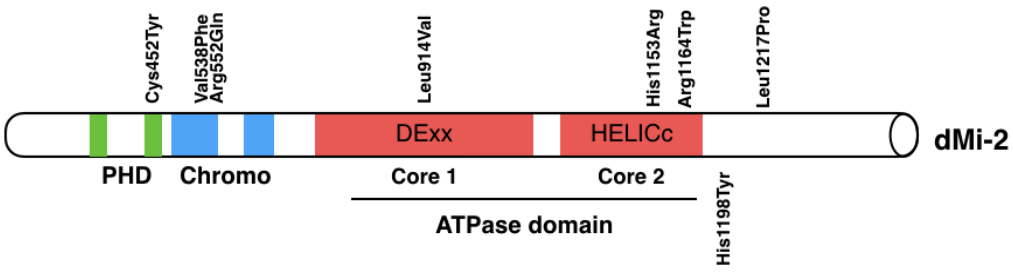
Cys452Tyr
Val538Phe
Arg552Gln
Leu914Val
His1153Arg
Arg1164Trp
Leu1217Pro
DExx
HELICc
dMi-2
PHD
Chromo
Core 1
Core 2
ATPase domain
His1198Tyr

Figure 4.1. Sequence alignment of dMi-2 and hCHD4.

(A) Part of sequence in green showing PHD finger 1 (amino acid residue 370 to 417 in CHD4 and 377 to 424 in dMi-2) and PHD finger 2 (amino acid residue 449 to 496 in CHD4 and 437 to 484 in dMi-2), in blue chromodomain 1 (amino acid residue 494 to 594 in CHD4 and 488 to 566 in dMi-2) and chromodomain 2 (amino acid residue 622 to 697 in CHD4 and 612 to 673 in dMi-2), in red ATPase domain core 1 (amino acid residue 738 to 922 in CHD4 and 742 to 924 in dMi-2) and ATPase domain core 2 (amino acid residue 1054 to 1176 in CHD4 and 1056 to 1179 in dMi-2). Cancer associated residues that are biochemically analysed in this study are indicated with black boxes. Conserved helicase motifs of the ATPase domain are indicated by black lines above the alignment. Brace indicated in purple, Brace-II, NegC and C-terminal bridge region in green. **(B)** Schematic overview of mutations analysed in this study.

The sequence alignment revealed that many amino acids in functional domains and regions are conserved between CHD4 and dMi-2. Several mutations identified in these domains and regions were selected for further work. More specifically, the PHD finger mutant C452Y, chromodomain mutants V538F and R552Q, ATPase domain region mutants L914V, H1153R and R1164Q, as well as C-terminal region mutants H1198Y (brace) and L1217P (putative brace-II/ NegC/C-terminal bridge region) are analysed in this thesis (Figure 4.1 A and B) (Le Gallo et al. 2012, Zhao et al. 2013.).

4.1.2. Characterisation of mutations in the N-terminal region of dMi-2 and the Core 1 region

4.1.2.1. A PHD finger point mutant shows moderately reduced enzymatic activity

The PHD fingers of human CHD4 contact histone H3 and bind methylated H3K9 or unmodified H3K4 (Mansfield et al. 2011, Musselman et al. 2011). One of the cancer derived point mutations (Cys452Tyr in *Drosophila*) changes one of the key cysteines located in the second PHD finger. This cysteine is part of highly conserved $Cys_4His_1Cys_3$ residues that are responsible for coordinating zinc ions (Zhao et al. 2012, Mansfield RE et al. 2011) (Figure 4.2.).

Previous studies from Watson and colleagues have shown that deleting both PHD fingers of human CHD4 leads to moderately decreased ATPase activity, while Musselman and colleagues have shown that PHD fingers are required for CHD4 mediated repression (Watson et al. 2012, Musselman et al. 2011). Considering these findings, it was interesting to investigate the biochemical activity of this novel PHD finger point mutant.

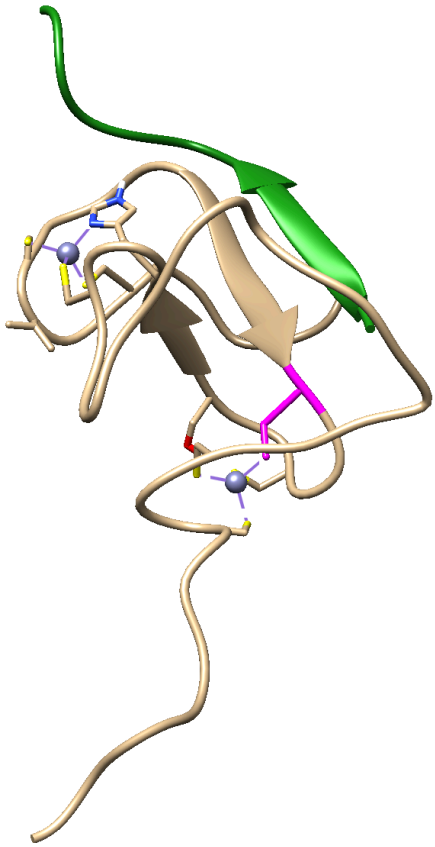

Figure 4.2. Structure of the second PHD finger showing positon of C452 in complex with H3

Crystal structure showing the second PHD finger of human CHD4 (2L75) with the conserved $Cys_4His_1Cys_3$ motif indicated in yellow with the affected cysteine residue indicated in pink. Part of histone H3 is indicated in green (Modified from Mansfield RE *et al.* 2011).

A C452Y point mutation was introduced into dMi-2 by site-directed mutagenesis as described in 3.2.2.1 and the protein was expressed and purified as described in 3.2.3.1 and 3.2.3.2. Considering that dMi-2 is a nucleosome stimulated ATPase (Wang et al. 2001), it was incubated with polynucleosomes that were assembled on a plasmid containing 12x601 Widom nucleosome positioning sequences as described in 3.2.4.3. When nucleosomes were added to the reaction there was a strong increase in ATP hydrolysis. C452Y mutant was tested in an ATPase assay to investigate if this PHD finger point mutation had any consequence on ATP hydrolysis. The C452Y point mutant retained about 50% of WT activity (Figure 4.3.A). To test wether this reduced ability to hydrolyse ATP is due to the

protein's inability to properly coordinate ATP binding, I performed a filter binding assay with radioactively labelled ATP as described in 3.2.3.9. Briefly, samples were incubated with radioactively labelled ATP and incubated for 30 minutes at 26°C. 2μL of each reaction was spotted on nitrocellulose membrane under vacuum and washed with BC100 buffer to remove unbound ATP. Membranes were airdried and exposed to a phosphpoimager screen and radioactive signals were quantified. Quantification of signals showed that the point mutant still retains ATP binding near the level of the WT protein (Figure 4.3.B and C). This indicates that the C452Y point mutant's reduced ATPase activity is probably not due to its inability to properly bind ATP. To determine if this point mutation is affecting the protein’s ability to interact with and bind nucleosomes, I implemented a nucleosome bandshift assay as deccribed in 3.2.4.6. In this assay it is possible to detect differences in nucleosome binding. An unbound nucleosome has a faster electrophoretic mobility than a nucleosome-protein complex, which allows the detection of nucleosome binding activity. In this case the dMi-2-nucleosome complex is mostly too large to enter the gel and it is retained in the loading well. When tested for nucleosome binding ability, the C452Y point mutant was indistinguishable from the WT protein, indicating that this point mutation is not affecting dMi-2's ability to interact with nucleosomes. (Figure 4.3.D)

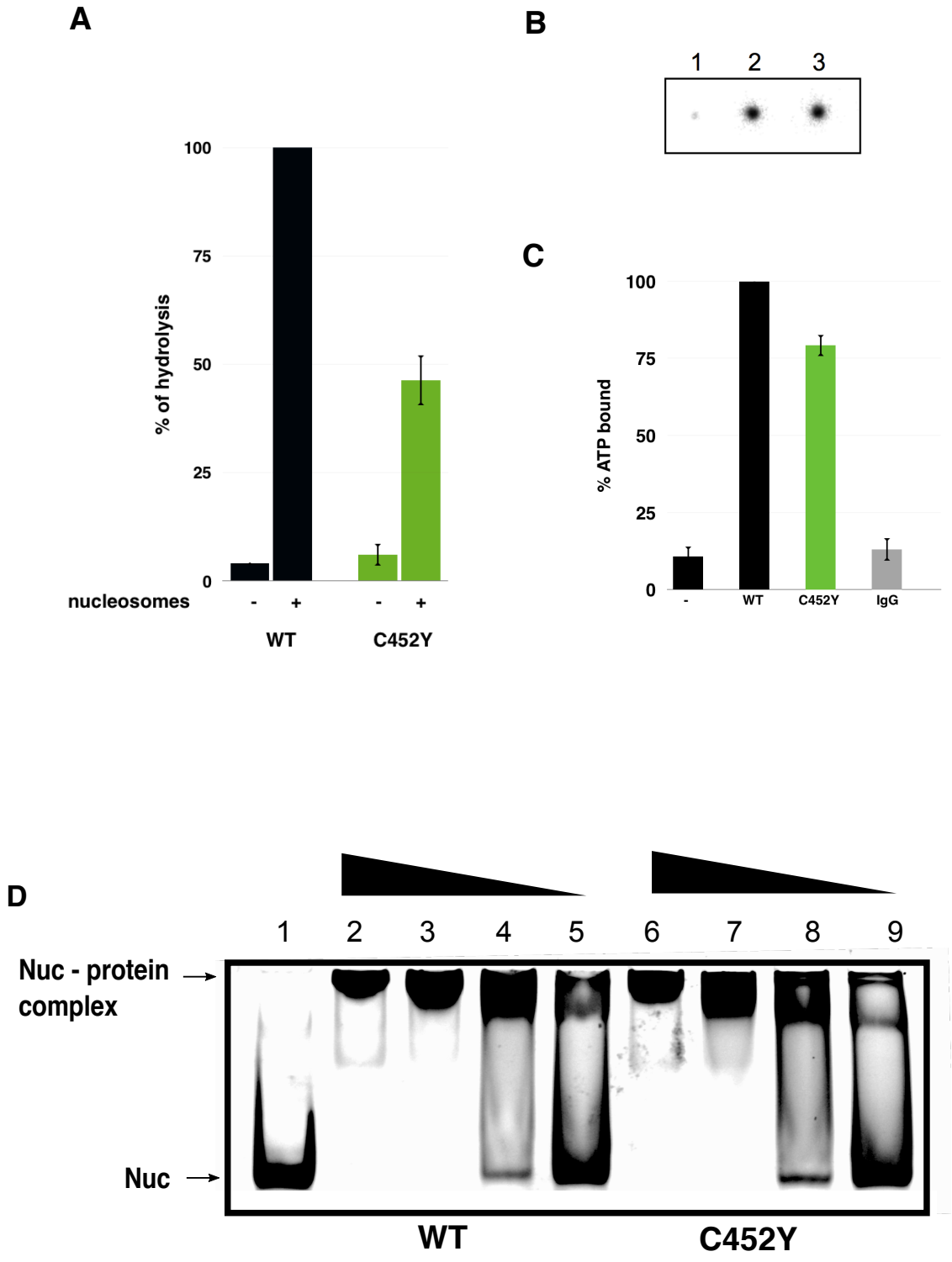
A
100
75
50
25
0
% of hydrolysis
nucleosomes
-
+
-
+
WT
C452Y
B
1
2
3
C
100
75
50
25
0
% ATP bound
-
WT
C452Y
IgG
D
1
2
3
4
5
6
7
8
9
Nuc - protein complex
Nuc
WT
C452Y

Figure 4.3. PHD finger point mutant retains ATP hydrolyis, ATP binding and nucleosome binding ability

(A) ATPase assay with saturating amounts of polynucleosomes assembled on a plasmid containing 12x601 Widom nucleosome positioning sequence. ATP hydrolysis levels of WT protein compared to C452Y in presence (+) or abscence of polynucleosomes (-) are shown. Error bars represent SEM and are derived from 3 independent experiments. **(B)** ATP binding assay of sample without protein (1), WT protein (2) and C452Y point mutant (3) in presence of radioactive ATP. **(C)** Quantification of data from B, IgG served as negative control. **(D)** Nucleosome binding assay with 150nM of end positioned mononucleosome assembled on 601 Widom sequence with 80bp DNA overhang, incubated with decreasing amounts (900nM, 450nM, 225nM and 113nM) of dMi-2 WT (lanes 2-5) and C452Y point mutant (lanes 6-9).

To test whether nuleosome remodeling activity was affected by the point mutation, a nucleosome sliding assay and a restriction enzyme accessibility assay (REA) were performed as described in 3.2.4.5 and 3.2.4.6. The nucleosome sliding assay was performed with two different nucleosomal templates, an end positioned mononucleosome (0-77) and a centrally positioned mononucleosome (77-77), to determine potential preferences of the mutant for differently positioned nucleosomes. These assays allow the detection of changes in nucleosome positioning that significantly alter nucleosome electrophoretic mobility. Nucleosomes were incubated with increasing amounts of protein and incubated for 45 minutes at 26°C. Reactions were stopped with competitor DNA, loaded on a 5% native polyacrylamide gel and run at 120V for approximately 3 hours. The samples with dMi-2 WT without ATP were included in the experiment to ensure that any nucleosome mobilisation detected is ATP dependent (Figure 4.4.A. Lanes 2-5). It is noticeable that the dMi-2 WT protein slides the nucleosome from the end (Figure 4.4.A. Lanes 6-9, lower bands) to more central positions (upper bands) with increasing protein concentrations. This is demonstrated by formation of three differently positioned mononucleosomes with decreased gel mobility, indicating shifts to more central positions. The dMi-2 C452Y point mutant displayed noticably diminished remodelling ability. This is shown by reduced population of centrally positioned nucleosomes at the two highest concentrations of C452Y used. (Figure 4.4.A.;

compare lanes 6 and 7, with lanes 10 and 11). Similar observations were made with the centrally positioned nucleosomal template that has 77 base pairs extending from each side of the nucleosome. Here, the centrally positioned nucleosome (highest band) was shifted towards the end of the DNA fragment (lowest bands) (Figure 4.4.B). While WT protein is able to slide nucleosomes from the center towards the end of DNA fragment at lower protein concetrations (Figure 4.4.B.; lanes 6-7), C452Y required higher protein concentration to achieve the same pattern of remodelling.

In order to more directly quantify the difference in remodelling activity, I performed an REA (restriction enzyme accessibility) assay (Kreher et al. 2017, Bouazoune and Kingston 2012, Narlikar et al. 2001, Logie and Peterson, 1997). With this assay it is possible to measure the ability of a remodeller to expose a MfeI restriction site (+28bp inside the nucleosome) that is usually protected by the nucleosome, as described in 3.2.4.5. This provides a more quantitive way of monitoring the remodelling reaction compared to the nucleosome sliding assay, since the REA assay couples the activity of the nucleosome remodeller that exposes DNA with the restriction enzyme that immediately and irreversibly cuts the exposed DNA. This way the amount of exposed DNA - as a measure of remodeling activity - can be monitored by quantifying the corresponding DNA fragment on the gel.

Radioactively body-labelled nucleosomes (20nM) were incubated with a constant concentration of protein (115nM) in presence of saturating amounts of MfeI restriction enzyme. Time points were taken at 5, 10, 20 and 40 minutes. With WT protein (Figure 4.4.C.; middle panel) an increased percentage of DNA was cut over time, indicating that there is increased remodelling, as shown in the quantification panel (Figure 4.4.D.) Unlike the WT protein, the C452Y mutant showed a reduced remodelling ability, which results in a reduced exposure of MfeI restriction site (Figure 4.5.C.; lower panel and Figure 4.4.D.). All together, these results show that reduced hydrolysis levels, due to a PHD finger point mutation, correlate with reduced remodelling activity, suggesting the

possibility that remodelling is reduced due to reduction of ATP hydrolysis. This further emphasises the importance of PHD fingers for dMi-2 enzymatic activity.

A

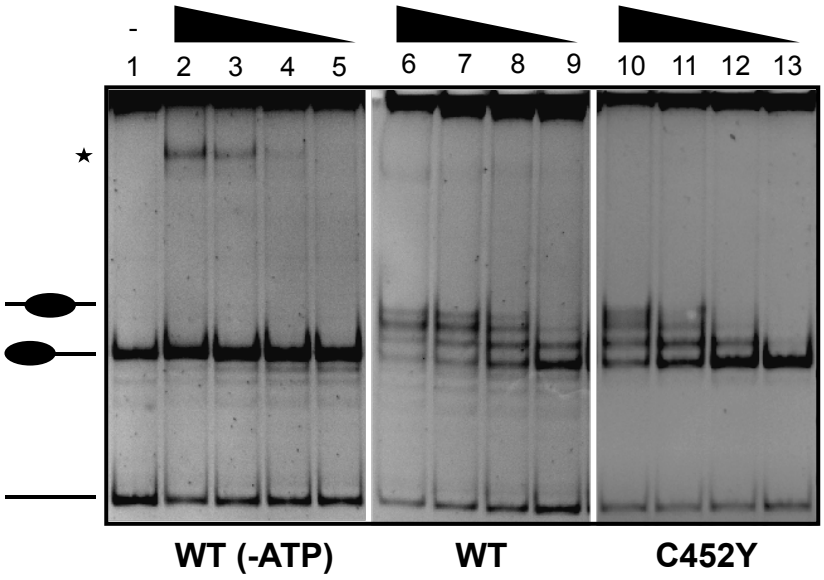

B

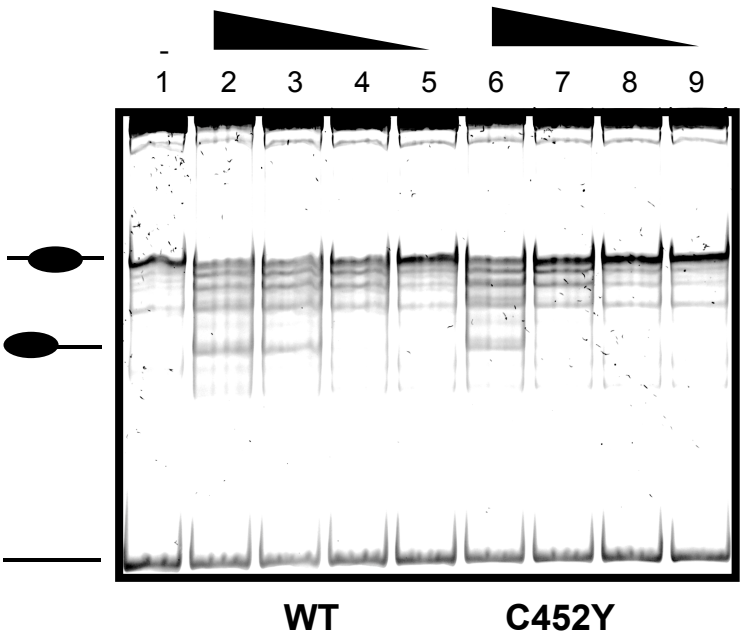

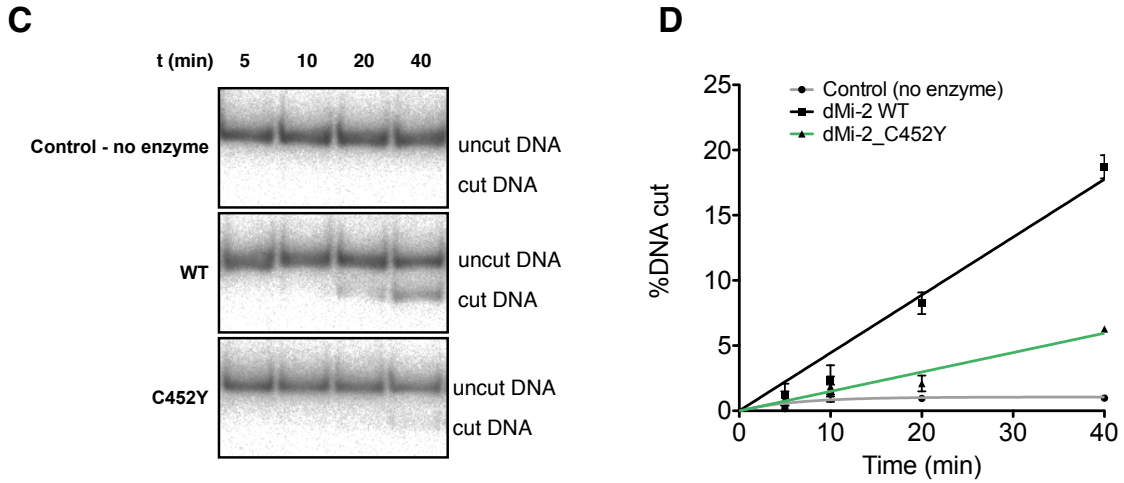

Figure 4.4. dMi-2 C452Y remodells nucleosomes *in vitro*

(A) Nucleosome sliding assay with 150nM of '0-77' end positioned mononucleosome incubated with decreasing amounts of protein (900nM, 450nM, 225nM, 113nM) incubated at 26°C for 45 min. Samples without ATP were incubated with the aforementioned amounts of WT protein (Lanes 2-5). Rections were stopped with addition of 2 μg of competitor DNA and incubated for 10 min on ice. Black star indicates a nucleosome-protein complex that was formed in the reaction independent of remodelling. All panels shown are derived from the same experiment, except C452Y. Gels were stained with SYBR Gold reagent. **(B)** Nucleosome sliding assay with 150nM of '77-77' centrally positioned mononucleosome with increasing amounts of protein (900nM, 450nM, 225nM, 113nM) incubated at 26°C for 45 min. Samples without ATP were incubated with the aforementioned amounts of WT protein (Lanes 2-5). Reactions were stopped with addition of 2 μg of competitor DNA and incubated for 10 min on ice. Gels were stained with SYBR Gold reagent. Black star indicates a nucleosome-protein complex that was formed in the reaction independent from remodelling. **(C)** REA assays of WT (middle panel), C452Y mutant (lower panel) and samples with no remodeller (upper panel). Radioactively labelled DNA was visualised by exposing the gels to Phosphoimager screen. **(D)** Quantification of gel from C. Cut and uncut DNA was quantified and ratio of cut and total DNA (cut plus uncut) was plotted as '% DNA cut'. Error bars represent SEM and are derived from 3 independent experiments. Plotting was done in GraphPad Prism using the one phase decay equation.

4.1.2.2. Chromodomain point mutants show severely impaired enzymatic activity

Many chromodomain containing proteins bind methylated histone tails, like HP1 (Jacobs et al. 2001, Schwartz and Pirrotta, 2007). It has been shown by our lab that the dMi-2 chromodomains bind the nucleosome through contacts with nucleosomal DNA. Deletion of both chromodomains causes a significant reduction in dMi-2 binding to nucleosomal DNA (Bouazoune et al. 2002). Two distinct mutations in the chromodomains were identified in CHD4 by exome sequencing (Le Gallo et al. 2012.). These mutations were separately introduced into dMi-2 by site directed mutagenesis and the enzyme was purified as described in 3.2.3.1 and 3.2.3.2. Val538Phe and Arg552Gln (from here on referred to as V538F and R552Q) are located in the first chromodomain of dMi-2. These point mutations were tested for their impact on the ATPase activity. An ATPase assay was performed as described in 3.2.4.3. and 4.1.2.1. Upon incubation with radioactively labelled ATP and polynucleosomes ATP hydrolysis by both mutants was severely reduced. This suggested that both mutated residues could have a direct role in ATP hydrolysis or that the mutations result in structural changes that have a negative effect on ATP hydrolysis. (Figure 4.5.A). A filter binding assay was used to investigate if these point mutations have an effect on ATP binding. The experiment was performed as described in 3.2.3.9. and 4.1.2.1. Quantification showed that both mutants still retain ATP binding ability. ATP binding by R552Q was more reduced and it measured 31% of WT protein ATP binding ability. On the other hand, V538F showed ATP binding levels similar to WT protein, measured at 90% of WT ATP binding ability (Figure 4.5.B and C). Given that deletion of the double chromodomain region abrogates nucleosome binding (Boauzoune et al. 2002) it was interesting to test if the two point mutations in the chromodomain were sufficient to affect nucleosome and DNA binding. Nucleosome bandshift experiments were performed as described in 3.2.4.6. and 4.1.2.1. DNA bandshift assays were performed the same way as the nucleosome bandshift, except naked DNA fragments were used, as described in 3.2.4.6. Interestingly,

both DNA (Figure 4.5.D) and nucleosome binding (Figure 4.5.E) were retained by the chromodomain mutants, but reduced. This reduction was most noticable at the two highest protein concentrations. Comparing the two highest protein concentrations used in the nucleosome binding assay (Figure 4.5.D) between WT (lane 2 and 3), V538F (lane 6 and 7) and R552Q (lane 10 and 11) it is noticeable that R552Q and especially V538F have reduced binding to nucleosome, discernible by less nucleosome-protein complex that is shifted upwards in the gel. Similar observations were made with the DNA bandshift assay (Figure 4.5.E). Again, it is visible at the two highest concentrations that both point mutants have reduced binding to the DNA. When comparing WT (lanes 2 and 3) with V538F (lanes 6 and 7) and R552Q (lanes 10 and 11), both mutants display weaker binding to the DNA than the WT. This is visualized by less DNA forming DNA-protein complexes. These results show that both mutations have an impact on formation of DNA - protein or nucleosome - protein complexes. This difference could be the result of changes in direct contact that the mutated residues have with the nucleosome or DNA, or of structural changes in the chromodomain, such that direct contact by other residues are weakened.

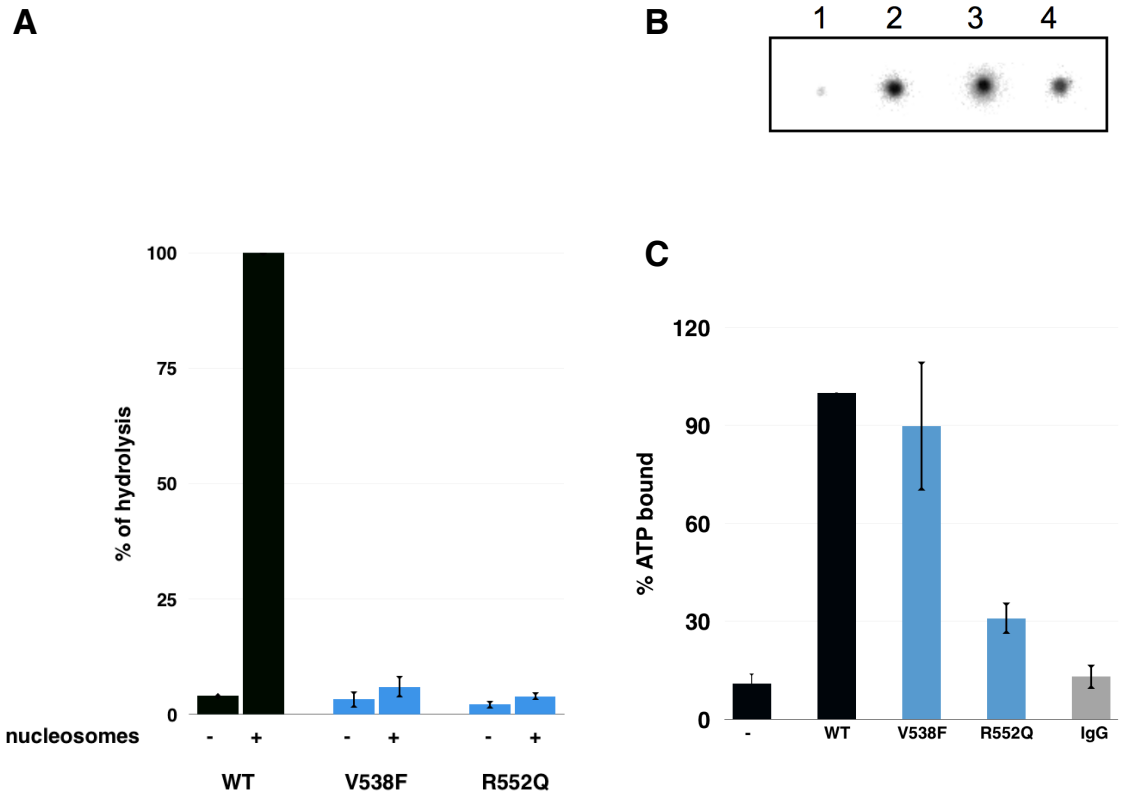
A
100
75
50
25
0
% of hydrolysis
nucleosomes
- + - + - +
WT
V538F
R552Q
B
1 2 3 4
C
120
90
60
30
0
% ATP bound
-
WT
V538F
R552Q
IgG

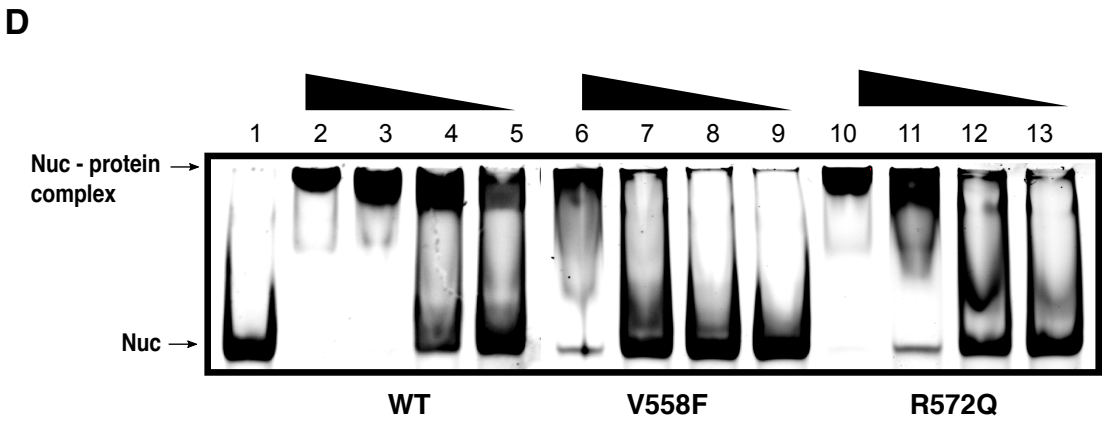
D
1 2 3 4 5 6 7 8 9 10 11 12 13
Nuc - protein complex
Nuc
WT
V558F
R572Q

E

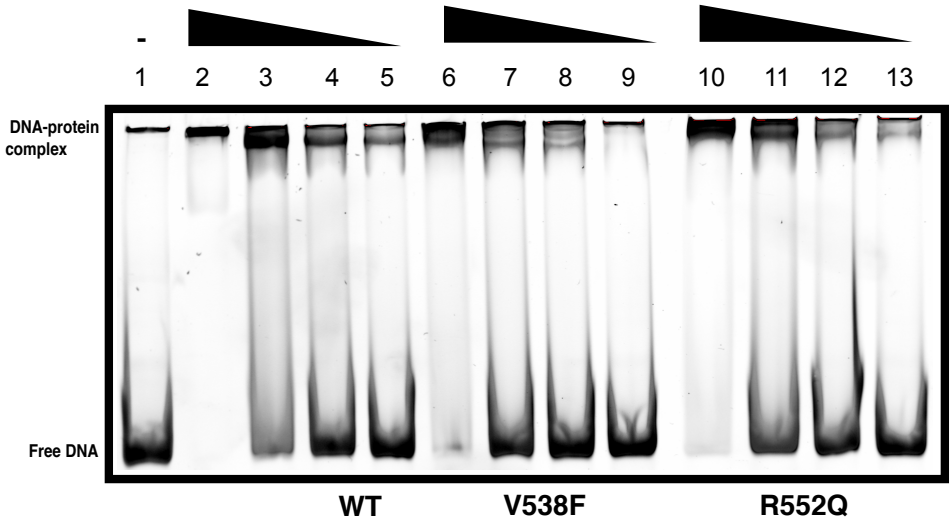

Figure 4.5. Chromodomain point mutants are severly impared in ATP hydrolysis, but retain ATP, DNA and nucleosome binding with moderately reduced affinity

(A) ATPase assay with saturating amounts of polynucleosomes assembled on a plasmid containing 12x601 Widom nucleosome positioning sequences. ATP hydrolysis levels of WT protein compared to V538F and R552Q in presence (+) or abscence of polynucleosomes (-) are shown. Error bars represent SEM and are derived from 3 independent experiments. **(B)** ATP binding assay of sample without protein (1)WT protein (2), V538F point mutant (3) and R552Q point mutant (4). **(C)** Quantification of data from B, IgG served as a negative control. **(D)** Nucleosome binding assay with 150nM of end positioned mononucleosome assembled on 601 Widom sequence with 80bp DNA overhang, incubated with decreasing amounts (900nM, 450nM, 225nM and 113nM) of dMi-2 WT (lane 2-5) and V538F point mutant (lanes 6-9) and R552Q point mutant (lanes 10-13). **(E)** DNA binding assay with 150nM of end positioned mononucleosome assembled on 601 Widom sequence with 80bp DNA overhang, incubated with decreasing amounts (900nM, 450nM, 225nM and 113nM) of dMi-2 WT (lanes 2-5), V538F point mutant (lanes 6-9) and R552Q point mutant (lanes 10-13).

In order to examine how these chromodomain mutations impact the protein's capability to remodel nucleosomes, REA and nucleosome sliding assays were carried out. Experiments were performed as described in 3.2.4.4, 3.2.4.5. and

4.1.2.1. Nucleosome sliding assays were performed with end positioned and centrally positioned nucleosomes. Again, nucleosomes were incubated with decreasing amounts of WT protein and the two chromodomain point mutants. Unlike WT dMi-2, chromatin remodelling by R552Q was undetectable in this assay. Nucleosome sliding to more cental positions is indicated by formation of a nucleosome with slower electrophoretic ability. For R552Q there was no detectable formation of centrally positioned nucleosomes (Figure 4.6.A. Lane 14-17). The V538F chromodomain point mutant displayed severely reduced levels of remodelling, but unlike R552Q, low nucleosome sliding levels could be detected. V538F was able to slide nucleosomes to more central positions which was reflected by formation of nucleosomes with slower electrophoretic mobility (Figure 4.6.A. Lanes 10-13). Similar observations were made when incubating chromodomain mutants with centrally positioned nucleosomes. Nucleosomes were incubated with decreasing amount of protein. At the highest concentration of protein, 5 distinct nucleosomal positions were generated (Figure 4.6.B. Lanes 6-9). Nucleosomes with faster electrophoretic mobility have the nucleosome shifted more to the end of the DNA fragment. The V538F point mutant showed modest remodelling ability by producing two bands of end positioned nucleosomes with faster electrophoretic mobility (Figure 4.6.B. Lanes 10-13). For the R552Q point mutant similar results as with end positioned nucleosomes were obtained: No nucleosome sliding was observed (Figure 4.6.B Lane 14-17). To more directly quantify these effects, REA assays were carried out. A constant amount of protein was incubated with radioactively labelled, end positioned nucleosomes and the reaction was stopped at different time points. Compared with the WT, no apparent remodelling was observed for either of the chromodomain mutants (Figure 4.6.C and D). Unlike in the nucleosome sliding assay, V538F showed no detectable remodelling in this assay. This might be due to the inability of this point mutant to remodel nucleosome enough to fully expose the MfeI restriction site. The R552Q point mutant showed no apparent remodelling, consistent with results obtained in nucleosome sliding assays. This analysis of chromodomain mutants showed that even one point mutation in the chromodomain might have an impact on dMi-2's ability to contact the

nucleosome and properly position itself for subsequent ATP hydrolysis and chromatin remodelling. When superimposing V538 and R552 onto the yeast CHD1 crystal structure it is noticeable how these two residues are flanking a recently identified basic loop (Figure 4.6.E). This loop was shown to cross link to nucleosomal DNA (Nodelman et al. 2017). It is possible that the mutations affect the interaction of the basic loop of CHD remodeler and the nucleosome.

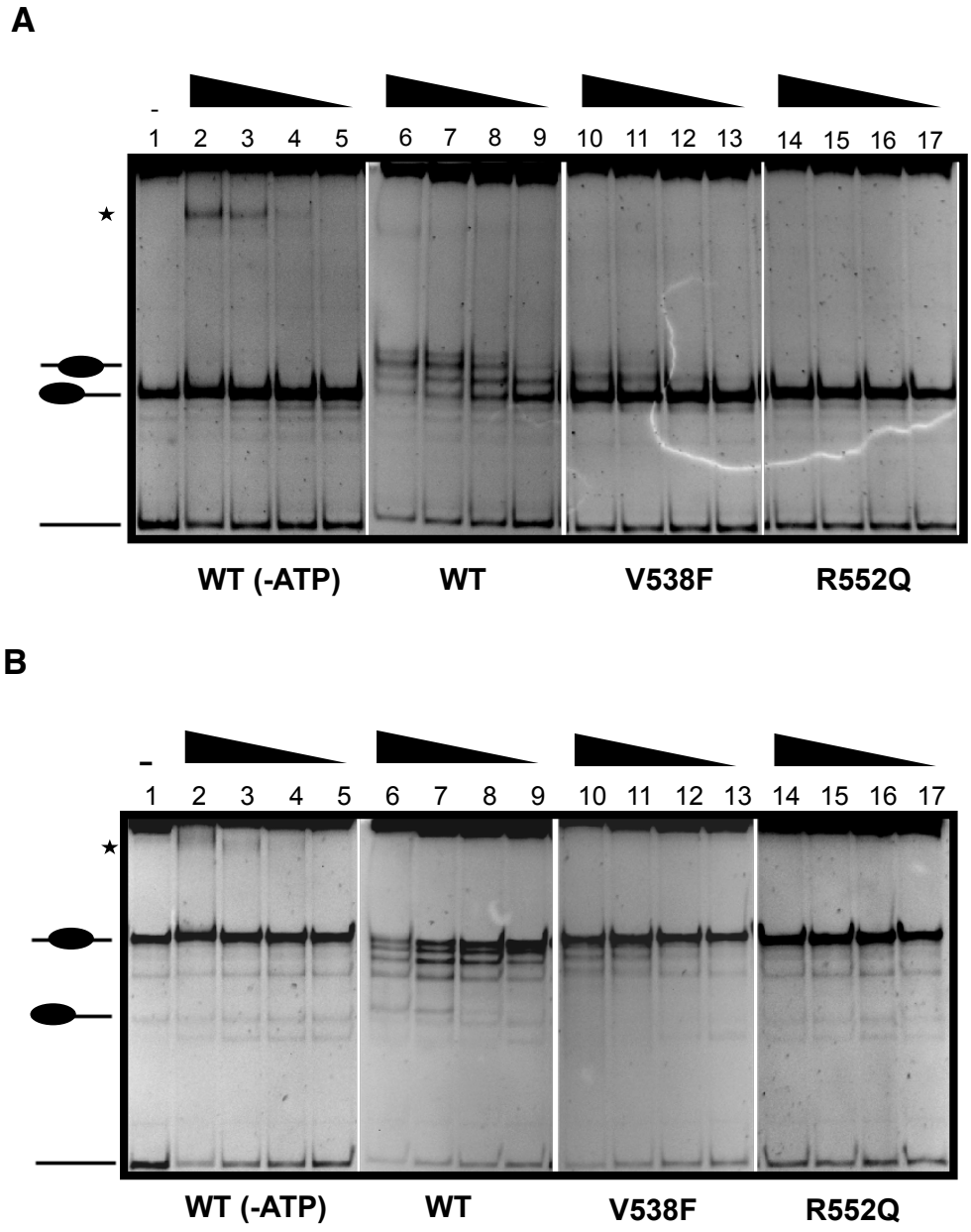

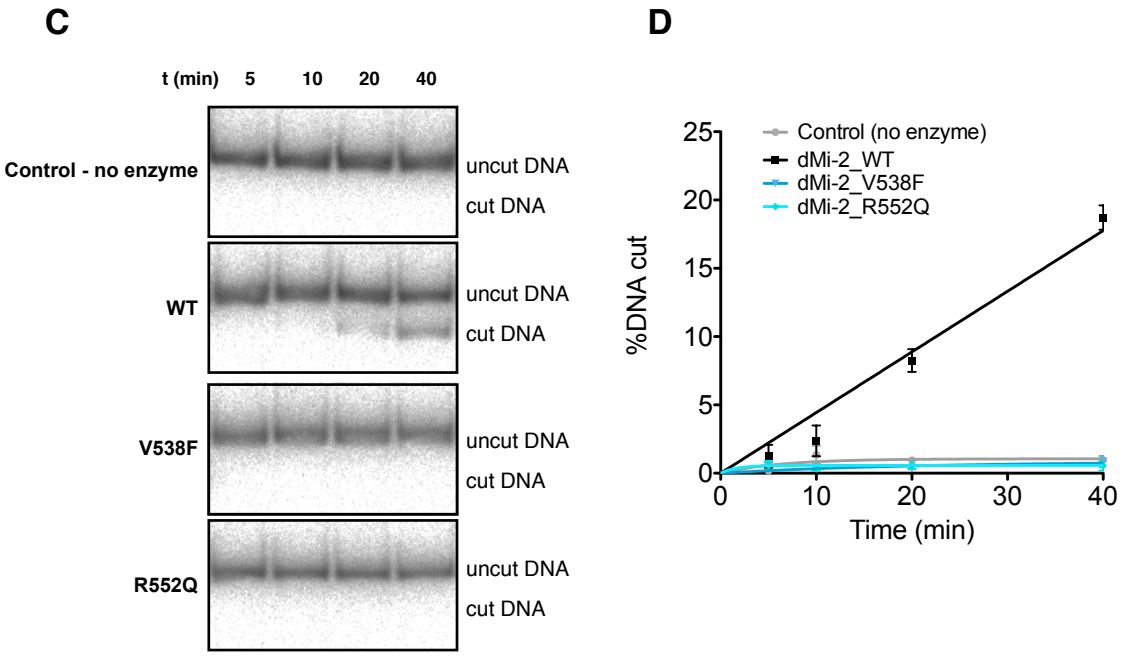
C
t (min) 5 10 20 40
Control - no enzyme
WT
V538F
R552Q
uncut DNA
cut DNA
D
Control (no enzyme)
dMi-2_WT
dMi-2_V538F
dMi-2_R552Q
%DNA cut
Time (min)
0
5
10
15
20
25
0
10
20
30
40

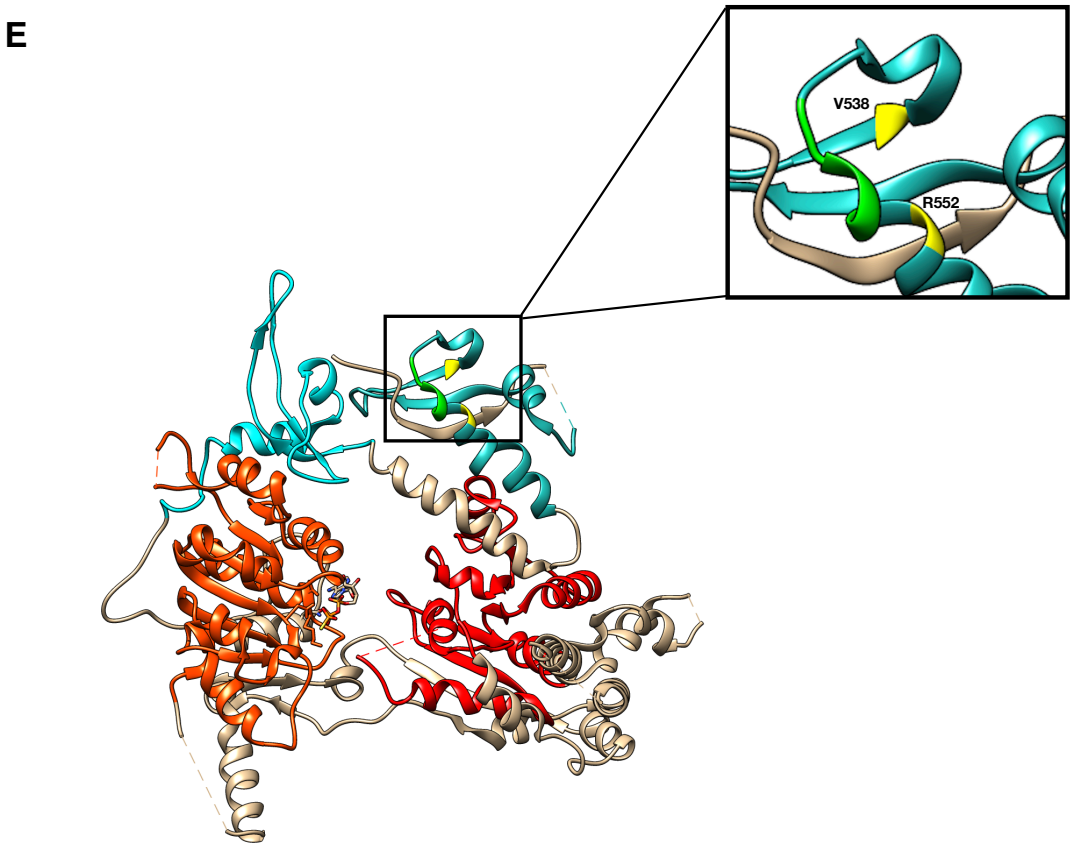
E
V538
R552

Figure 4.6. Chromodomain point mutanats are impaired for remodelling *in vitro*

(A) Nucleosome sliding assay with 150nM of '0-77' end positioned mononucleosome incubated with decreasing amounts of protein (900nM, 450nM, 225nM, 113nM) incubated at 26°C for 45 min. Samples without ATP were incubated with the aforementioned amounts of WT protein (lanes 2-5). Reactions were stopped with addition of 2 μg of competitor DNA and incubated for 10 min on ice. Black star indicates nucleosome-protein complex that was formed in the reaction independent of remodelling. All panels shown are derived from the same experiment. Gels were stained with SYBR Gold reagent. **(B)** Nucleosome sliding assay with 150nM of '77-77' centrally positioned mononucleosome with increasing amounts of protein (900nM, 450nM, 225nM, 113nM) incubated at 26°C for 45 min, stained with SYBR Gold reagent. Samples without ATP were incubated with aforementioned amounts of WT protein (lanes 2-5). Reactions were stopped with addition of 2 μg of competitor DNA and incubated for 10 min on ice. Gels were stained with SYBR Gold reagent. Black star indicates nucleosome-protein complex that was formed in the reaction independent from remodelling. **(C)** REA assays of WT, V538F and R552Q mutants and samples with no remodeller. Radioactively labelled DNA was visualised by exposing the gels to Phosphoimager screen. **(D)** Quantification of gel from C. Cut and uncut DNA was quantified and ratio of cut and total DNA (cut plus uncut) was plotted as '% DNA cut'. Error bars represent SEM and are derived from 3 independent experiments. Plotting was done in GraphPad Prism using the one phase decay equation. **(E)** yCHD1 structure (3MWY) with basic loop of chromodomain 1 indicated with green and superimposed relative positions of V538 and R552 in yellow (Chromodomain 1 in light blue, chromodomain 2 in cyan, ATPase domain core 1 orange red, ATPase domain core 2 in red).

4.1.2.3. Core 1 region point mutant Leu914Val shows significantly reduced enzymatic activity

The core 1 region, with its helicase motifs I, Ia, II, and III, is responsible for important mechanistic aspects of enyzmatic function. Successful interplay between the two cores and their motifs is crucial for catalytic activity (more in chapter 2.2.3.). One of the point mutations identified in endometrial cancer exome sequencing was Leu914Val (from here on referred to as L914V), a mutation located in the core 1 domain in close proximity to helicase motif III (Figure 4.1.A). This point mutation was introduced into dMi-2 by site-directed

mutagenesis as described in 3.2.2.1 and the protein was expressed and purified as described in 3.2.3.1 and 3.2.3.2. An ATPase assay was performed to quantify ATP hydrolysis compared to WT protein. The ATPase activity of the L914V mutant was reduced to around 10% of WT activity. Since the ATP binding pocket is located in the core 1 region (helicase motifs I and II), I investigated whether this point mutation has an effect on ATP binding. ATP binding ability of the mutant was at 64% of WT binding ability. This suggests that the severe impact on ATP hydrolysis is seemingly not only due to the impact on ATP binding. I examined if the reduced ATP hydrolysis was due to the mutant's inability to efficiently bind nucleosomes, for which I performed nucleosome bandshift assays (as described in 3.2.4.6) where decreasing amounts of protein were incubated with +80 mononucleosomes (Figure 4.7.D.). An effect on nucleosome binding of the L914V mutation was noticable at the 450nM concentration of the point mutant (Figure 4.7.D., lane 7). At this concentration a significant amount of nucleosomes remained unbound whereas this was not the case for WT dMi-2 (Figure 4.7.D., lane 3).

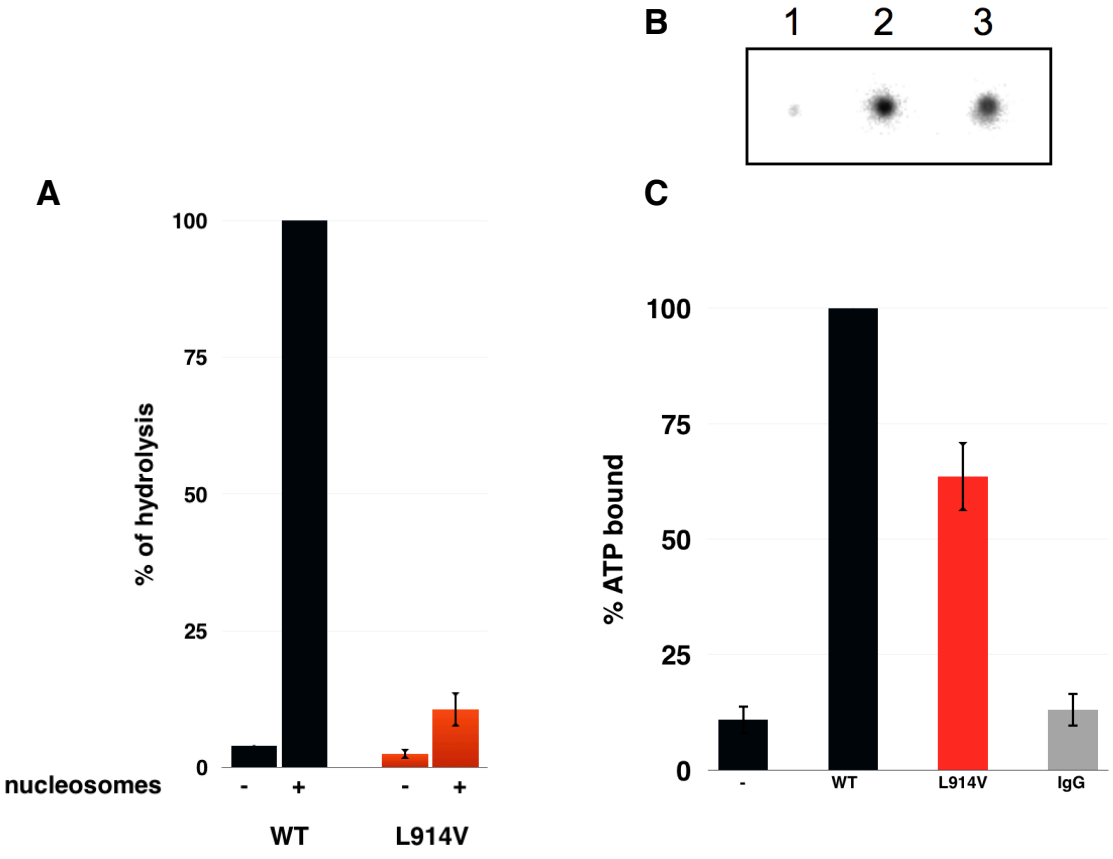

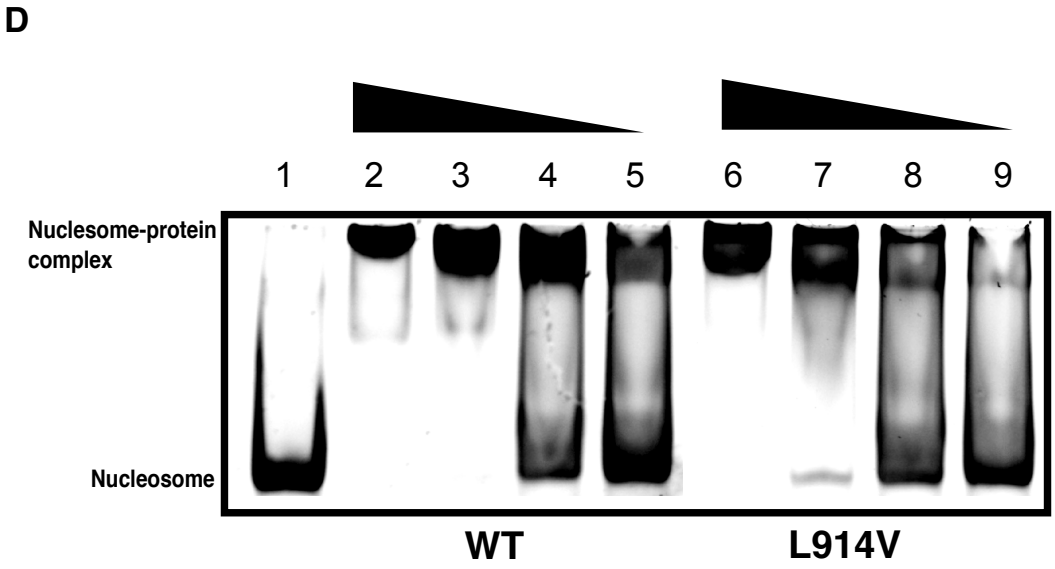

Figure 4.7. Core1 region point mutant L914V is significantly impaired in ATP hydrolysis, but retains ATP and nucleosome binding

(A) ATPase assay with saturating amounts of polynucleosomes assembled on a plasmid containing 12x601 Widom nucleosome positioning sequences. ATP hydrolysis levels of WT protein compared to L914V in presence (+) or abscence of polynucleosomes (-) are shown. Error bars represent SEM and are derived from 3 independent experiments. **(B)** ATP binding assay of sample without protein (1), WT protein (2) and L914V point mutant (3). **(C)** Quantification of data from B, IgG served as a negative control. **(D)** Nucleosome binding assay with 150nM of end positioned mononucleosome assembled on 601 Widom sequence with 80bp DNA overhang, incubated with decreasing amounts (900nM, 450nM, 225nM and 113nM) of dMi-2 WT (lanes 2-5) and L914V point mutant (lanes 6-9).

After establishing that L914V is still binding nucleosomes, I wanted to determine if the significant impact on ATP hydrolysis, also reflects on the point mutant's capability to remodel nucleosomes. Once again, nucleosome sliding and REA assays were carried out on 0-77 end-positioned, 77-77 centrally positioned and +80 end positioned nucleosomes. When the nucleosome sliding assay was performed on 0-77 end positioned nucleosomes, formation of a nucleosome with slower electrophoretic mobility was observed at the highest concentration of protein. This indicated a sliding of a nucleosome to a more centrally

positioned location (Figure 4.8.A Lane 10). This was well in line with ATPase activity of this mutant, indicating that the decreased ability to efficiently hydrolyse ATP is a possible reason for decreased remodelling activity. Incubating the mutant with centrally positioned nucleosome did not produce any noticable formation of more end postioned nucleosome, showing that end positioned nucleosome is a prefered substrate (Figure 4.8.B). To quantify these results, an REA assay was performed, as described previously (3.2.4.5). No detectable remodelling was observed (Figure 4.8.D). Again, this might be due to the inability of L914V to remodel nucleosomes enough to expose the MfeI restriction site. Analysis of this mutant showed that while still retaining the ability to perform ATP hydrolysis, albeit at very low levels of 10% WT protein hydrolysis activity, it was severly impaired in its remodelling ability. Extremely low levels of remodelling were detected for end positioned nucleosomes, while centrally positioned nucleosomes showed no apparent remodelling; it was also not able to expose nucleosomal DNA to the MfeI restriction enzyme in the REA assay. This indicates an important role of the L914 residue for ATP hydrolysis and chromatin remodelling.

A

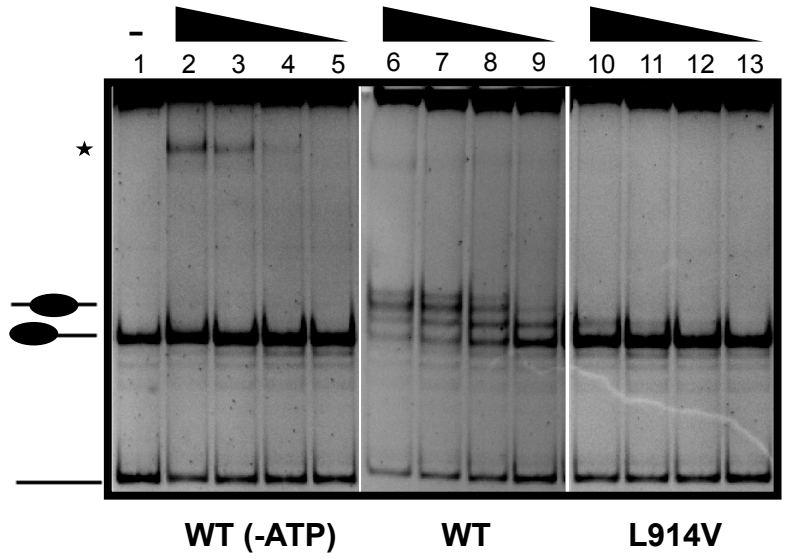

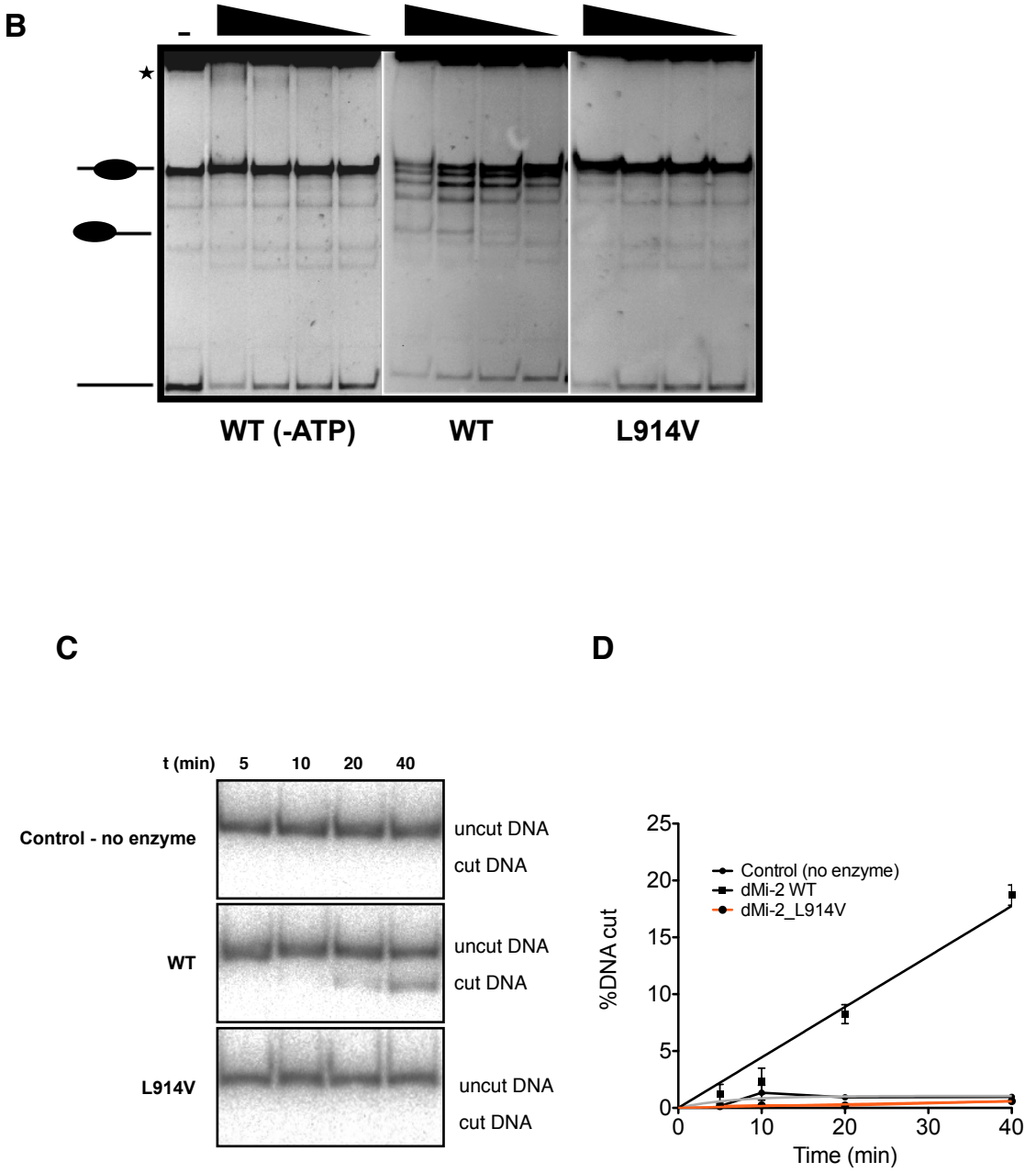

Figure 4.8. L914V point mutant is severly affected in its remodelling ability

(A) Nucleosome sliding assay with 150nM of '0-77' end positioned mononucleosome incubated with decreasing amounts of protein (900nM, 450nM, 225nM, 113nM) incubated at 26°C for 45 min. Samples without ATP were incubated with the aforementioned amounts of WT protein (Lanes 2-5). Reactions were stopped with addition of 2 μg of competitor DNA and incubated for 10 min on ice. Black star indicates nucleosome-protein complex that was formed in the reaction independent from remodelling. All panels shown are derived from same experiment. Gels were

stained with SYBR Gold reagent. **(B)** Nucleosome sliding assay with 150nM of '77-77' centrally positioned mononucleosome with increasing amounts of protein (900nM, 450nM, 225nM, 113nM) incubated at 26°C for 45 min. Samples without ATP were incubated with the aforementioned amounts of WT protein (Lanes 2-5). Reactions were stopped with addition of 2 *μ*g of competitor DNA and incubated for 10 min on ice. Gels were stained with SYBR Gold reagent. Black star indicates nucleosome-protein complex that was formed in the reaction independent from remodelling. **(C)** REA assays of WT, L914V and samples with no remodeller. Radioactively labelled DNA was visualised by exposing the gels to Phosphoimager screen. **(D)** Quantification of gel from C. Cut and uncut DNA was quantified and ratio of cut and total DNA (cut plus uncut) was plotted as '% DNA cut'. Error bars represent SEM and are derived from 3 independent experiments. Plotting was done in GraphPad Prism using one phase decay equation.

4.1.2. Characterisation of mutations in the Core 2 domain and in the region adjacent to core 2

Core 2 domain contains motifs IV, V and VI are important for nucleic acid binding, translocation along the DNA and binding of the ATP. Interaction between these motifs and core 1 motifs are crucial for efficient ATP hydrolysis and chromatin remodelling (Flaus et al. 2006, Liu et al. 2017). Furthermore, the region adjacent to core 2 on its C-terminal side has a regulatory role in many chromatin remodellers (Hauk et al. 2010, Clapier and Cairns, 2012, Liu et al. 2017). In this study several cancer derived point mutants in core 2 and its C terminal adjacent region were biochemically analysed.

4.1.2.3. Core 2 region point mutants His1153Arg and Arg1164Gln show a variety of effects on enzymatic activity

His1153 and Arg1164 are both located in a highly conserved part of the core 2 region. His1153 is located between motifs V and VI, while Arg1164 is part of the helicase motif VI (arginine fingers) and it is involved in the interaction with core 1 domain motif I during ATP hydrolysis (Liu et al. 2017. Flaus et al. 2006) (Figure 4.1.A). Considering the functional relevance and the level of

conservation of these residues, biochemical effects of two cancer derived point mutations were analysed - His1153Arg (from here on referred as H1153R) and Arg1164Gln (from here on referred as R1164Q). Point mutations were introduced into dMi-2 by site-directed mutagenesis as described in 3.2.2.1 and proteins were expressed and purified as described in 3.2.3.1 and 3.2.3.2. ATPase assay analysis showed very different effects of these point mutations. The H1153R mutant had moderately decreased ATPase activity of about 60-70% of WT activity. R1164Q had a more severe effect on ATP hydrolysis: its ATP hydrolysis levels were decreased to 18% (Figure 4.9.A). I assessed the ATP binding activity of both mutants and found that they both retained their ability to bind ATP, although to a different extent; H1153R had moderately reduced ATP binding of 66% of WT binding activity, while the binding activity of R1164Q was increased to about 150% of WT binding activity. This indicates that the decreased ATPase activity of the R1164Q mutant can not be attributed to reduced ATP binding (Figure 4.9. B and C). Next, I investigated the impact of these mutations on dMi-2's ability to bind nucleosomes by nucleosome bandshift assays (3.2.4.6). Like WT dMi-2, both point mutants shifted the nucleosomes quantitatively at the two highest protein concentrations used (Figure 4.9. D, Lane 2-3, 6-7 and 10-11). This shows that the ability to bind nucleosome was not affected by these mutations.

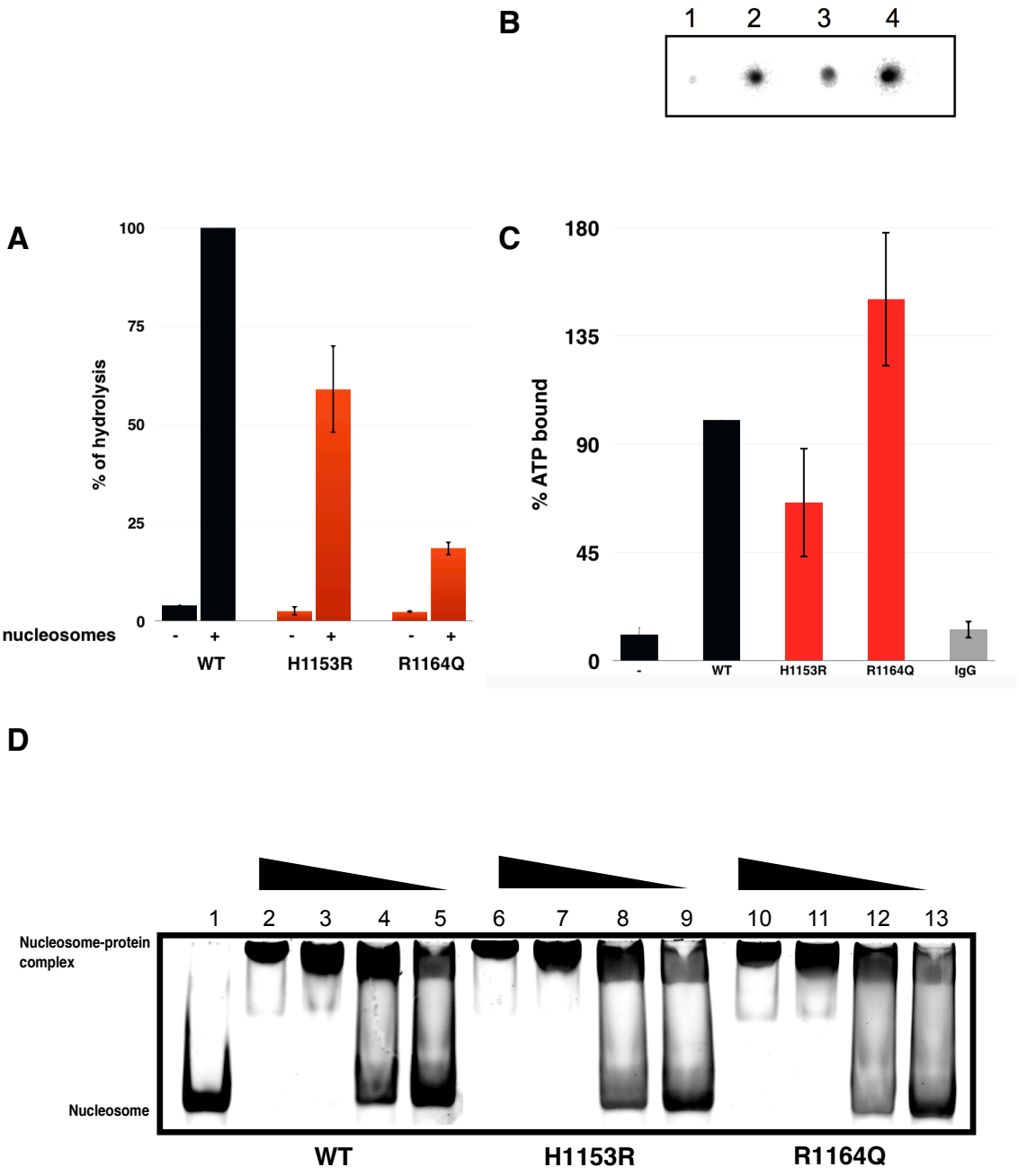

Figure 4.9. Core 2 region point mutants H1153R and R1164Q show distinct effects on ATP hydrolysis, but no significant effect on ATP binding, and retain nucleosome binding

(A) ATPase assay with saturating amounts of polynucleosomes assembled on a plasmid containing 12x601 Widom nucleosome positioning sequences. ATP hydrolysis levels of WT protein compared to H1153R and R1164Q point mutant in presence (+) or abscence of polynucleosomes (-) are shown. Error bars represent SEM and are derived from 3 independent

experiments. **(B)** ATP binding assay of sample without protein (1), WT protein (2) H1153R (3) and R1164Q (4). **(C)** Quantification of data from B, IgG served as negative control. **(D)** Nucleosome binding assay with 150nM of end positioned mononucleosome assembled on 601 Widom sequence with 80bp DNA overhang, incubated with decreasing amounts (900nM, 450nM, 225nM and 113nM) of dMi-2 WT (lanes 2-5) H1153R point mutant (lanes 6-9) and R1164Q point mutant (lane 10-13).

Furthermore, nucleosome sliding and REA assays were carried out to determine the effects of these mutations on dMi-2's remodelling ability. In nucleosome sliding assays with end positioned mononucleosomes the R1164Q mutant was able to form an additional nucleosome position with slower electrophoretic mobility at the highest concentration of protein. This indicated movement of a nucleosome over a short distance to more central positon. (Figure 4.10.A. - lane 14). Suprisingly, H1153R was not able to slide nucleosomes (Figure 4.10.A. Lane 10-13). With centrally positioned nucleosomes, similar results were obtained; there was no apparent remodelling observed for H1153R as in the experiment with end positioned nucleosome. (Figure 4.10.B. Lane 10-13). Also, for R1164Q no remodelling was detected, indicating again that centrally positioned nucleosomes are less favourable substrates for dMi-2. (Figure 4.10.B) To verify and quantify these results, I performed REA assays with radioactively labelled end positioned nucleosomes, where similar results were observed; no detectable remodelling for H1153R, and about 2% remodelled nucleosomes for R1164Q mutant at the last time point. (Figure 4.10.C and D).

In summary, the analysis of these two mutants which fall within core 2 domain showed different effects of these point mutations on dMi-2's enzymatic function. The arginine finger mutant R1164Q was significantly affected by this point mutation, with both drastically reduced ATP hydrolysis and remodelling activities. The other core 2 domain mutant - H1153R - showed varying effects on its enzymatic functions. While retaining more more than 60% of ATPase capability, it was not able to remodel end positioned, nor centrally positioned nucleosomes. These results confirm the importance of arginine finger motif VI

for chromatin remodelling and ATP hydrolysis. Moreover, they identify a mutant, H1153R, which decouples ATP hydrolysis from chromatin remodelling, indicating the importance of this residue for bringing these two different enzymatic functions together.

A

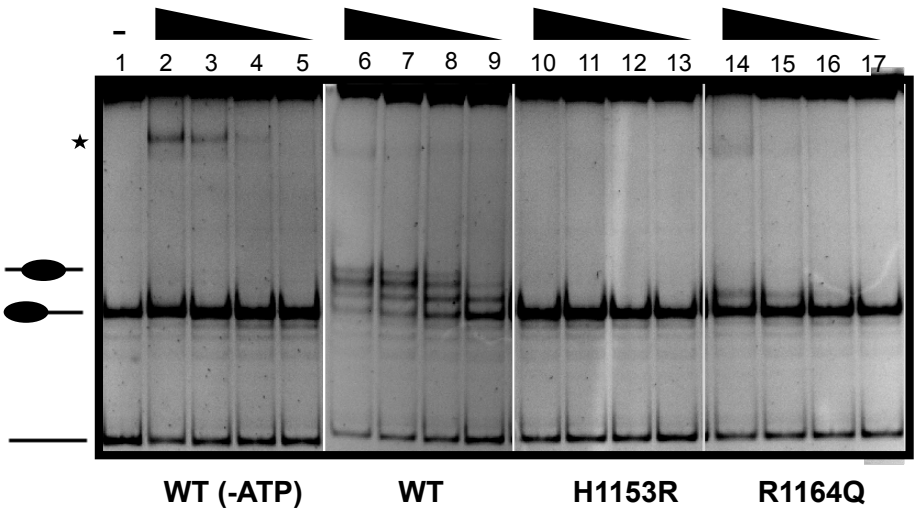

B

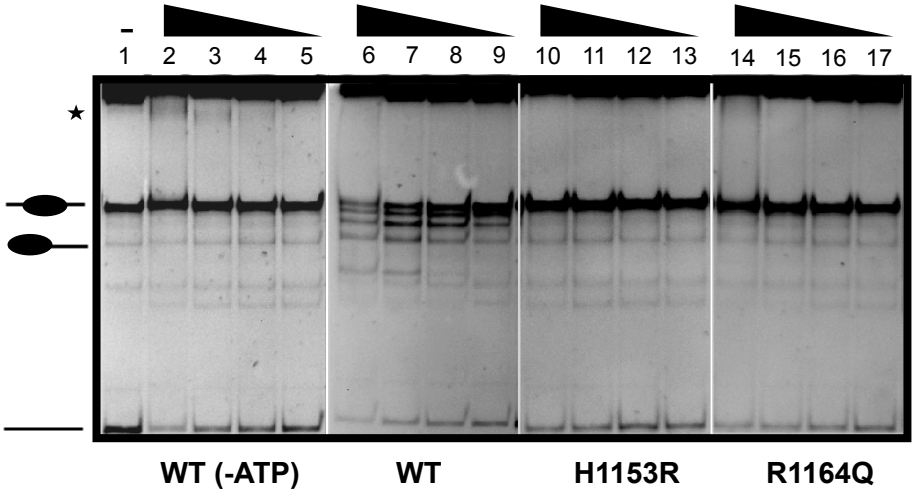

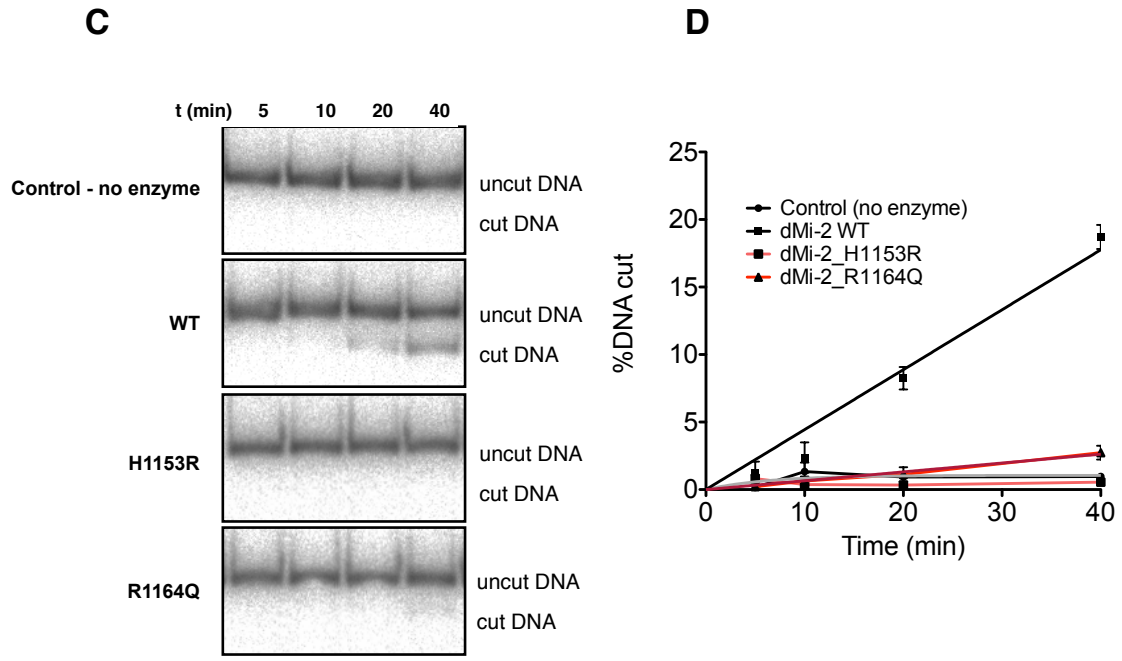

Figure 4.10. Core 2 region mutants show impaired chromatin remodelling

(A) Nucleosome sliding assay with 150nM of '0-77' end positioned mononucleosome incubated with decreasing amounts of protein (900nM, 450nM, 225nM, 113nM) incubated at 26°C for 45 min. Samples without ATP were incubated with the aforementioned amounts of WT protein (Lanes 2-5). Rections were stopped with addition of 2 μg of competitor DNA and incubated for 10 min on ice. Black star indicates nucleosome-protein complex that was formed in the reaction independent of remodelling. All panels shown are derived from same experiment. Gels were stained with SYBR Gold reagent. **(B)** Nucleosome sliding assay with 150nM of '77-77' centrally positioned mononucleosome with increasing amounts of protein (900nM, 450nM, 225nM, 113nM) incubated at 26°C for 45 min. Samples without ATP were incubated with the aforementioned amounts of WT protein (Lanes 2-5). Reactions were stopped with addition of 2 μg of competitor DNA and incubated for 10 min on ice. Gels were stained with SYBR Gold reagent. Black star indicates nucleosome-protein complex that was formed in the reaction independent from remodelling. **(C)** REA assays of WT, H1153R, R1164Q and sample with no remodeller. Radioactively labelled DNA was visualised by exposing the gels to Phosphoimager screen. **(D)** Quantification of gel from C. Cut and uncut DNA was quantified and ratio of cut and total DNA (cut plus uncut) was plotted as '% DNA cut'. Error bars represent SEM and are derived from 3 independent experiments. Plotting was done in GraphPad Prism using one phase decay equation.

4.1.2.3. Mutations adjacent to the Core 2 region of the ATPase domain show remarkably diverse effects on enzyme activity

Residues adjacent to the core 2 region have been shown to play a regulatory role in several different chromatin remodellers (Sen et al. 2011, Clapier and Cairns, 2012). In yeast CHD1 the C-terminal bridge connects both core regions of the ATPase domain (Hauk et al. 2010). In ISWI, the corresponding region forms the NegC domain which negatively regulates remodeling activity (Clapier and Cairns, 2012, Yan et al. 2016). In yeast SNF2 the corresponding region forms two alpha helices called Brace-I and Brace-II which together regulate remodelling activity. Two different mutations in this region of dMi-2 were biochemically analyzed. Leu1217Pro (from here on referred as L1217P) which resides in the putative Brace-II/NegC/C-terminal bridge region and His1198Tyr (H1198Y) which falls within the putative Brace region of dMi-2 (Figure 4.1.A). Point mutations were introduced into dMi-2 by site-directed mutagenesis as described in 3.2.2.1 and proteins were expressed and purified as described in 3.2.3.1 and 3.2.3.2. ATPase assays were performed and the activities of mutant dMi-2 was compared to the activity of WT protein. Interestingly, the two mutations showed remarkably different effects on ATPase function; while H1198Y was almost indistinguishable from WT with approximately 90% of WT ATPase activity, L1217P showed extremely low levels of hydrolysis (Figure 4.11). I analysed ATP binding of both mutants and found that they both fully retained their ability to bind ATP, showing that decreased ATPase activity of the L1217P mutant is not due to inability to bind ATP. When testing these point mutants in nucleosome bandshift assays, H1198Y bound nucleosomes with affinity equivalent to the WT protein. At the same time, the L1217P mutant displayed a moderately reduced affinity in binding to the nucleosome. At concentrations of 450nM and 225nM of L1217P protein the reduction in the binding to the nucleosome is readily apparent (Figure 4.11 D compare lanes 3 and 4 with 11 and 12).

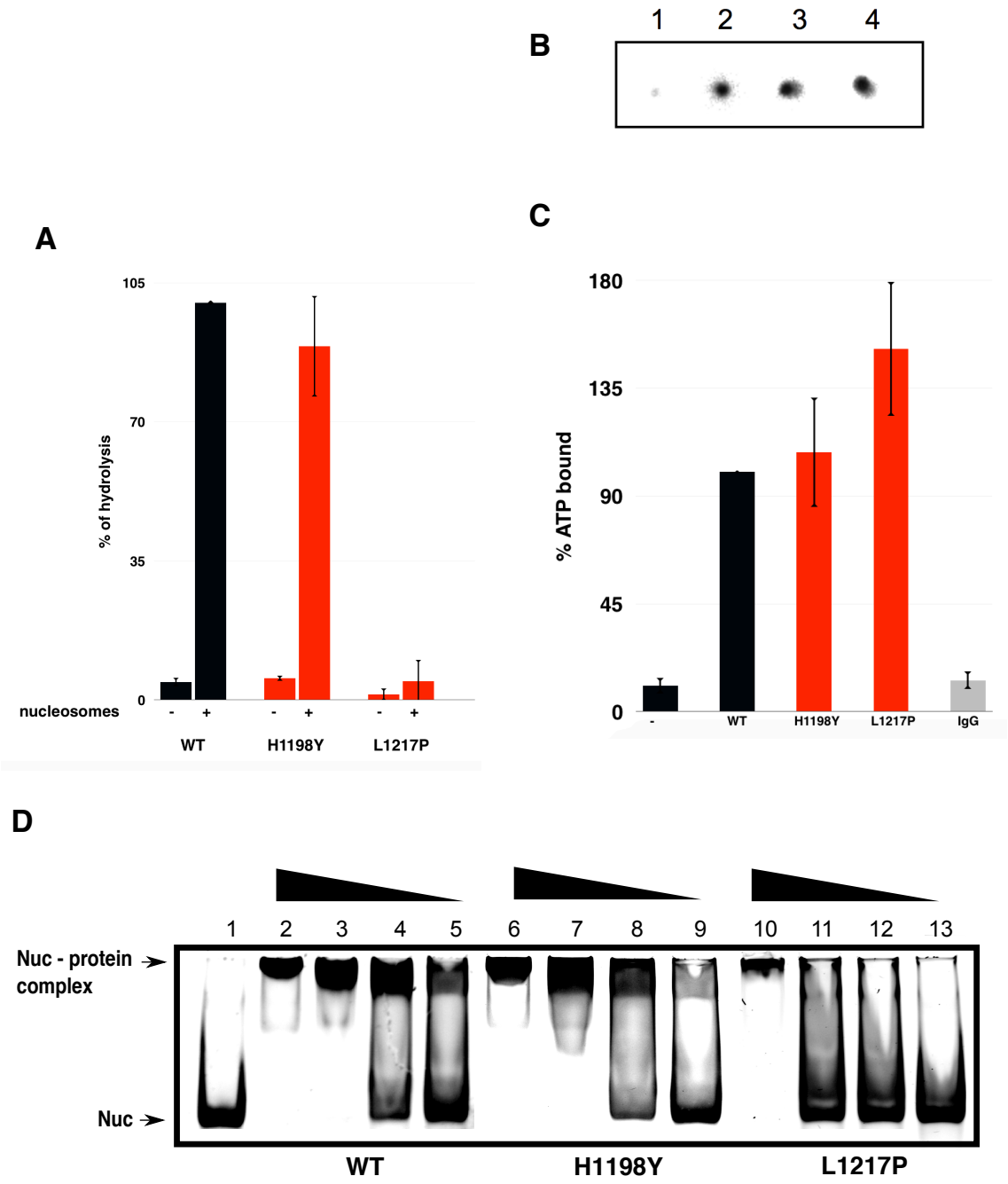

Figure 4.11. Mutants in Core 2 region differ in ATP hydrolysis, while retaining WT levels of ATP and nucleosome binding

(A) ATPase assay with saturating amounts of polynucleosomes assembled on a plasmid containing 12x601 Widom nucleosome positioning sequences. ATP hydrolysis levels of WT protein compared to H1198Y and L1217P point mutant in presence (+) or abscence of polynucleosomes (-) are shown. Error bars represent SEM and are derived from 3 independent

experiments. **(B)** ATP binding assay of sample without protein (1), WT protein (2) H1198Y (3) and L1217P (4) point mutant. **(C)** Quantification of data from B, IgG served as negative control. **(D)** Nucleosome binding assay with 150nM of end positioned mononucleosome assembled on 601 Widom sequence with 80bp DNA overhang, incubated with decreasing amounts (900nM, 450nM, 225nM and 113nM) of dMi-2 WT (lanes 2-5) H1198Y point mutant (lanes 6-9) and L1217P point mutant (lanes 10-13).

In order to determine their remodelling ability, I tested the mutants in nucleosome sliding and REA assays. Remarkably, in nucleosome sliding assays with end positioned mononucleosomes, the H1198Y mutant showed a higher remodelling capability than WT. H1198Y was able to move the histone octamer over a short distance at the lowest concentration of 14,12nM, while WT protein showed no detectable remodelling at concentrations lower than 56,5nM (Figure 4.12. A, lower panel, compare lanes 6-8, with lanes 13-15). At the higher concentration, it was observable that the WT protein preferred to slide nucleosomes from the end position to the central position (Figure 4.12.A, upper panel, lane 2-4). Unlike the WT protein, the H1198Y mutant generated a more equal distribution of nucleosomes at higher concentrations, suggesting that H1198Y slides nucleosomes both to the center and to the end of the DNA fragment with similar efficiency (Figure 4.13. A, lower panel, lanes 9-12). Similar results were obtained with centrally positioned nucleosomes. Moreover, the H1198Y mutant produced additional nucleosome positions with higher electrophoretic mobility, indicating a shift to the very end of the DNA fragment (Figure 4.12. B). In stark contrast, no remodelling was detected for the L1217P mutant using end or centrally positioned nucleosomes (Figure 4.12. A, lanes 10-13, Figure 4.12. C, lanes 14-17). To confirm the results from the sliding assays, the point mutants were analysed in the REA assay. Again, H1198Y exposed the MfeI restriction site to restriction enzyme more efficiently than the WT protein. At the 5 minute time point, when remodeling by WT dMi-2 can barely be detected, H1198Y had already remodelled about 10% of nucleosomes. At the 40 minute time point, WT protein had exposed about 20% of restriction sites to MfeI, while the H1198Y mutant had exposed about 50%. The L1217P mutant showed no detectable remodelling activity in the REA

assay. In conclustion, these results indicate that H1198Y belongs to the brace regulatory region of dMi-2, while L1217P resides in a new regulatory region of dMi-2 that is similar to the Brace-II/NegC/C-terminal bridge region of other remodelers.

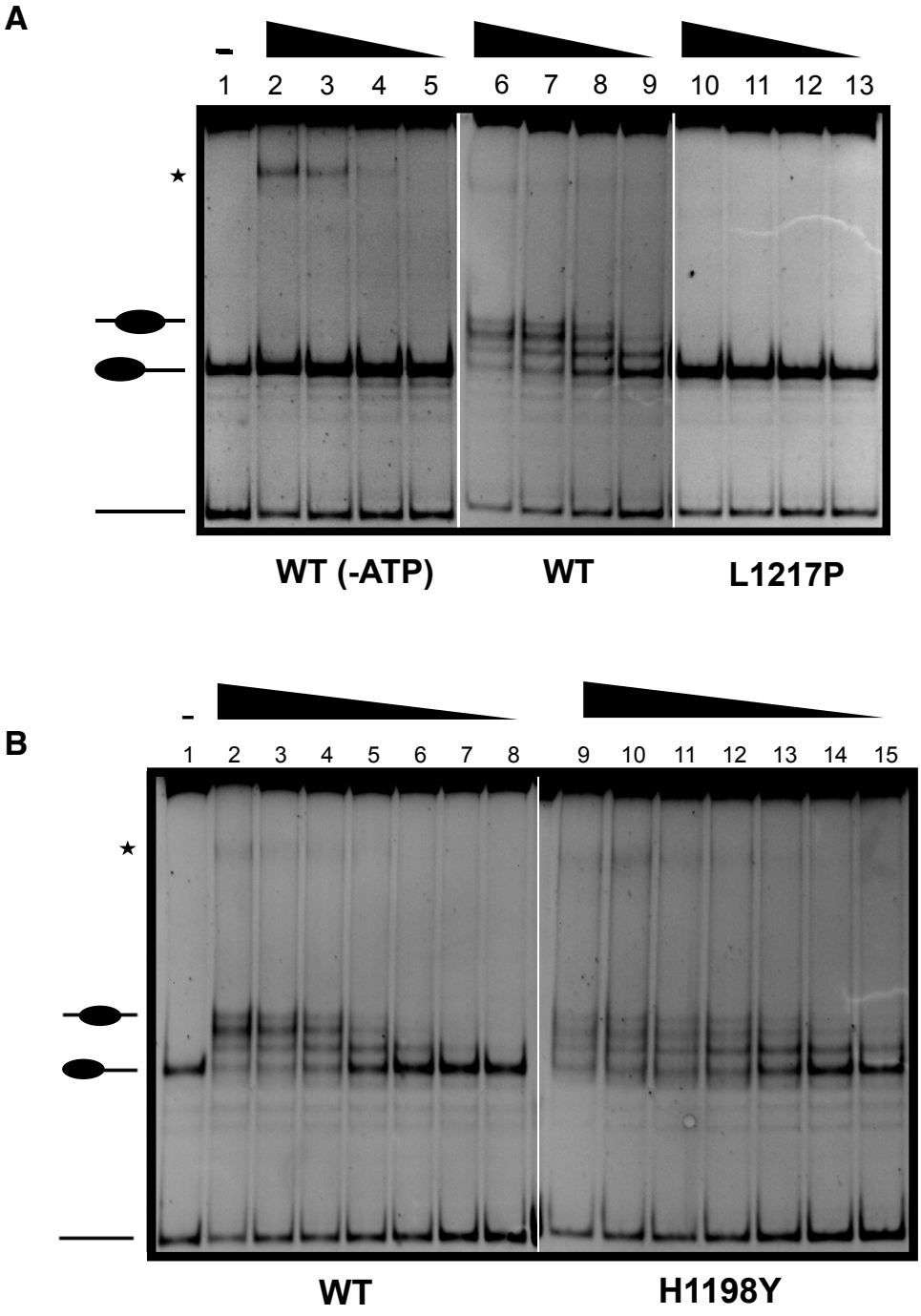

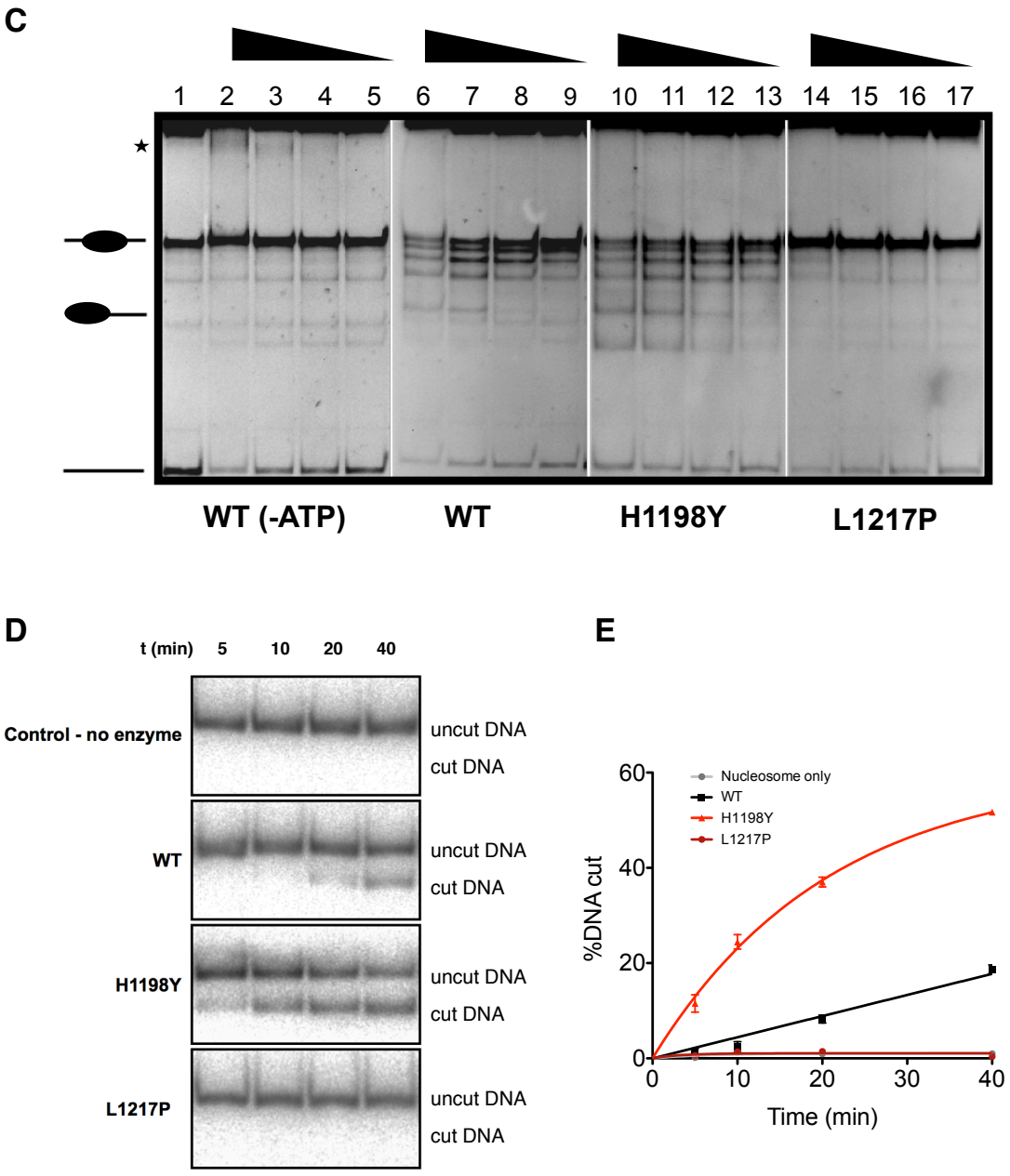

Figure 4.12. H1198Y and L1217P show remarkably different effects on chromatin remodelling

(A) Nucleosome sliding assay with 150nM of '0-77' end positioned mononucleosome incubated with decreasing amounts of WT and L1217P (900nM, 450nM, 225nM, 113nM) incubated at 26°C for 45 min. Samples without ATP were incubated with the aforementioned amounts of WT protein (Lane 2-5). Rections were stopped with addition of 2 μg of competitor DNA and incubated for 10 min on ice. Black star indicates nucleosome-protein complex that was formed in the reaction independent from remodelling. All panels shown are derived from same

experiment. Gels were stained with SYBR Gold reagent. **(B)** Nucleosome sliding assay with 150nM of '0-77' end positioned mononucleosome incubated with decreasing amounts of WT and H1198Y (900nM, 450nM, 225nM, 113nM, 56,5nM, 28,25nM, 14,12 nM) incubated at 26°C for 45 min. Reaction was stopped with addition of 2 μg of competitor DNA and incubated for 10 min on ice. Black star indicates nucleosome-protein complex that was formed in the reaction independent from remodelling. Gels were stained with SYBR Gold reagent. **(C)** Nucleosome sliding assay with '77-77' centrally positioned mononucleosome with increasing amounts of protein (900nM, 450nM, 225nM, 113nM) incubated at 26°C for 45 min. Samples without ATP were incubated with aforementioned amounts of WT protein (Lanes 2-5). Reaction was stopped with addition of 2 μg of competitor DNA and incubated for 10 min on ice. Gels were stained with SYBR Gold reagent. Black star indicates nucleosome-protein complex that was formed in the reaction independent from remodelling **(D)** REA assays of WT, H1198Y, L1217P and sample with no remodeller. Radioactively labelled DNA was visualised by exposing the gels to Phosphoimager screen. **(E)** Quantification of gel from C. Cut and uncut DNA was quantified and ratio of cut and total DNA (cut plus uncut) was plotted as '% DNA cut'. Error bars represent SEM and are derived from 3 independent experiments. Plotting was done in GraphPad Prism using the one phase decay equation.

4.2. *In vivo* analysis of dMi-2 cancer derived point mutants

The biochemical analysis uncovered that cancer derived point mutations cause a variety of different effects of dMi-2 enzymatic function. The mutants analysed have shown a plethora of effects, including loss or gain of function and uncoupling of ATP hydrolysis from chromatin remodeling. Since all mutations identified in endometrial cancer are heterozygous, this suggests that the mutants exert dominant negative or gain of function effects to contribute to oncogenesis. The next step in the analysis was to introduce these mutations into an *in vivo* system. This way it is possible to investigate if ectopic expression of mutants can affect cell proliferation and differentiation in *Drosophila melanogaster.*

4.2.1. Ectopic expression of dMi-2 point mutants using the UAS/ GAL4 system

After biochemical analysis of dMi-2 mutants, the question remained how are these biochemical effects manifested in an *in vivo* system? To answer that question, selected point mutants were introduced to *Drosophila*. C-terminally FLAG tagged dMi-2 WT and point mutants of interest were subcloned into the pUASt-attB target vector by Topo cloning and the Gateway system as described in 3.2.5.1. Using these plasmid constructs, transgenic flies carrying inducible UAS-dMi-2 WT or point mutant were created using the ϕ-C31 based integration system. In brief, vectors were injected into *Drosophila* embryos containing an attP docking site on the 3rd chromosome (3.2.5.1). Successful vector transformation into flies was confirmed by genomic DNA isolation and sequencing as described in 3.2.2.2. In the UAS/GAL4 expression system, the transgene of interest is under control of UAS (upstream activating sequence) sites that contain GAL4 binding sites. In order for the transgene to be expressed, flies carrying the transgene need to be crossed with driver lines containing an appropriate GAL4 gene, that will direct expression of the transgene to a particular tissue. In this study a GAL4 driver line called *engrailed* was used to direct the ectopic expression of dMi-2 to the posterior part of the developing wing. 5 different mutants - C452Y, R1164Q, L1217P, H1153R, H1198Y - and WT were used for ectopic expression in flies. Crosses were performed as described in 3.2.5.1 and the progeny of crossed flies was analysed for changes in posterior wing phenotype. The analysis of flies ectopically expressing WT dMi-2 revealed gain of posterior cross vein (PCV) material (Figure 4.13 A and C). This was an indication that it is possible to disrupt the differentiation of the PCV by an increase in dMi-2 activity. Ectopic expression of dMi-2 point mutants led to several different PCV phenotypes. These were divided into two main categories - gain of PCV and loss of PCV vein phenotype. The gain of PCV phenotype was further divided into two main classes - mild gain of PCV (ectopic PCV dot or ectopic PCV branch) and strong gain of PCV (ectopic PCV delta or ectopic PCV two branches) (Figure 4.13 A

and C). The loss of PCV vein phenotype is characterised by the loss of the connection to L4, L5 or both, indicating a disruption in the normal PCV differentiation programme and resulting irregular vein formations (Figure 4.13 B and C). Ectopic expression of any of the constructs, whether they were enzymatically active (WT, C452Y and H1198Y) or enzymatically impaired (L1217P, H1153R and R1164Q) gave rise to gain of PCV vein phenotypes, while the loss of PCV material phenotypes were exclusive to enzymatically impaired dMi-2 point mutants, indicating that they have a dominant negative or gain of function effect over endogenous dMi-2 protein. Over-expression of wild type dMi-2 showed mostly mild gain of PCV vein phenotypes (45,42%), a very low percentage (2,89%) of strong PCV vein phenotype and 51,69% of flies had no phenotype. Very similar effects were scored for the PHD finger point mutant which produced only mild gain of PCV phenotypes and no strong gain of PCV phenotype, with 0,65% of flies showing a loss of vein phenotype. For the hyperactive H1198Y mutant a high percentage of 20,63% wings displayed a strong gain of PCV phenotype and 67,92% a mild gain of PCV phenotype. Ectopic expression of L1217P, H1153R and R1164Q produced noticably different effects in fly wings. L1217P fly wings showed loss of PCV phenotype in 5,88 % of wings and gain in 62,95%, while the R1164Q point mutant showed a remarkably higher effect of 28,29% loss and 60,23% gain of vein phenotype. H1153R, the decoupling mutant, showed 8,89% of lost vein material, with 76,35% gain of phenotype (Figure 4.13 C). In all cases, loss of vein material manifested in shortening of PCV and loss of contact between L4 or L5, or both (Figure 4.13. B).

In conclusion, these results show that ectopic expression of dMi-2 WT, remodeling impaired point mutants or a hyperactive point mutant all affect wing development. Proteins that are still enzymatically active had an overall gain of PCV material, while loss of function mutants produced in addition loss of vein phenotypes. This suggests that dMi-2 could have a role in vein formation and regulation of wing patterning.

A

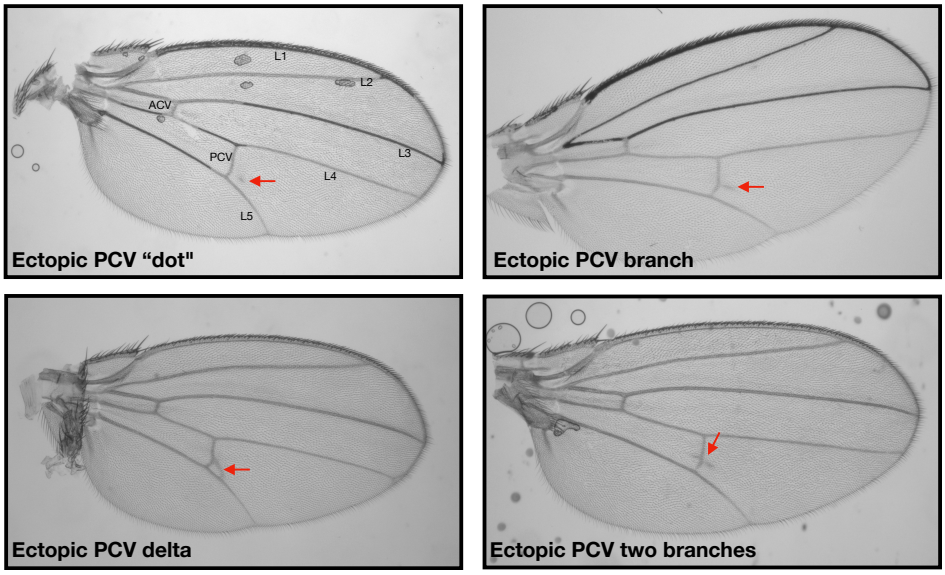
L1
L2
ACV
PCV
L3
L4
L5
Ectopic PCV “dot"
Ectopic PCV branch
Ectopic PCV delta
Ectopic PCV two branches

B

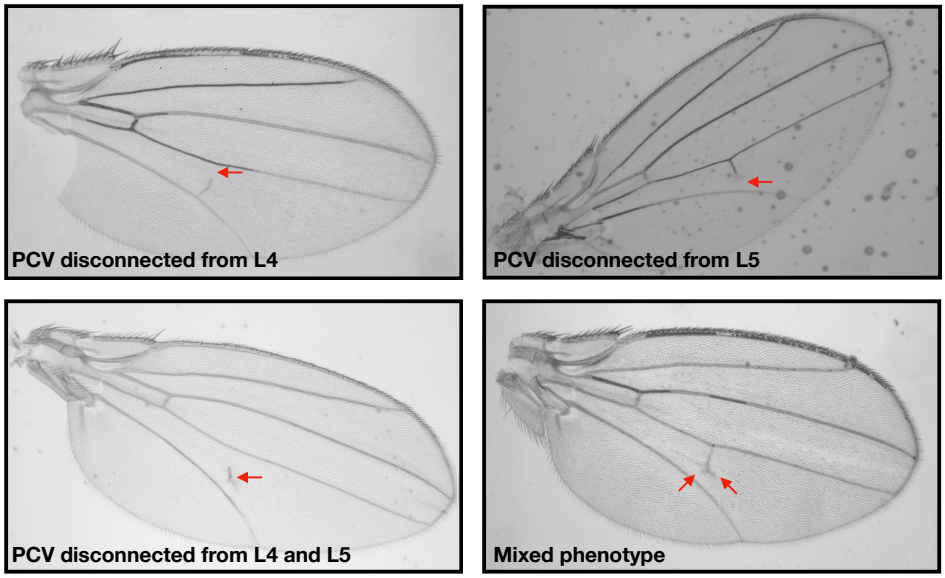
PCV disconnected from L4
PCV disconnected from L5
PCV disconnected from L4 and L5
Mixed phenotype

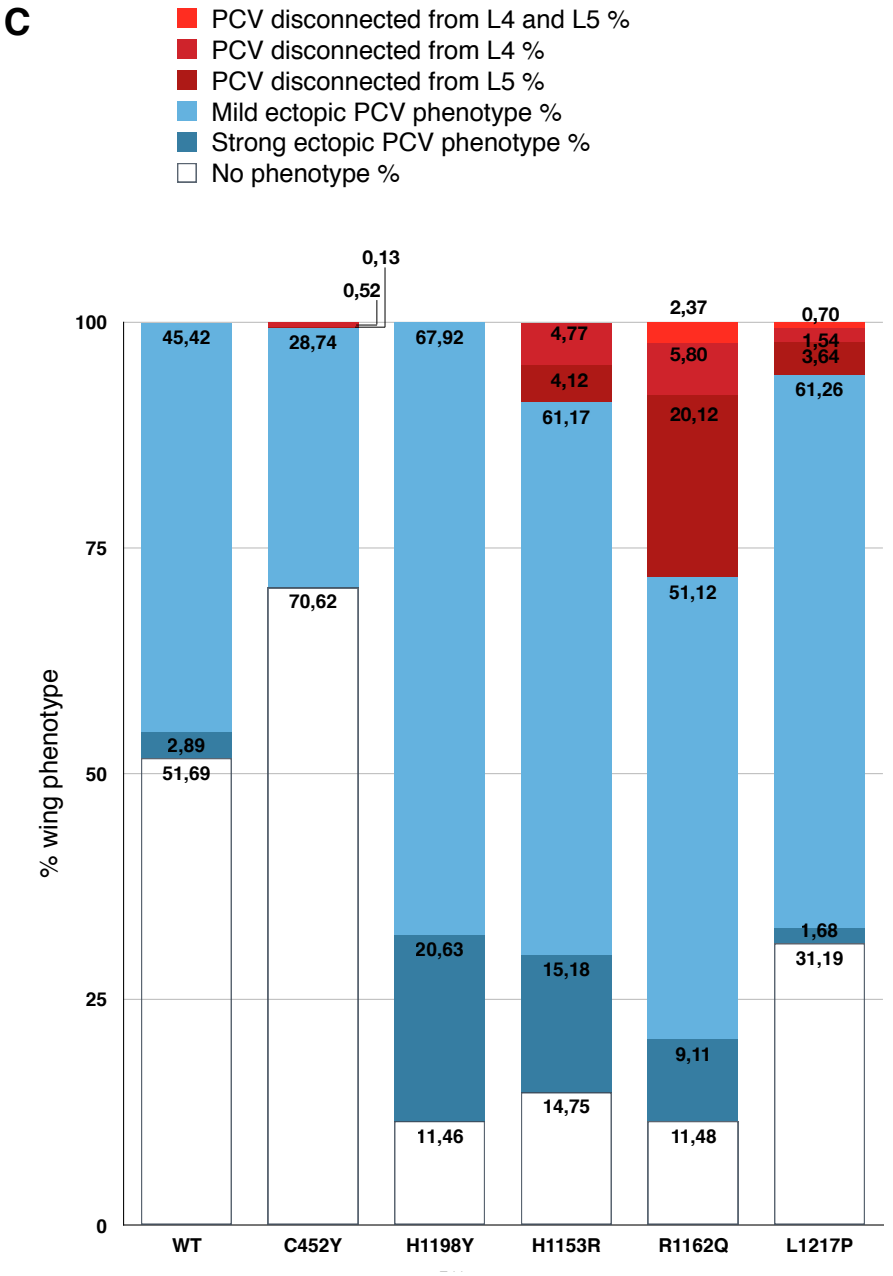

Figure 4.13. Over-expression of dMi-2 WT and point mutants leads to disruptions in the formation of wing structures

(A) Gain of PCV material phenotypes. Mild phenotype is characterised by formation of an additional 'dot' of PCV cells that is disconnected from the PCV (upper panel, left) or branching out of the PCV - ectopic PCV branch (upper panel, right). Strong gain phenotypes are

characterised by additional formation of a PCV delta (lower panel, left) or two ectopic PCV branches (lower panel, right). Malformed PCV structures are indicated by red arrows. The positions of longitudinal veins (L1 to L5), the anterior (ACV) and posterior (PCV) crossveins are indicated in the first panel on the left. **(B)** Loss of PCV material phenotypes. Loss of PCV connection to L4 (upper panel, left) or L5 (upper panel, right). Strong loss of PCV material is characterised by disconnection from both L4 and L5 (lower panel, left). A small percentage of wings showed a mixed phenotype with both gain and loss of vein material (lower panel, right). **(C)** Graph showing distribution (in %) of gain (blue) and loss (red) of PCV material for expression of WT and mutant dMi-2 as indicated. Relative ATPase and nucleosome remodelling activities are given for WT and point mutants below as determined in chapter 4.1.

5. Discussion

This thesis describes the first systematic analysis of the effects of endometrial cancer-derived point mutations on the enzymatic abilities of an ATP-dependent nucleosome remodeler. Several point mutations were introduced into PHD fingers, chromodomains and ATPase domain, as well as the C-terminal region of dMi-2. The biochemical analysis included ATP binding, nucleosome binding, ATP hydrolysis, nucleosome sliding, as well as ability to make nucleosomal DNA accessible for a restriction enzyme. This analysis revealed a plethora of effects that these mutations have on dMi-2's enzymatic and non-enzymatic functions. Studying these mutants revealed a new regulatory region outside of the ATPase domain that is important for modulating its activity. Additionally, this study used *Drosophila* as a model system, to investigate the effects of these point mutations in an *in vivo* system and demonstrated that cancer-derived point mutations in a nucleosome remodeler can change cell fate.

5.1. Point mutations produce a variety of effects on dMi-2's enzymatic activities

Cancer relevant point mutations in the chromatin remodeller dMi-2 are analysed *in vitro* and *in vivo* for the first time in this study. All identified mutations were predicted to severely effect enzymatic properties, since most of them map to the protein’s functional domains. Mutated residues within these domains are highly conserved throughout the CHD family and some, like R1164Q, in the entire SF2 superfamily. This study has revealed that these mutations do not always result in an inactive enzyme. Mutations impacted dMi-2 ATPase and remodelling functions in a variety of ways. Some mutants showed a moderate decrease in ATP hydrolysis and nucleosome remodelling, like the PHD finger mutant C452Y. On the other hand, H1198Y, a mutation located in putative brace region resulted in significantly higher activity in remodelling. Other mutations affected ATP hydrolysis in a relatively graded manner, while remodelling was severely

affected in all of them. This study provides new insights into how the chromatin remodelling machinery is affected in endometrial cancer.

5.2. Decoupling of ATP hydrolysis and nucleosome remodelling in dMi-2 mutants

In the past, amino acid substitutions and deletions of certain regions within chromatin remodellers have been shown to decouple ATP hydrolysis from chromatin remodelling. In yeast SWI/SNF, deletion of the highly conserved STRAGGLG sequence located in core 2, corresponding to helicase motif V, significantly reduced nucleosome sliding, while ATP hydrolysis was not affected (Smith and Peterson, 2005). Decoupling point mutants were also identified in other remodellers. In yeast CHD1, the N-terminal region between ATPase domain and DNA binding domain was identified to have a significant role in coupling ATPase activity with nucleosome remodelling. More specifically, mutations of amino acid residues in proximity of the core 2 domain of the ATPase motor were shown to severely impair nucleosome sliding. At the same time, ATP hydrolysis was only slightly reduced, indicating that the mutated residues are important for coupling efficiency of ATP hydrolysis and nucleosome remodelling (Patel et al. 2011). In yeast RSC, mutations located in the protrusion 1 domain of Sth1, positioned between the two ATP core domains, can improve coupling of ATP hydrolysis and nucleosome remodelling (Clapier et al. 2016).

In this study, two different mutants were identified to affect the coupling of ATP hydrolysis and nucleosome remodelling. H1153R in the core 2 domain and H1198Y in the brace region adjacent to the core 2. This is the first time decoupling mutants were identified in cancer cells. In both cases of decoupling mutants, histidine was the amino acid that was affected. Histidine is a polar amino acid with an imidazole side chain. It is often found in enzyme active sites. The pK_a of histidine is around 6.5, which is close to the physiological pH,

meaning that its side chain can relatively easily switch from neutral to positive charge. Because of this, it can be found both at positions that are buried inside of the protein core and exposed on the surface of the protein. Given all of its unique properties, histidine mutations can severly impact protein structure and function.

The H1153 residue is located in a highly conserved region, between motif V and VI of the second HELICc lobe (Figure 5.1.). Both of these motifs have significant roles in protein function. Motif V is involved in DNA binding, translocation and was shown to be crucial in coupling ATP hydrolysis with nucleosome remodelling (Smith and Peterson 2005). Motif VI contains highly conserved arginine finger that is important for ATP binding and hydrolysis. H1153 and the

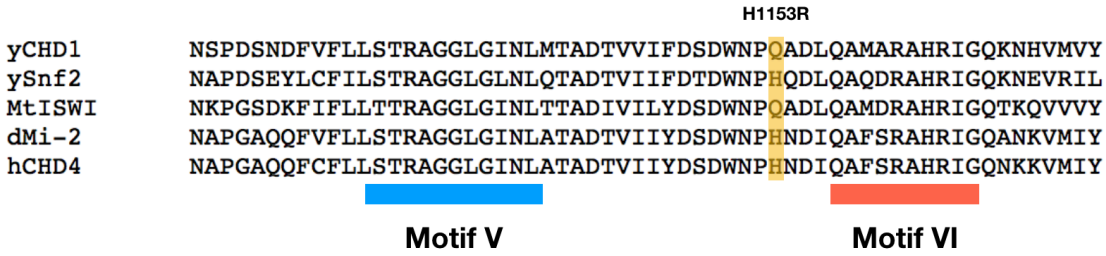

Figure 5.1. Decoupling mutant H1153R is located between helicase motif V and VI

Part of multiple sequence alignment of yeast CHD1, yeast Snf2, *Myceliophthora thermophila* ISWI, human CHD4 and *Drosophila* Mi-2 showing the motif V in blue and motif VI in red. Position of H1153R is marked in yellow.

region surrounding it are not a part of these motifs and their role in protein enzymatic function has been so far unknown. Considering the high level of conservation of residues surrounding H1153 as well as motifs V and VI in relative proximity, it is expected that mutation of this residue could have significant consequences on the catalytic function of dMi-2. Indeed, mutation to arginine seemed to disrupt translocation ability of dMi-2, since this mutant was inactive in both remodelling assays in this study (Figure 4.10.). At the same

time, this mutant kept relatively robust levels of ATP hydrolysis (Figure 4.9.A). This is reminiscent on deletions of motif V in related the chromatin remodeler in yeast Swi2/Snf2. Deletion of the entire motif V significantly impaired remodelling function of the protein, while leaving ATP hydrolysis mostly intact (Smith and Peterson, 2005).

In related proteins, it is noticeable that often histidine can be changed with glutamine, which could perform similar function to histidine, as it is also often found in protein active sites. Mutation to arginine, brings in a positively charged residue. Arginine is often involved in the formation of salt bridges, so it is conceivable that introducing this residue could form new interactions with neighbouring residues. This could affect communication between catalytically important parts of the protein. Taking all this into consideration, these results show that this residue is important for successful interaction between parts of the protein important for DNA and ATP binding and for its translocation along the DNA. It is conciveable that H1153 and its surrounding area are part of an important conserved catalytical motif. This mutation could also introduce changes to the structure of the region in a fundamental way. This change can in turn influence the interaction between key parts of the protein that would ultimately lead to the decoupling effect.

The second identified mutant to show altered coupling of ATP hydrolysis and nucleosome remodelling is H1198Y. This mutation is located in the C-terminal region of CHD4/dMi-2, adjacent to the core 2 domain. In other related remodellers, like *Drosophila* ISWI and yeast Snf2, this region is corresponding to the brace helix (Figure 5.2). This helix functions in the core 1 - core 2 communication in many SF2 proteins and it is important for coupling ATP hydrolysis with nucleosome remodelling (Yan et al. 2016, Liu et al. 2017). The brace helix interacts with other parts of the protein to regulate enyzmatic function. In Snf2 it interacts with another brace helix, known as brace II. In ISWI it interacts with the NegC domain and in CHD1 with the C-terminal bridge. They

all have an inhibitory effect on ATPase domain. Inhibition is released after binding of the protein to the nucleosome.

Unlike the other decoupling mutant H1153R, this mutant showed highly increased translocation ability. In both remodelling assays it was able to remodel more nucleosomes than the WT protein (Figure 4.12.). This indicates that an inhibitory role of the brace helix is weakened by introduction of tyrosine at this position. Nevertheless, although weakened, the brace helix is still able to maintain its inhibitory role, as the H1198Y mutant was still depending on the nucleosomes for effective ATP hydrolysis (Figure 4.11.A). ATP hydrolysis levels of this mutant were not significantly different from the WT protein. This result indicates that ATP hydrolyis is not a reason for increased nucleosome remodelling. It goes in favour of the hypothesis, that the increased nucleosome remodelling is a consequence of a diminished inhibitory effect of the brace helix on the ATPase domain.

Mutation of histidine to tyrosine introduced significant changes to dMi-2 enzymatic properties. The question remains how does this change arise? Both histidine and tyrosine contain an side chain with aromatic properties. Aromatic rings are often involved in stacking interactions with other aromatic side chains. However, functional groups of histidine and tyrosine could have different impact on enzymatic reaction, due to different pKa values of their side chain, histidine at 6.5, while tyrosine is at 10.4. Additionally, the histidine side chain has lower rotational degree of freedom and higher free energy compared to tyrosine due to its chemical structure (Doig, 1996). Taking all this together, this mutation could lead to lowering of the energy of the transition state during the enzymatic reaction, finally leading to more product, in this case a remodelled nucleosome. Interestingly, the corresponding residue to dMi-2 H1153 in yeast CHD1 is tyrosine. Introducing more neutral mutations, like alanine, at this position in dMi-2, could answer the question if the observed effects are really due to tyrosine at this position. Furthermore, mutating this residue in other related

remodelers could give more insight into the function of this residue, as well as the brace helix in CHD proteins.

This results demonstrate that H1198Y has improved coupling of ATP hydrolysis and nucleosome remodelling. These effects are reminiscent of mutations in the Sth1 protrusion 1 domain, where point mutations increase the levels of nucleosome sliding, while largely retaining the ATP hydrolysis levels (Clapier et al. 2016). In nucleosome sliding H1198Y showed that, besides an increased levels of remodelling with both end-positioned and centrally positioned nucleosomes, its remodelling produced a different nucleosome positioning patterns when using an end-positioned nucleosome template (Figure 4.12.B and C). These results reveal another potential consequence of this mutation *in vivo*. It is possible this mutant could produce differently positioned nucleosomes which could affect transcription of some genes in the cell. Aberrant transcription of some genes could lead to development of cancer. All taken together, these results show that coupling of ATP hydrolysis and nucleosome remodelling can be positively and negatively affected in cancer cells.

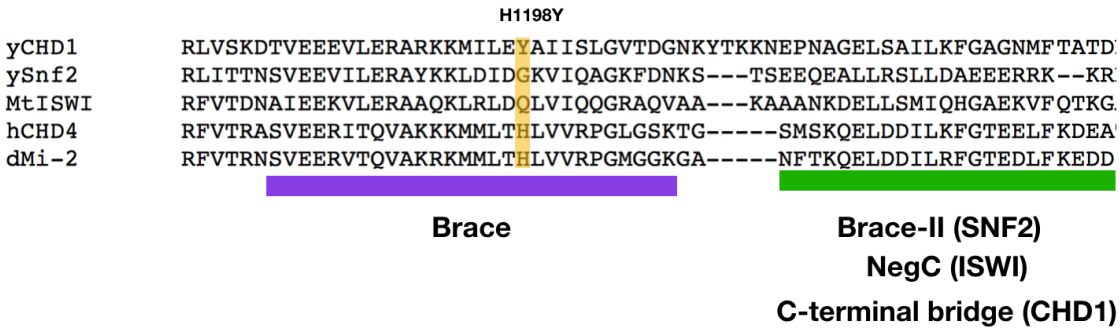

Figure 5.2. Decoupling mutation H1198Y resides in the Brace regulatory region of dMi-2

Part of multiple sequence alignment of yeast CHD1, yeast Snf2, *Myceliophthora thermophila* ISWI, human CHD4 and *Drosophila* Mi-2 showing the Brace region in purple and the Brace-II/ NegC/C-terminal bridge regions in green. Position of H1198Y is marked in yellow.

5.3. Mutations of PHD finger and chromodomains have distinct effects on enzymatic activity

Mutation of C452 affected dMi-2 in a modest manner. This residue in the PHD finger is involved in coordinating zinc binding together with other highly conserved residues of a $Cys_4His_1Cys_3$ motif. Considering the high conservation and functional importance of this residue it was interesting to investigate its consequences in a biochemical manner. Indeed, this mutant showed reduction in ATP hyrdolysis, which consequently resulted in a similar decrease of nucleosome remodelling (Figure 4.3. A and 4.4.). This reduction was observed with both end positioned and centrally positioned nucleosomes. These results agree well with previously published data from human CHD4, where deletion of the PHD fingers resulted in a moderate reduction in ATPase and remodelling capabilities. This reduction of ATP hydrolysis of the PHD finger mutant was only apparent with unmodified nucleosomes, while H3K4me modified histones did not show this reduced activity (Watson et al. 2012). This might be due to H3K4 methylation reducing the binding affinity of the CHD4 PHD fingers (Mansfield et al. 2011). In this study, nucleosomes were assembled with histones purified from *Drosophila* embryos. This means they contain a mixture of modified and unmodified histones. In the future, to determine how this mutation affects binding in the context of histone modifications, experiments will need to be performed with unmodifed and H3K4 methylated histones separately. In summary, these results reveal that a point mutation in one of the key cysteines in the PHD finger can have an effect on dMi-2 ATP hydrolysis and nucleosome remodelling abilities. Previously, it was demonstrated that deletion of PHD2 *in vivo* in B cells, causes a strong activation of the NuRD complex repressed gene *mb-1*, compared to deletion of PHD1 finger which caused weaker derepression (Musselman et al. 2012). Subsequently, it was shown that PHD2 has a role in the initiation of CHD4 recruitment to the nucleosome and that PHD1 interacts with the nucleosome after PHD2 binding, underlining the more important role of PHD2 for CHD4 nucleosome recruitment (Gatchalian et al. 2017). This taken

into account, it is conceivable, that C452Y could have similar consequences on CHD4's interaction with the nucleosome, hence reducing the protein's recruitment and stabilisation on the nucleosome. However, considering that C452Y demonstrated WT levels of nucleosome binding, this outcome seems unlikely (Figure 4.3.D.). Therefore, it is more likely that overall reduction in enzymatic activity of this mutant is due to disruption of intramolecular interactions. In addition, it is possible that this point mutation could have an effect on subunit interactions within the NuRD complex in cancer cells, as it is known that PHD fingers are required for CHD4 interaction with the HDAC1 subunit of the NuRD complex (Zhang et al. 1998).

Mutations within the chromodomains had strikingly different effects compared to the PHD finger mutation. Two mutations in the first chromodomain had a strong negative effect on the protein's ATP hydrolysis and nucleosome remodelling abilities (Figure 4.5 and 4.6). This indicated a functional importance of the region to which these mutation reside. The results presented in this thesis demonstrated that even a single point mutation in the chromodomains can have a severe impact on enzymatic functions. In the past, it was shown that dMi-2's chromodomains are DNA binding modules, which are binding to the nucleosome mostly through DNA-protein interactions. Deletion of the chromodomains critically impairs ATP hydrolysis, as well as nucleosome binding and remodelling (Bouazoune et al. 2002). More recently crystal structure studies of the related chromatin remodeler CHD1, revealed that chromodomains act as negative regulators of CHD1 ATPase activity. Chromodomains interact with both ATPase cores through a negatively charged alpha helix - the chromo wedge - and keep it in an inactive open conformation that is less susceptible to hydrolysis (Hauk et al. 2010). In this structure, residues corresponding to dMi-2 V538 and R552 are located on the opposite side from the ones making contacts with the ATPase domain (Figure 5.3). The question that is posed here is, why do single point mutations in this region affect the protein activity in such a dramatic way?

Some recent studies could provide an answer to this question. A study from the Bowman lab identified a short basic loop in the chromodomain 1 of Chd1 that directly contacts nucleosomal DNA at SHL1 (Nodelman et al. 2017). This interaction was also identified in the recent cryo-EM structure of yeast CHD1 bound to the nucleosome from the Patrick Cramer lab (Farnung et al. 2017). It is suggested that when CHD1 first interacts with the nucleosome, the chromodomains rotate from the ATPase domain and bind the nucleosome via this small basic loop. This rotation is supposed to disrupt the inhibitory effect of the chromo-wedge on the ATPase domain, by which it promotes ATP hydrolysis and chromatin remodelling. Interestingly, when overlapping dMi-2 amino acid residues V538 and R552 onto the crystal structure of yCHD1 it is revealed that these amino acid residues fall in the region flanking this basic loop (Figure 5.3. A and B). This suggests that these dMi-2 residues could have a role in interacting with nucleosomal DNA. It is also possible that mutations are bringing in structural changes that are affecting binding of other residues to nucleosomal DNA. These results support the hypothesis that the basic loop and the region between V538 and R552 are critical for establishing contacts between nucleosome and protein that are crucial for ATP hydrolysis and chromatin remodelling.

A

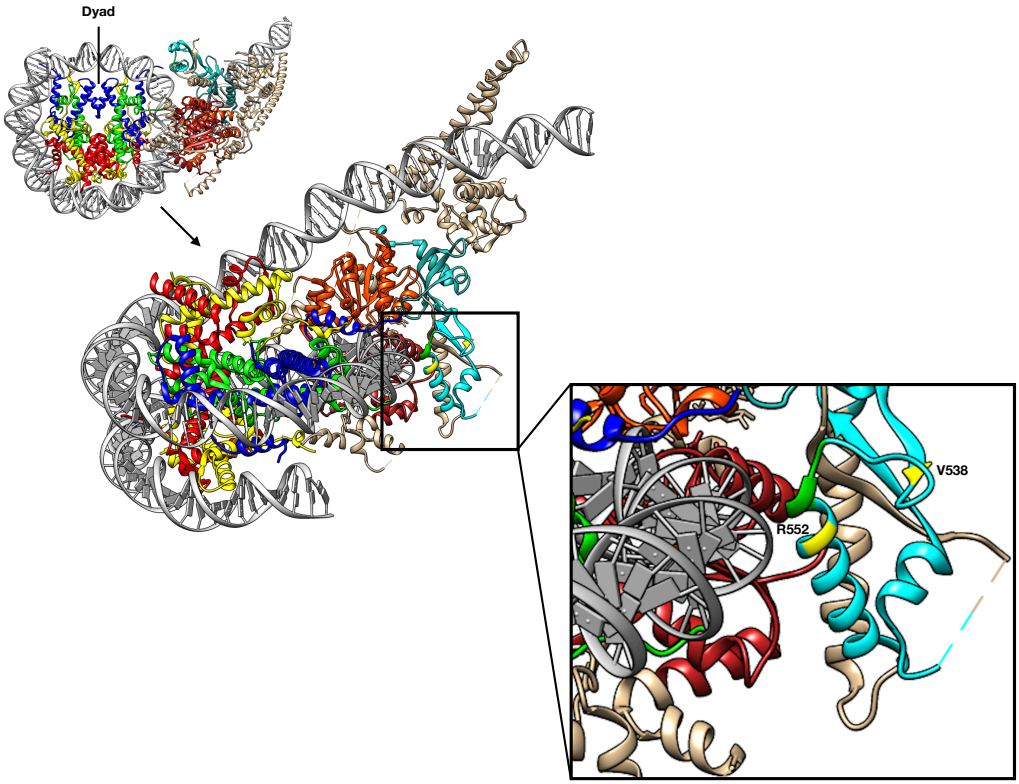

B

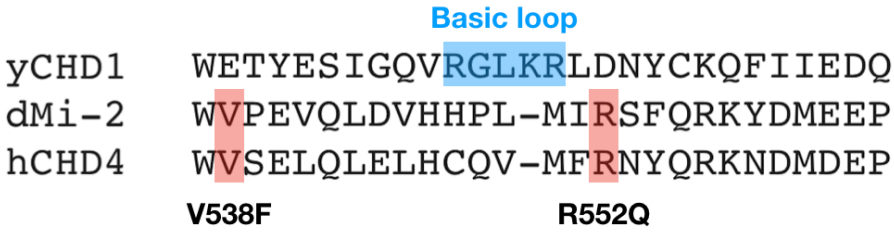

Figure 5.3. Role of chromodomain V538 and R552 residues in dMi-2 chromatin remodelling

(A) yCHD1 in complex with nucleosome (5O9G) with basic loop of chromodomain 1 indicated with green and superimposed relative positions of V538 and R552 in yellow (Chromodomain 1 in light blue, chromodomain 2 in cyan, ATPase domain core 1 orange red, ATPase domain core 2 in red. Core histones are shown in different colours; H3 in blue, H4 in green, H2A in yellow and H2B in red, nucleosomal DNA in gray), modified after Farnung et al. 2017 **(B)** Part of multiple sequence alignement of yeast CHD1, human CHD4 and *Drosophila* Mi-2 with basic loop indicated in blue. V538 and R558 residues indicated in red in CHD4 and dMi-2.

5.4. A mutation in a putative regulatory region which lies adjacent to the core 2 region

One of the mutations identified in endometrial cancer is affecting a leucine residue at the C-terminal side of the ATPase domain core 2 of CHD4. Mutation from leucine to proline in this position had a strong effect on ATP hydrolysis of dMi-2, which was strongly decreased (Figure 4.11). Accordingly, this reduction affected levels of nucleosome remodelling, which were not detectable in all of the remodelling assays in this study (Figure 4.12). The question that is presented here is why does a mutation to proline at this position, outside of any identified catalytical and regulatory regions in dMi-2, so dramatically affect protein enzymatic abilities? In related chromatin remodelers, a C-terminal side of the ATPase domain core 2 and brace has been identified as a regulatory region that controls the activity of the ATPase motor. In CHD1 this is a C-terminal bridge, in ISWI this region is called NegC, and in Snf2 Brace-II (Hauk et al. 2010, Clapier and Cairns, 2012, Liu et al. 2017). By superimposing the dMi-2 sequence on the CHD1 structure it is observable that L1217 falls within this alpha helix (Figure 5.3. B). Leucine is a hydrophobic amino acid that prefers alpha helical structures. The corresponding residue to dMi-2's L1217 in yeast Snf2 is L1254. This leucine falls within the Brace-II region of Snf2 and when mutated to aspartic acid (L1254D) it was shown to reduce DNA and nuclesome stimulated ATP hydrolysis activity by two to five fold. Even more importantly, this mutant was shown to have severely diminished nucleosome remodelling (Liu et al. 2017). Considering this published data about a related remodeller, high conservation levels of this leucine and results of this study it is possible to conclude that this residue has an important role.

However, Snf2 - L1254D still shows measurable levels of ATP hydrolysis, but dMi-2 - L1217P did not. This raises a question why L1217P showed no detectable ATP hydrolysis? An answer could be in the nature of amino acid change. Proline is an amino acid with distinct features compared to other amino

acids. It is often found in turns and outside of alpha helices and beta sheets. Because of its unique structure, mutations to proline often lead to disruption of entire regions and lead to protein instability. Therefore, it is conciveable that the effects that are observed in this study are combined effects of removing a functionally important leucine and its exchange with proline, an amino acid that will break the alpha helix in which this residue is likely located. This would lead to destabilisation of the protein structure and loss of enzymatic activity (Figure 5.3.B). Interestingly, this mutation also affected the nucleosome binding ability of dMi-2, indicating that this region could have a possible regulatory role in dMi-2's nucleosome binding (Figure 4.11.D). It is plausible, that the disruption of the entire region by introduction of proline could affect its interaction with the nucleosome. Furthermore, it is also feasible that leucine is directly binding to the nucleosome and loss of this interaction is leading to weaker binding to the nucleosome or formation of less stable nucleosome-protein complex.

In conclusion, this mutation caused a severe reduction in ATP hydrolysis and remodelling activities. This can be due to disruption of intramolecular interactions within the protein, possibility that this region has a role in regulating protein-nucleosome interaction or that leucine is directly involved in nucleosome binding resulting in weaker interaction with the nucleosome when mutation is introduced. These three possibilities are not mutually exclusive and are to be resolved in future studies. This study identifies a putative regulatory region adjacent to the brace in CHD4/dMi-2 enzymes, that has a similar role to regions identified in CHD1, ISWI, and Snf2.

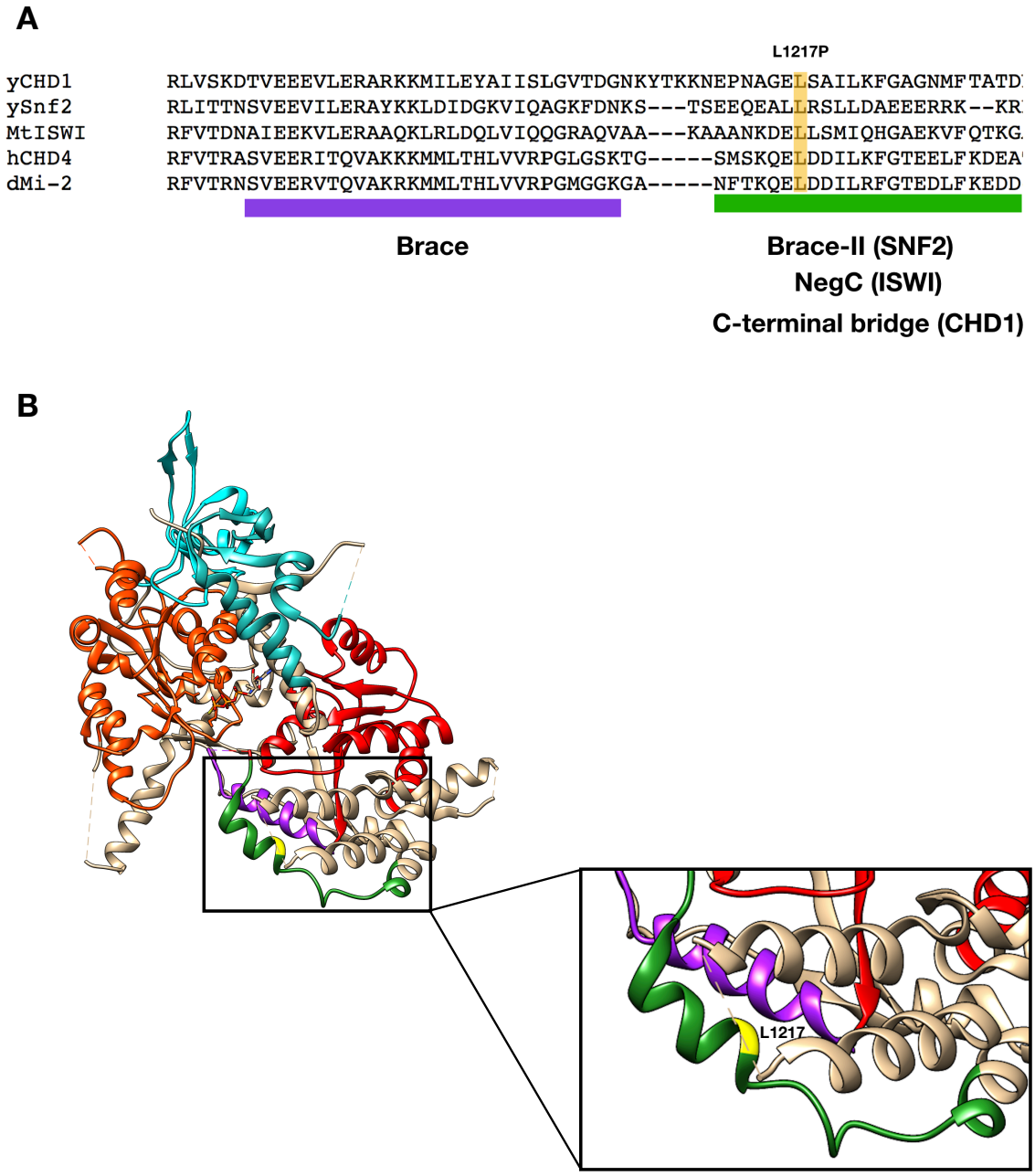

Figure 5.4. L1217 belongs to putative regulatory region in dMi-2

(A) Part of multiple sequence alignement of yeast CHD1, yeast Snf2, *Myceliophthora thermophila* ISWI, human CHD4 and *Drosophila* Mi-2 showing Brace region in purple and Brace-II/NegC/C-terminal bridge region in green. Position of L1217P is marked with yellow. **(B)** yCHD1 structure (3MWY) with Brace in purple and C-terminal bridge in green, with superimposed dMi-2-L1217 amino acid residue indicated in yellow (Chromodomain 1 in light blue, chromodomain 2 in cyan, ATPase domain core 1 orange red, ATPase domain core 2 in red) Modified after Hauk et al. 2010.

5.5. Other missense mutations within the ATPase domain

5.5.1. An arginine finger mutant is crucial for efficient coupling of ATP hydrolysis and nucleosome remodelling

The only residue that was identified in exome sequencing to be affected by a mutation in several patients was arginine 1162, belonging to the highly conserved arginines in the helicase motif VI (Le Gallo et al 2012, Zhao et al. 2012, The Cancer Genome Atlas Research Network, 2013) (Figure 5.5). In humans, this R1162 of CHD4 corresponds to R1164 in *Drosophila* dMi-2. This residue has been shown to be a hotspot, since the corresponding arginine was found to be mutated in CHD1 in prostate cancer (Huang et al. 2012). This motif located in ATPase domain core 2 is responsible for efficient coupling of ATP hydrolysis with nucleosome remodelling. The functional importance of this residue is in interaction of motif VI with ATP binding site of motif I in core 1 (Liu et al. 2017). Rotation of core 2 from its initial position by 40° to core 1 brings this two motifs together to couple efficient ATP hydrolysis with translocation (Farnung et al. 2017).

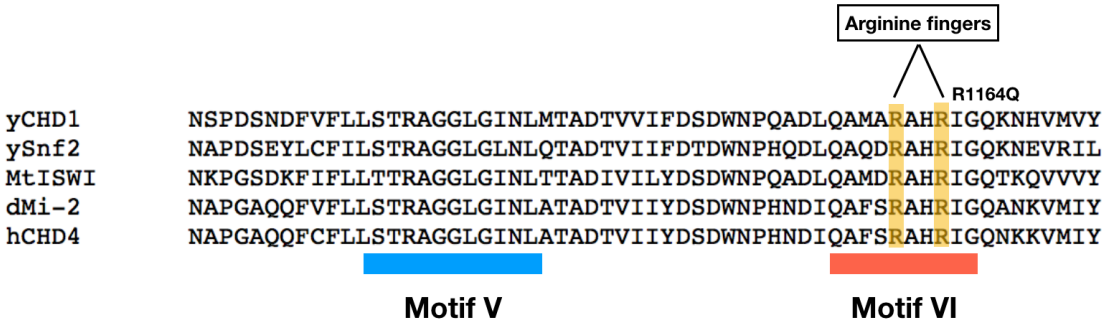

Figure 5.5. Arginine finger mutant in motif VI

Part of multiple sequence alignement of yeast CHD1, yeast Snf2, *Myceliophthora thermophila* ISWI, human CHD4 and *Drosophila* Mi-2 showing part of the core 2 sequence with motif V indicated with blue, motif VI indicated in red and two arginine finger, with R1164Q indicated, marked with yellow.

In the related SF2 protein, *Drosophila* RNA unwinding helicase Vasa, arginines corresponding to dMi-2 arginine fingers (R1161 and R1162) were identified to have somewhat distinct features. Arginine corresponding to R1161 was found to bind simultaneously α-, β-, and γ-phosphates, while arginine corresponding to R1164 was shown to interact with γ-phosphate (Sengoku et al. 2006). In this study introducing glutamine at the position of the highly conserved R1164, caused considerable decrease in ATP hydrolysis and subsequently nucleosome remodelling (Figure 4.9. and 4.10.). However, ATP hydrolysis and nucleosome remodelling were not completely lost, indicating that R1164Q mutant is still able to perform hydrolysis and couple it to remodelling. Interestingly, in the related SF2 helicase DbpA of *E.coli*, mutation of arginines corresponding to the arginine fingers in dMi-2, conferred different effects on the protein. Mutation of first arginine in the DbpA arginine finger (R1161 in *Drosophila*), to alanine had a more dramatic effect on the protein function, with dramatically reduced ATPase activity and no helicase activity. Meanwhile, mutation of the second arginine in the arginine finger (R1164 in *Drosophila*) had considerably less drastic effects, although still significantly reduced ATPase activity (Elles et al. 2007). Considering this published data and results of the study presented here, this could argue that in the R1164Q mutant, arginine at position 1161 is still interacting with ATP, which results in low levels of ATP hydrolysis and nucleosome remodelling. However, these results indicate that both arginines are essential for efficient ATP hydrolysis and remodelling.

Additionaly, a mutation from arginine to glutamine is introducing changes which are affecting charge and interaction with other amino acids. This change can also cause disruption of salt bridges which in turn would prevent efficient coupling of ATP hydrolysis with nucleosome remodelling.

5.5.2. The core 1 region mutation L914V leads to impaired ATP hydrolysis and nucleosome remodelling

The core 1 domain point mutant investigated in this study is L914V. This leucine is highly conserved throughout different chromatin remodellers (Figure 5.6) Exchanging this leucine with valine had a strong effect on ATP hydrolysis of dMi-2 (Figure 4.7.A). L914 is not a part of any known identified SF2 helicase motifs, but it is highly conserved throughout the Snf2 family of chromatin remodellers. It is located in the so-called conserved block H. These blocks are defined as unique structural features of Snf2 family enzymes (Flaus et al. 2006). Conserved block H comes right after helicase motif III and contains a few highly conserved aromatic residues (Figure 5.6). Motif III is involved in coupling of ATP

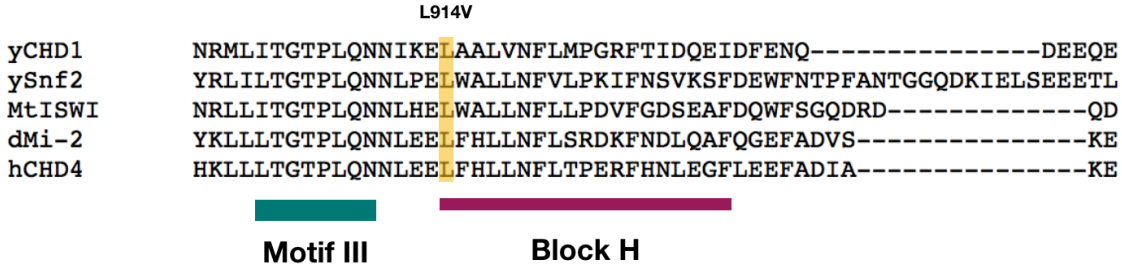

Figure 5.6. Highly conserved core 1 mutant L914V is located in Block H in proximity of helicase motif III

Part of multiple sequence alignement of yeast CHD1, yeast Snf2, *Myceliophthora thermophila* ISWI, human CHD4 and *Drosophila* Mi-2 showing part of the core 1 sequence with motif III indicated with green, block H in purpule and position of L914V indicated in yellow.

hydrolysis and translocation. More specifically, it is interacting with ATP binding motif II (Walker B) in core 1 and with motifs V and VI in the core 2 domain that are involved in DNA binding and translocation (motif V), and interaction with motif I and II in ATP binding (motif VI) (Sengoku et al. 2006, Flaus et al. 2006). Mutation of L914 to valine resulted in significant loss of ATP hydrolysis and nucleosome remodelling. The change from leucine to valine represents a

conservative mutation. However, it is possible that this point mutation brings in subtle structural changes that are difficult to tolerate. It is conceivable that the mutation from leucine to valine is changing intramolecular interactions in the region. Indeed, it is known that structurally, valine has a lower rotational degree of freedom and higher free energy compared to leucine (Doig, 1996). This could have a significant effect on amino acid interactions in this region and result in impaired enzymatic function.

When observing the CHD1 structure it is noticeable that L914 is part of an alpha helix, preceded by a motif III loop region. Changes brought on by this mutation could affect motif III, which would subsequently affect its interaction with motifs II, V and VI. In fact, this mutation had an effect on nucleosome binding which was mildly reduced in the nucleosome bandshift assay (Figure 4.7.D). Considering that motif V has a role in binding of nucleosomal DNA it is conceivable that interaction between motif III and V is affected. This weaker interaction of protein and nucleosome could lead to inappropriate positioning of helicase motifs in relation to the nucleosome and ATP. Indeed, in the related *S. cerevisiae* chromatin remodeler Snf2 the core 1 and core 2 domains stack together in the resting state. Upon binding of the nucleosome, these domains rotate by approximately 80° which generates a new core 1 - core 2 interface (Liu et al, 2017). It is conciveable that L914 is involved in the generation of these new core interactions. Introduction of valine could disrupt some of these interactions that result in impaired ATP hydrolysis and translocation.

In order to futher investigate the importance of this region, additional point mutations or deletions could be performed to more directly determine the role of this residue.

5.6. dMi-2 mutants disrupts *Drosophila* wing differentiation

Mutations introduced into dMi-2 exhibited a plethora of effects on protein activity *in vitro*. Different levels of ATP hydrolysis and nucleosome sliding suggested that, depending on the mutation, different consequences of these remodelling outcomes could be expected *in vivo*. To address this issue, several point mutations were introduced into *Drosophila*. Mutants analysed in this study were identified in endometrial cancer (Zhao et al. 2012., Le Gallo et. al 2012). Endometrial cancer develops when differentiation of epithelial cells of the endometrium is disrupted, which causes overproliferation. In order to study the consequences of these point mutations in an *in vivo* system, expression of point mutants was directed to the posterior part of the developing wing to study vein formation. Development of the *Drosophila* wing is an established model for epithelial morphogenesis (Restrepo et al. 2014).

Overexpression of WT dMi-2 or the mutants caused perturbations in normal posterior crossvein (PCV) differentiation, as formation of additional vein material was observed in all cases. Mutants that were active in remodelling *in vitro* displayed only gain of vein material, while mutants impaired in remodelling *in vitro* displayed in addition loss of vein material. Interestingly, remodelling levels of each protein correlate with both penetrance and severity of the different PCV phenotypes (Figure 4.13. C). The hyperactive mutant H1198Y displayed increased remodeling activity compared to the WT protein *in vitro*. This increase of activity was reflected in a stronger penetrance of the gain of vein material phenotype compared to ectopic expression of the WT protein. Similarily, a high penetrance of phenotype was also observed in mutants that are impaired in remodelling *in vitro*, but they also displayed significant loss of vein material. However, the extent of reduced remodelling activity *in vitro* did not completely mirror the severity of the loss of vein material phenotype. Some mutants with severe loss of remodelling like H1153R and L1217P had a lower penetrance of

the loss of vein material phenotype, compared to R1164Q whose translocation ability was still detectable in remodelling assays, but showed the most striking loss of PCV material. This could be explained by different expression levels of the various mutants. Additionally, mutants could exhibit differences in remodelling that were not observable in remodelling assays used in this study. Testing these mutants on different nucleosomal templates, like di- or tri-nucleosomes, could determine more fine difference in remodelling, that could explain their phenotype.

5.7. PCV differentiation and implications for endometrial cancer

In this experimental set up of the fly wing assay, overproliferation of epithelial cells was not observed. However, this analysis indicates that ectopic expression of dMi-2 is sufficient to perturb PCV differentiation. PCV differentiation is mostly under control of the TGF-β/BMP signalling pathway. In vertebrates the TGF-β (transforming growth factor β)/BMP (bone morphogenetic protein) axis plays an important role in bone organogenesis via activation of receptor serine/threonine kinases. Disturbance in this pathway can lead to the development of different types of clinical outcomes - skeletal anomalies, cardiovascular and autoimmune diseases or cancer (Rahman et al. 2015). In *Drosophila,* Decapentaplegic (Dpp), a homologue of BMP, is a morphogen that controls anterior-posterior patterning and growth of the wing (Matsuda et al. 2016). Similar phenotypes to the one observed in this study were detected with other chromatin regulators. *Drosophila* COMPASS-like complex, Cmi-Trr coactivator complex, contains Cmi as a core component which controls wing vein patterning through the conserved Dpp signaling pathway (Chauhan et al. 2013). Wing patterning was also found to be affected when LSD1/CoREST was depleted, which seems to affect the TGFβ/Dpp pathway (Curtis et al. 2012). Another example of a chromatin regulator and its role in wing patterning is given by *Drosophila* snr1, an essential component of the Brahma (SWI/SNF) complex. Impaired snr1 showed clear

defects in wing patterning, more specifically in PCV formation (Zraly et al. 2004). These examples together with the results of this study show that PCV differentiation is very sensitive to epigenetic imbalance brought on by disruption of a certain chromatin regulator. These results suggest that dMi-2 mutants that are impaired in remodelling, change the outcome of TGF-β/BMP signalling. Several examples of mammalian CHD4 influencing the TGF-β/BMP pathway through interaction with its components or by regulation of its target genes have been shown previously. As a part of the NuRD complex, CHD4 interacts with ZNF521, a zinc finger protein that is involved in BMP signaling (Bond et al. 2007). CHD4 was found to repress Sox9 during BMP2 induced chondrogenesis (Sun et al. 2013). In *Xenopus*, mutations of transcription factor Zeb2 (zinc-finger E-box-binding homeobox 2; also known as ZFHX1B or Sip1) lead to loss of NuRD recruitment and subsequent loss of transcriptional repression activity on the BMP4 gene promoter, another component of the BMP pathway (Verstappen et al. 2008). Another example of Zeb2 and NuRD interaction influencing TGF-β/BMP signalling pathway was reported in Schwann cell differentiation (Wu et al. 2016). Considering all the published reports and the data from this study it is possible to postulate that impaired or hyperactive dMi-2 can influence the outcome of TGF-β/BMP signalling pathway. How can this be done?

Aberrant dMi-2 activity can influence expression of its target genes by different remodelling levels, that lead to altered nucleosome positioning. For the hyperactive H1198Y mutant it was observed that it remodels nuclesomes in a different pattern than the WT protein. While the WT protein mostly moved nucleosome to the central position, H1198Y did not show this type of preference, and it was remodeling nucleosomes with no preference for a certain position (Figure 4.12. B and C). This kind of remodelling activity indicates that *in vivo* this mutant could either occlude or provide access to the transcription machinery at transcription factor binding sites. This could result in different expression levels of the target genes *in vivo* or aberrant expression of unrelated genes. In case of loss of function mutants, similar scenarios could be expected. Depending on the remodeling activities of the mutants, dMi-2 could

produce different remodelling outcomes. Since nucleosomes could protect some transcription factor binding sites the outcome could be insufficent or lack of expression of the TGF-β/BMP target genes and misregulation of entire signaling pathway. Furthermore, since CHD4 is, together with HDAC, a part of the NuRD complex it is possible that reduced or increased remodelling levels could lead to more or less deacetlyation, which would affect transcription levels of many target genes. This types of misregulation finally can affect differentiation of the wing cells.

The importance of the TGF-β/BMP pathway has been documented in the development and metastasis of endometrial cancer. Disturbing expression of TGF-β/BMP pathway components TGFβRII and SMAD4 can lead to the development of type I endometrial carcinomas (Piestrzeniewicz-Ulanska et al. 2004). Another study reported that TGF-β/BMP signaling has a role in driving tumorigenesis in endometrial cancer cells (Lei et al. 2009). Taken together, it is conceivable that dMi-2 mutants that obstructed proper PCV differentiation, use related molecular mechanisms to the ones used by CHD4 mutants in a transformation of epithelial cells of the endometrium that ultimately lead to cancer. Recently, a role od CHD4/NuRD in cell type transition was demonstrated in oral cancer. More specifically, loss of NuRD subunit DOC1 (deleted in oral cancer 1), was shown to affect NuRD-dependent repression of EMT (epithelial-mesenchymal transition) factors. Loss of NuRD-dependent repression drives the transition from mesenchymal to the epithelial cell type that leads to detachment of carcinoma cells and development of metastases in oral cancer (Mohd-Sarip et al. 2017).

5.8. Gain-of-function and dominant negative effect of CHD4 in endometrial cancer

Most of the identified mutations in CHD4 are falling within highly conserved regulatory domains and are predicted to negatively impact enzymatic function

(Zhao et al. 2012., Le Gallo et. al 2012). In that regard, together with the results of this study, where most of the analysed mutants show reduced or completely impaired enzymatic activity, it is possible that cancerogenesis is driven by a general reduction in CHD4 activity. Considering that most of the mutations identified in exome sequencing were missense mutations (89%), this seems unlikely. Haploinsufficiency is usually driven by the loss of one copy of the gene, which results in lower levels of the protein. This is mostly caused by frameshift mutations and deletions that are very rare in endometrial cancer. Since most of the mutation in endometrial cancer are missense, it is assumed that CHD4 also contributes to cancerogenesis through gain-of-function or dominant negative effect mechanisms. This is supported by my results of ectopic expression in the fly wing. In these experiments, expression of dMi-2 mutants was sufficient to disturb PCV differentiation, although flies still retain two copies of the endogenous dMi-2 gene (Figure 4.13. A and B).

As described above, these mutations could have an impact on nucleosome positioning *in vivo*. This was particularly clear for H1198Y that no longer has preferred directionality towards the center of the DNA fragment like the WT protein (Figure 4.12.B). Lower remodelling levels of these mutants could as well result in a different distribution of the nucleosomes, thereby changing expression levels of certain genes. These types of scenarios could lead to, for example, silencing of tumour suppressor genes (TSGs) like it was shown for human CHD4: In colorectal cancer, CHD4 can have an oncogenic function. More specifically, high expression of CHD4 was shown to maintain tumour suppressor gene silencing in colorectal cancer. To maintain this silencing and recruit other necessary factors, CHD4 ATPase activity is critical (Xia et al. 2017).

5.9. Conclusion

In summary, this thesis has given a detailed biochemical analysis of CHD4 cancer derived mutants. Analysed mutations revealed a plethora of effects on dMi-2 ATP hydrolysis and nucleosome remodelling. They displayed decreased ATP hydrolysis, impaired or increased nucleosome remodelling, decoupling of ATP hydrolysis from nucleosome remodelling, and changes in the pattern of nucleosome positioning. The difference in enzymatic activity and nucleosome positioning of each mutant will need to be taken into account when designing new drugs for cancer treatment. Therefore, in the design of new drugs for cancer treatment, a personalised approach might need to be taken. Drugs will need to be designed in a way that restores WT activity of CHD4. Furthermore, analysis of these mutants revealed possible new regulatory regions of dMi-2/CHD4, and has given strong biochemical support to recent structural studies and models about the remodeller's interaction with the nucleosome and how this interaction induces conformational changes that are relevant for the remodelling reaction.

6. References

Aasland, R., Gibson, T. J. & Stewart, A. F. The PHD finger: implications for chromatin-mediated transcriptional regulation. Trends Biochem. Sci. 20, 56—59 (1995).

Arents, G., Burlingame, R. W., Wang, B. C., Love, W. E. & Moudrianakis, E. N. The nucleosomal core histone octamer at 3.1 A resolution: a tripartite protein assembly and a left-handed superhelix. Proc. Natl. Acad. Sci. U. S. A. 88, 10148—10152 (1991).

Bagchi, A. et al. CHD5 Is a Tumor Suppressor at Human 1p36. Cell 128, 459–475 (2007).

Bajaj, K. et al. Stereochemical criteria for prediction of the effects of proline mutations on protein stability. PLoS Comput. Biol. 3, e241 (2007).

Banerjee, T. & Chakravarti, D. A peek into the complex realm of histone phosphorylation. Mol. Cell. Biol. 31, 4858—4873 (2011).

Bao, Y. et al. Nucleosomes containing the histone variant H2A.Bbd organize only 118 base pairs of DNA. EMBO J. 23, 3314—3324 (2004).

Barski, A. et al. High-resolution profiling of histone methylations in the human genome. Cell 129, 823—837 (2007).

Bergs, J. W. et al. Differential expression and sex chromosome association of CHD3/4 and CHD5 during spermatogenesis. PLoS One 9, e98203 (2014).

Bischof, J., Maeda, R. K., Hediger, M., Karch, F. & Basler, K. An optimized transgenesis system for Drosophila using germ-line-specific phiC31 integrases. Proc. Natl. Acad. Sci. U. S. A. 104, 3312—3317 (2007).

Black, B. E. et al. Structural determinants for generating centromeric chromatin. Nature 430, 578—582 (2004).

Blanc, R. S. & Richard, S. Regenerating muscle with arginine methylation. Transcription 8, 175—178 (2017).

Bond, H. M. et al. Early hematopoietic zinc finger protein-zinc finger protein 521: a candidate regulator of diverse immature cells. Int. J. Biochem. Cell Biol. 40, 848—854 (2008).

Bouazoune, K. & Kingston, R. E. Chromatin remodeling by the CHD7 protein is impaired by mutations that cause human developmental disorders. Proc. Natl. Acad. Sci. 109, 19238–19243 (2012).

Bouazoune, K. et al. The dMi-2 chromodomains are DNA binding modules important for ATP-dependent nucleosome mobilization. EMBO J. 21, 2430–2440 (2002).

Boyer, L. A. et al. Essential role for the SANT domain in the functioning of multiple chromatin remodeling enzymes. Mol. Cell 10, 935—942 (2002).

Boyer, L. A., Latek, R. R. & Peterson, C. L. The SANT domain: a unique histone-tail-binding module? Nat. Rev. Mol. Cell Biol. 5, 158—163 (2004).

Bradford, M. M. A rapid and sensitive method for the quantitation of microgram quantities of protein utilizing the principle of protein-dye binding. Anal. Biochem. 72, 248–254 (1976).

Brehm, a et al. dMi-2 and ISWI chromatin remodelling factors have distinct nucleosome binding and mobilization properties. EMBO J. 19, 4332–4341 (2000).

Burd, C. J., Kinyamu, H. K., Miller, F. W. & Archer, T. K. UV radiation regulates Mi-2 through protein translation and stability. J. Biol. Chem. 283, 34976—34982 (2008).

Burgess RJ, Zhang Z. Histone chaperones in nucleosome assembly and human disease. Nat Struct Mol Biol. 2013;20(1):14—22. doi:10.1038/nsmb.2461.

Cairns, B. R., Erdjument-Bromage, H., Tempst, P., Winston, F. & Kornberg, R. D. Two actin-related proteins are shared functional components of the chromatin-remodeling complexes RSC and SWI/SNF. Mol. Cell 2, 639—651 (1998).

Cairns, B. R., Kim, Y. J., Sayre, M. H., Laurent, B. C. & Kornberg, R. D. A multisubunit complex containing the SWI1/ADR6, SWI2/SNF2, SWI3, SNF5, and SNF6 gene products isolated from yeast. Proc. Natl. Acad. Sci. U. S. A. 91, 1950—1954 (1994).

Carlson, M., Osmond, B. C. & Botstein, D. Mutants of yeast defective in sucrose utilization. Genetics 98, (1981).

Changolkar, L. N. & Pehrson, J. R. Reconstitution of nucleosomes with histone macroH2A1.2. Biochemistry 41, 179—184 (2002).

Chauhan, C., Zraly, C. B. & Dingwall, A. K. The Drosophila COMPASS-like Cmi-Trr coactivator complex regulates dpp/BMP signaling in pattern formation. Dev. Biol. 380, 185–198 (2013).

Chen, Z., Yang, H. & Pavletich, N. P. Mechanism of homologous recombination from the RecA-ssDNA/dsDNA structures. Nature 453, 489—484 (2008).

Chow, C.-M. et al. Variant histone H3.3 marks promoters of transcriptionally active genes during mammalian cell division. EMBO Rep. 6, 354–60 (2005).

Clapier, C. R. & Cairns, B. R. The biology of chromatin remodeling complexes. Annu Rev Biochem 78, (2009).

Clapier, C. R. et al. Regulation of DNA Translocation Efficiency within the Chromatin Remodeler RSC/Sth1 Potentiates Nucleosome Sliding and Ejection. Mol. Cell 62, 453—461 (2016).

Clapier, C. R. & Cairns, B. R. Regulation of ISWI involves inhibitory modules antagonized by nucleosomal epitopes. Nature 492, 280–284 (2012).

Corona, D. F. V & Tamkun, J. W. Multiple roles for ISWI in transcription, chromosome organization and DNA replication. Biochim. Biophys. Acta 1677, 113—119 (2004).

Costanzi, C. & Pehrson, J. R. Histone macroH2A1 is concentrated in the inactive X chromosome of female mammals. Nature 393, 599—601 (1998).

Cox, M. M. Regulation of bacterial RecA protein function. Crit. Rev. Biochem. Mol. Biol. 42, 41—63 (2007).

Curtis, B. J., Zraly, C. B. & Dingwall, A. K. Drosophila LSD1-CoREST demethylase complex regulates DPP/TGFβ Signaling during wing development. Genesis 51, 16–31 (2013).

Dang, W. & Bartholomew, B. Domain Architecture of the Catalytic Subunit in the ISW2-Nucleosome Complex. Mol. Cell. Biol. 27, 8306–8317 (2007).

Deciphering Developmental Disorders Study. Prevalence and architecture of de novo mutations in developmental disorders. Nature 542, 433—438 (2017).

Delmas, V., Stokes, D. G. & Perry, R. P. A mammalian DNA-binding protein that contains a chromodomain and an SNF2/SWI2-like helicase domain. Proc. Natl. Acad. Sci. U. S. A. 90, 2414–8 (1993).

Denslow, S. A. & Wade, P. A. The human Mi-2/NuRD complex and gene regulation. Oncogene 26, 5433—5438 (2007).

Deuring, R. et al. The ISWI chromatin-remodeling protein is required for gene expression and the maintenance of higher order chromatin structure in vivo. Mol. Cell 5, 355—365 (2000).

Doig, A. J. Thermodynamics of amino acid side-chain internal rotations. Biophys. Chem. 61, 131—141 (1996).

Elles, L. M. S. & Uhlenbeck, O. C. Mutation of the arginine finger in the active site of Escherichia coli DbpA abolishes ATPase and helicase activity and confers a dominant slow growth phenotype. Nucleic Acids Res. 36, 41—50 (2008).

F.X. Wilhelm, M.L Wilhelm, M. Erard, M. P. D. Reconstitution of chromatin: assembly of the nucleosome. Nucleic Acids Res. 5, 3493–3502 (1978).

Falkenberg, K. J. & Johnstone, R. W. Histone deacetylases and their inhibitors in cancer, neurological diseases and immune disorders. Nat. Rev. Drug Discov. 13, 673—691 (2014).

Fan, H.-Y., He, X., Kingston, R. E. & Narlikar, G. J. Distinct strategies to make nucleosomal DNA accessible. Mol. Cell 11, 1311—1322 (2003).

Farnung, L., Vos, S. M., Wigge, C. & Cramer, P. Nucleosome-Chd1 structure and implications for chromatin remodelling. Nature 550, 539—542 (2017).

Fasulo, B. et al. The Drosophila MI-2 chromatin-remodeling factor regulates higher-order chromatin structure and cohesin dynamics in vivo. PLoS Genet. 8, e1002878 (2012).

Feng, Q. & Zhang, Y. The MeCP1 complex represses transcription through preferential binding, remodeling, and deacetylating methylated nucleosomes. Genes Dev. 15, 827—832 (2001).

Fischle, W. et al. Regulation of HP1-chromatin binding by histone H3 methylation and phosphorylation. Nature 438, 1116—1122 (2005).

Flanagan, J. F. et al. Double chromodomains cooperate to recognize the methylated histone H3 tail. Nature 438, 1181—1185 (2005).

Flaus, A., Martin, D. M. A., Barton, G. J. & Owen-Hughes, T. Identification of multiple distinct Snf2 subfamilies with conserved structural motifs. Nucleic Acids Res. 34, 2887–2905 (2006).

Gamble, M. J. & Kraus, W. L. Multiple facets of the unique histone variant macroH2A: from genomics to cell biology. Cell Cycle 9, 2568—2574 (2010).

Gatchalian, J. et al. Accessibility of the histone H3 tail in the nucleosome for binding of paired readers. Nat. Commun. 8, 1489 (2017).

Gautier, T. et al. Histone variant H2ABbd confers lower stability to the nucleosome. EMBO Rep. 5, 715—720 (2004).

Greer, E. L. & Shi, Y. Histone methylation: a dynamic mark in health, disease and inheritance. Nat. Rev. Genet. 13, 343–357 (2012).

Grüne, T. et al. Crystal structure and functional analysis of a nucleosome recognition module of the remodeling factor ISWI. Mol. Cell 12, 449—460 (2003).

Hake, S. B. et al. Serine 31 phosphorylation of histone variant H3.3 is specific to regions bordering centromeres in metaphase chromosomes. Proc. Natl. Acad. Sci. U. S. A. 102, 6344—6349 (2005).

Hamiche, A., Sandaltzopoulos, R., Gdula, D. A. & Wu, C. ATP-dependent histone octamer sliding mediated by the chromatin remodeling complex NURF. Cell 97, 833—842 (1999).

Hauk, G., McKnight, J. N., Nodelman, I. M. & Bowman, G. D. The Chromodomains of the Chd1 Chromatin Remodeler Regulate DNA Access to the ATPase Motor. Mol. Cell 39, 711–723 (2010).

Hoffmeister, H. et al. CHD3 and CHD4 form distinct NuRD complexes with different yet overlapping functionality. Nucleic Acids Res. 1–21 (2017). doi: 10.1093/nar/gkx711

Hoppmann, V. et al. The CW domain, a new histone recognition module in chromatin proteins. EMBO J. 30, 1939—1952 (2011).

Huang, S. et al. Recurrent deletion of CHD1 in prostate cancer with relevance to cell invasiveness. Oncogene 31, 4164—4170 (2012).

Ito, T., Bulger, M., Pazin, M. J., Kobayashi, R. & Kadonaga, J. T. ACF, an ISWI-containing and ATP-utilizing chromatin assembly and remodeling factor. Cell 90, 145—155 (1997).

Ito, T. et al. ACF consists of two subunits, Acf1 and ISWI, that function cooperatively in the ATP-dependent catalysis of chromatin assembly. Genes Dev. 13, 1529–1539 (1999).

Jacobs, S. A. et al. Specificity of the HP1 chromo domain for the methylated N-terminus of histone H3. EMBO J. 20, 5232–5241 (2001).

Jin, C. & Felsenfeld, G. Nucleosome stability mediated by histone variants H3.3 and H2A.Z. Genes Dev. 21, 1519—1529 (2007).

Jones, D. O., Cowell, I. G. & Singh, P. B. Mammalian chromodomain proteins: Their role in genome organisation and expression. BioEssays 22, 124–137 (2000).

Kalashnikova, A. A., Porter-Goff, M. E., Muthurajan, U. M., Luger, K. & Hansen, J. C. The role of the nucleosome acidic patch in modulating higher order chromatin structure. J. R. Soc. Interface 10, 20121022 (2013).

Kassabov, S. R., Zhang, B., Persinger, J. & Bartholomew, B. SWI/SNF unwraps, slides, and rewraps the nucleosome. Mol. Cell 11, 391—403 (2003).

Kim, J. et al. Blocking promiscuous activation at cryptic promoters directs cell type-specific gene expression. Science 356, 717—721 (2017).

Kim, M. S., Chung, N. G., Kang, M. R., Yoo, N. J. & Lee, S. H. Genetic and expressional alterations of CHD genes in gastric and colorectal cancers. Histopathology 58, 660—668 (2011).

Kouzarides, T. Chromatin modifications and their function. Cell 128, 693—705 (2007).

Kreher, J. et al. EcR recruits dMi-2 and increases efficiency of dMi-2-mediated remodelling to constrain transcription of hormone-regulated genes. Nat. Commun. 8, 14806 (2017).

Kunert, N. & Brehm, A. Mass production of Drosophila embryos and chromatographic purification of native protein complexes. Methods Mol. Biol. 420, 359—371 (2008).

Kunert, N. et al. dMec: a novel Mi-2 chromatin remodelling complex involved in transcriptional repression. EMBO J. 28, 533–44 (2009).

Längst, G., Bonte, E. J., Corona, D. F. V. & Becker, P. B. Nucleosome movement by CHRAC and ISWI without disruption or trans-displacement of the histone octamer. Cell 97, 843–852 (1999).

Längst, G. & Manelyte, L. Chromatin Remodelers: From Function to Dysfunction. Genes (Basel). 6, 299—324 (2015).

Le Gallo, M. et al. Exome sequencing of serous endometrial tumors identifies recurrent somatic mutations in chromatin-remodeling and ubiquitin ligase complex genes. Nat. Genet. 44, 1310–5 (2012).

Lei, X., Wang, L., Yang, J. & Sun, L.-Z. TGFbeta signaling supports survival and metastasis of endometrial cancer cells. Cancer Manag. Res. 2009, 15—24 (2009).

Leonard, J. D. & Narlikar, G. J. A Nucleotide-Driven Switch Regulates Flanking DNA Length Sensing by a Dimeric Chromatin Remodeler. Mol. Cell 57, 850–859 (2015).

Levenstein, M. E. & Kadonaga, J. T. Biochemical analysis of chromatin containing recombinant Drosophila core histones. J. Biol. Chem. 277, 8749—8754 (2002).

Liu, X., Li, M., Xia, X., Li, X. & Chen, Z. Mechanism of chromatin remodelling revealed by the Snf2-nucleosome structure. Nature 544, 440–445 (2017).

Logie, C. & Peterson, C. L. Catalytic activity of the yeast SWI/SNF complex on reconstituted nucleosome arrays. EMBO J. 16, 6772–82 (1997).

Lowary, P. . & Widom, J. New DNA sequence rules for high affinity binding to histone octamer and sequence-directed nucleosome positioning. J. Mol. Biol. 276, 19–42 (1998).

Luger, K., Mäder, a W., Richmond, R. K., Sargent, D. F. & Richmond, T. J. Crystal structure of the nucleosome core particle at 2.8 A resolution. Nature 389, 251–260 (1997).

Luo, J., Su, F., Chen, D., Shiloh, A. & Gu, W. Deacetylation of p53 modulates its effect on cell growth and apoptosis. Nature 408, 377—381 (2000).

Lusser, A., Urwin, D. L. & Kadonaga, J. T. Distinct activities of CHD1 and ACF in ATP-dependent chromatin assembly. Nat. Struct. Mol. Biol. 12, 160–166 (2005).

Malik, H. S. & Henikoff, S. Phylogenomics of the nucleosome. Nat. Struct. Biol. 10, 882—891 (2003).

Manning, B. J. & Yusufzai, T. The ATP-dependent chromatin remodeling enzymes CHD6, CHD7, and CHD8 exhibit distinct nucleosome binding and remodeling activities. J. Biol. Chem. 292, 11927–11936 (2017).

Mansfield, R. E. et al. Plant homeodomain (PHD) fingers of CHD4 are histone H3-binding modules with preference for unmodified H3K4 and methylated H3K9. J. Biol. Chem. 286, 11779–11791 (2011).

Marfella, C. G. A. & Imbalzano, A. N. The Chd family of chromatin remodelers. Mutat. Res. 618, 30—40 (2007).

Marmorstein, R. & Berger, S. L. Structure and function of bromodomains in chromatin-regulating complexes. Gene 272, 1—9 (2001).

Martens, J. A. & Winston, F. Recent advances in understanding chromatin remodeling by Swi/Snf complexes. Curr. Opin. Genet. Dev. 13, 136—142 (2003).

Masliah-Planchon, J., Bièche, I., Guinebretière, J.-M., Bourdeaut, F. & Delattre, O. SWI/SNF chromatin remodeling and human malignancies. Annu. Rev. Pathol. 10, 145—171 (2015).

Mathieu, E.-L. et al. Recruitment of the ATP-dependent chromatin remodeler dMi-2 to the transcribed region of active heat shock genes. Nucleic Acids Res. 40, 4879—4891 (2012).

Matsuda, S., Harmansa, S. & Affolter, M. BMP morphogen gradients in flies. Cytokine Growth Factor Rev. 27, 119–127 (2016).

McNeill, H. Sticking together and sorting things out: adhesion as a force in development. Nat. Rev. Genet. 1, 100—108 (2000).

Mito, Y., Henikoff, J. G. & Henikoff, S. Genome-scale profiling of histone H3.3 replacement patterns. Nat. Genet. 37, 1090—1097 (2005).

Mizuguchi, G., Tsukiyama, T., Wisniewski, J. & Wu, C. Role of nucleosome remodeling factor NURF in transcriptional activation of chromatin. Mol. Cell 1, 141—150 (1997).

Mizuguchi, G. et al. ATP-driven exchange of histone H2AZ variant catalyzed by SWR1 chromatin remodeling complex. Science 303, 343—348 (2004).

Mohd-Sarip, A. et al. DOC1-Dependent Recruitment of NURD Reveals Antagonism with SWI/SNF during Epithelial-Mesenchymal Transition in Oral Cancer Cells. Cell Rep. 20, 61—75 (2017).

Mohrmann, L. et al. Differential targeting of two distinct SWI/SNF-related Drosophila chromatin-remodeling complexes. Mol. Cell. Biol. 24, 3077—3088 (2004).

Morrison, A. J. & Shen, X. Chromatin remodelling beyond transcription: the INO80 and SWR1 complexes. Nat. Rev. Mol. Cell Biol. 10, 373—384 (2009).

Muchardt, C. & Yaniv, M. ATP-dependent chromatin remodelling: SWI/SNF and Co. are on the job. J Mol Biol 293, (1999).

Muchardt, C. & Yaniv, M. When the SWI/SNF complex remodels...the cell cycle. Oncogene 20, 3067—3075 (2001).

Murawska, M., Hassler, M., Renkawitz-Pohl, R., Ladurner, A. & Brehm, A. Stress-induced PARP activation mediates recruitment of Drosophila Mi-2 to promote heat shock gene expression. PLoS Genet. 7, e1002206 (2011).

Murawska, M. et al. dCHD3, a novel ATP-dependent chromatin remodeler associated with sites of active transcription. Mol. Cell. Biol. 28, 2745—2757 (2008).

Musselman, C. A. et al. Bivalent recognition of nucleosomes by the tandem PHD fingers of the CHD4 ATPase is required for CHD4-mediated repression. Proc. Natl. Acad. Sci. 109, 787–792 (2012).

Musselman, C. A. et al. Binding of the CHD4 PHD2 finger to histone H3 is modulated by covalent modifications. Biochem. J. 423, 179—187 (2009).

Narlikar, G. J., Phelan, M. L. & Kingston, R. E. Generation and interconversion of multiple distinct nucleosomal states as a mechanism for catalyzing chromatin fluidity. Mol. Cell 8, 1219—1230 (2001).

Neigeborn, L. & Carlson, M. Genes Affecting the Regulation of SUC2 Gene Expression by Glucose Repression in SACCHAROMYCES CEREVISIAE. Genetics 108, 845–858 (1984).

Nodelman, I. M. et al. Interdomain Communication of the Chd1 Chromatin Remodeler across the DNA Gyres of the Nucleosome. Mol. Cell 65, 447–459.e6 (2017).

O'Shaughnessy, A. & Hendrich, B. CHD4 in the DNA-damage response and cell cycle progression: not so NuRDy now. Biochem. Soc. Trans. 41, 777–82 (2013).

Oppikofer, M. et al. Expansion of the ISWI chromatin remodeler family with new active complexes. EMBO Rep. 18, 1697—1706 (2017).

Owen, D. J. et al. The structural basis for the recognition of acetylated histone H4 by the bromodomain of histone acetyltransferase Gcn5p. EMBO J. 19, 6141–6149 (2000).

Paro, R. & Hogness, D. S. The Polycomb protein shares a homologous domain with a heterochromatin-associated protein of Drosophila. Proc. Natl. Acad. Sci. 88, 263–267 (1991).

Patel, A., McKnight, J. N., Genzor, P. & Bowman, G. D. Identification of residues in chromodomain helicase DNA-binding protein 1 (Chd1) required for coupling ATP hydrolysis to nucleosome sliding. J. Biol. Chem. 286, 43984–43993 (2011).

Piestrzeniewicz-Ulanska, D. et al. TGF-beta signaling is disrupted in endometrioid-type endometrial carcinomas. Gynecol. Oncol. 95, 173—180 (2004).

Polo, S. E., Kaidi, A., Baskcomb, L., Galanty, Y. & Jackson, S. P. Regulation of DNA-damage responses and cell-cycle progression by the chromatin remodelling factor CHD4. EMBO J. 29, 3130–9 (2010).

Potts, R. C. et al. CHD5, a brain-specific paralog of Mi2 chromatin remodeling enzymes, regulates expression of neuronal genes. PLoS One 6, (2011).

Pyle, A. M. Translocation and unwinding mechanisms of RNA and DNA helicases. Annu. Rev. Biophys. 37, 317—336 (2008).

Rahman, M. S., Akhtar, N., Jamil, H. M., Banik, R. S. & Asaduzzaman, S. M. TGF-β/BMP signaling and other molecular events: regulation of osteoblastogenesis and bone formation. Bone Res. 3, 15005 (2015).

Rasmussen, T. P. et al. Messenger RNAs encoding mouse histone macroH2A1 isoforms are expressed at similar levels in male and female cells and result from alternative splicing. Nucleic Acids Res. 27, 3685—3689 (1999).

Restrepo, S., Zartman, J. J. & Basler, K. Coordination of patterning and growth by the morphogen DPP. Curr. Biol. 24, R245—55 (2014).

Rogakou, E. P., Pilch, D. R., Orr, A. H., Ivanova, V. S. & Bonner, W. M. DNA double-stranded breaks induce histone H2AX phosphorylation on serine 139. J. Biol. Chem. 273, 5858—5868 (1998).

Rogakou, E. P., Pilch, D. R., Orr, A. H., Ivanova, V. S. & Bonner, W. M. Double-stranded Brekas Induce Histone H2AX phosphorylation on Serine 139. J. Biol. Chem. 273, 5858–5868 (1998).

Rossetto, D., Avvakumov, N. & Côté, J. Histone phosphorylation: a chromatin modification involved in diverse nuclear events. Epigenetics 7, 1098—1108 (2012).

Rowe, C. E. & Narlikar, G. J. The ATP-dependent remodeler RSC transfers histone dimers and octamers through the rapid formation of an unstable encounter intermediate. Biochemistry 49, 9882–9890 (2010).

Sambrook, J. and Russell, D.W. Molecular cloning a laboratory manual. Cold Spring Harbor Laboratory Press, Cold Spring Harbor, New York. (2001).

Schindler, U., Beckmann, H. & Cashmore, A. R. HAT3.1, a novel Arabidopsis homeodomain protein containing a conserved cysteine-rich region. Plant J. 4, 137—150 (1993).

Schmidt, D. R. & Schreiber, S. L. Molecular association between ATR and two components of the nucleosome remodeling and deacetylating complex, HDAC2 and CHD4. Biochemistry 38, 14711—14717 (1999).

Schwartz, Y. B. & Pirrotta, V. Polycomb silencing mechanisms and the management of genomic programmes. Nat. Rev. Genet. 8, 9—22 (2007).

Seelig, H. P., Renz, M., Targoff, I. N., Ge, Q. & Frank, M. B. Two forms of the major antigenic protein of the dermatomyositis-specific Mi-2 autoantigen. Arthritis Rheum. 39, 1769–1771 (1996).

Seelig, H. P. et al. The major dermatomyositis-specific mi-2 autoantigen is a presumed helicase involved in transcriptional activation. Arthritis Rheum. 38, 1389–1399 (1995).

Sen, P., Ghosh, S., Pugh, B. F. & Bartholomew, B. A new, highly conserved domain in Swi2/Snf2 is required for SWI/SNF remodeling. Nucleic Acids Res. 39, 9155—9166 (2011).

Sengoku, T., Nureki, O., Nakamura, A., Kobayashi, S. & Yokoyama, S. Structural basis for RNA unwinding by the DEAD-box protein Drosophila Vasa. Cell 125, 287—300 (2006).

Shahbazian, M. D. & Grunstein, M. Functions of site-specific histone acetylation and deacetylation. Annu. Rev. Biochem. 76, 75—100 (2007).

Sifrim, A. et al. Distinct genetic architectures for syndromic and nonsyndromic congenital heart defects identified by exome sequencing. Nat. Genet. 48, 1060—1065 (2016).

Singleton, M. R., Dillingham, M. S. & Wigley, D. B. Structure and mechanism of helicases and nucleic acid translocases. Annu. Rev. Biochem. 76, 23—50 (2007).

Smith, C. L. & Peterson, C. L. A conserved Swi2/Snf2 ATPase motif couples ATP hydrolysis to chromatin remodeling. Mol. Cell. Biol. 25, 5880—5892 (2005).

Sobel, R. E., Cook, R. G., Perry, C. A., Annunziato, A. T. & Allis, C. D. Conservation of deposition-related acetylation sites in newly synthesized histones H3 and H4. Proc. Natl. Acad. Sci. U. S. A. 92, 1237—1241 (1995).

Stern, M., Jensen, R. & Herskowitz, I. Five SWI genes are required for expression of the HO gene in yeast. J. Mol. Biol. 178, 853–868 (1984).

Stokes, D. G. & Perry, R. P. DNA-binding and chromatin localization properties of CHD1. Mol. Cell. Biol. 15, 2745—2753 (1995).

Stokes, D. G., Tartof, K. D. & Perry, R. P. CHD1 is concentrated in interbands and puffed regions of Drosophila polytene chromosomes. Proc. Natl. Acad. Sci. U. S. A. 93, 7137—7142 (1996).

Sun, F. et al. Chd4 and associated proteins function as corepressors of Sox9 expression during BMP-2-induced chondrogenesis. J. Bone Miner. Res. 28, 1950—1961 (2013).

Suto, R. K., Clarkson, M. J., Tremethick, D. J. & Luger, K. Crystal structure of a nucleosome core particle containing the variant histone H2A.Z. Nat. Struct. Biol. 7, 1121—1124 (2000).

Szerlong, H. et al. The HSA domain binds nuclear actin-related proteins to regulate chromatin-remodeling ATPases. Nat Struct Mol Biol. 2008 15, 469–476 (2008).

T. Ferreira, W. R. ImageJ User Guide IJ 1.46r. IJ 1.46r 185 (2012). doi:10.1038/nmeth.2019

Tachiwana, H. et al. Crystal structure of the human centromeric nucleosome containing CENP-A. Nature 476, 232—235 (2011).

Talbert, P. B. & Henikoff, S. Histone variants on the move: substrates for chromatin dynamics. Nat. Rev. Mol. Cell Biol. 18, 115–126 (2016).

Talbert, P. B. & Henikoff, S. Histone variants — ancient wrap artists of the epigenome. Nat. Rev. Mol. Cell Biol. 11, 264–275 (2010).

Tamkun, J. W. et al. brahma: a regulator of Drosophila homeotic genes structurally related to the yeast transcriptional activator SNF2/SWI2. Cell 68, 561—572 (1992).

Tang, L., Nogales, E. & Ciferri, C. Structure and function of SWI / SNF chromatin remodeling complexes and mechanistic implications for transcription. Prog. Biophys. Mol. Biol. 102, 122–128 (2010).

Tang, Y. et al. Linking long non-coding RNAs and SWI/SNF complexes to chromatin remodeling in cancer. Mol. Cancer 16, 42 (2017).

Torigoe, S. E., Urwin, D. L., Ishii, H., Smith, D. E. & Kadonaga, J. T. Identification of a rapidly formed nonnucleosomal histone-DNA intermediate that is converted into chromatin by ACF. Mol. Cell 43, 638—648 (2011).

Tsukada, Y. et al. Histone demethylation by a family of JmjC domain-containing proteins. Nature 439, 811—816 (2006).

Tsukiyama, T., Daniel, C., Tamkun, J. & Wu, C. ISWI, a member of the SWI2/SNF2 ATPase family, encodes the 140 kDa subunit of the nucleosome remodeling factor. Cell 83, 1021–1026 (1995).

Udugama, M., Sabri, A. & Bartholomew, B. The INO80 ATP-dependent chromatin remodeling complex is a nucleosome spacing factor. Mol. Cell. Biol. 31, 662—673 (2011).

Varga-Weisz, P. D. et al. Chromatin-remodelling factor CHRAC contains the ATPases ISWI and topoisomerase II. Nature 388, 598–602 (1997).

Venkatesh, S. & Workman, J. L. Histone exchange, chromatin structure and the regulation of transcription. Nat. Rev. Mol. Cell Biol. 16, 178—189 (2015).

Verstappen, G. et al. Atypical Mowat-Wilson patient confirms the importance of the novel association between ZFHX1B/SIP1 and NuRD corepressor complex. Hum. Mol. Genet. 17, 1175—1183 (2008).

Wang, H. B. & Zhang, Y. Mi2, an auto-antigen for dermatomyositis, is an ATP-dependent nucleosome remodeling factor. Nucleic Acids Res. 29, 2517—2521 (2001).

Watanabe, S. & Peterson, C. L. The INO80 family of chromatin-remodeling enzymes: Regulators of histone variant dynamics. Cold Spring Harb. Symp. Quant. Biol. 75, 35–42 (2010).

Watson, A. A. et al. The PHD and chromo domains regulate the atpase activity of the human chromatin remodeler CHD4. J. Mol. Biol. 422, 3–17 (2012).

Wei, Y., Mizzen, C. A., Cook, R. G., Gorovsky, M. A. & Allis, C. D. Phosphorylation of histone H3 at serine 10 is correlated with chromosome condensation during mitosis and meiosis in Tetrahymena. Proc. Natl. Acad. Sci. U. S. A. 95, 7480—7484 (1998).

Weiss, K. et al. De Novo Mutations in CHD4, an ATP-Dependent Chromatin Remodeler Gene, Cause an Intellectual Disability Syndrome with Distinctive Dysmorphisms. Am. J. Hum. Genet. 99, 934–941 (2016).

Wigley, D. B. & Bowman, G. D. A glimpse into chromatin remodeling. Nat. Struct. Mol. Biol. 24, 498—500 (2017).

Wong, L. H. et al. ATRX interacts with H3.3 in maintaining telomere structural integrity in pluripotent embryonic stem cells. Genome Res. 20, 351—360 (2010).

Workman, J. L. & Kingston, R. E. Alteration of Nucleosome Structure as a Mechanism of Transcriptional Regulation. Annu. Rev. Biochem. 67, 545–579 (1998).

Wu, L. M. N. et al. Zeb2 recruits HDAC-NuRD to inhibit Notch and controls Schwann cell differentiation and remyelination. Nat. Neurosci. 19, 1060—1072 (2016).

Wysocka, J. et al. A PHD finger of NURF couples histone H3 lysine 4 trimethylation with chromatin remodelling. Nature 442, 86—90 (2006).

Xia, L. et al. CHD4 Has Oncogenic Functions in Initiating and Maintaining Epigenetic Suppression of Multiple Tumor Suppressor Genes. Cancer Cell 31, 653—668.e7 (2017).

Xue, Y. et al. The human SWI/SNF-B chromatin-remodeling complex is related to yeast rsc and localizes at kinetochores of mitotic chromosomes. Proc. Natl. Acad. Sci. U. S. A. 97, 13015—13020 (2000).

Yan, L., Wang, L., Tian, Y., Xia, X. & Chen, Z. Structure and regulation of the chromatin remodeller ISWI. Nature 540, 466–469 (2016).

Yang, J. G., Madrid, T. S., Sevastopoulos, E. & Narlikar, G. J. The chromatin-remodeling enzyme ACF is an ATP-dependent DNA length sensor that regulates nucleosome spacing. Nat. Struct. Mol. Biol. 13, 1078—1083 (2006).

YANG, S. & YUJIANG, S. Histone Demethylation Mediated by the Nuclear Amine Oxidase Homolog LSD1. (2010).

Yang, X., Zaurin, R., Beato, M. & Peterson, C. L. Swi3p controls SWI/SNF assembly and ATP-dependent H2A-H2B displacement. Nat. Struct. Mol. Biol. 14, 540—547 (2007).

Yuan, J., Adamski, R. & Chen, J. Focus on histone variant H2AX: to be or not to be. FEBS Lett. 584, 3717—3724 (2010).

Zhao, S., Choi, M., Overton, J. D. & Santin, A. D. Landscape of somatic single-nucleotide and copy-number mutations in uterine serous carcinoma. PNAS (2012).

Zhou, C. Y., Johnson, S. L., Gamarra, N. I. & Narlikar, G. J. Mechanisms of ATP-Dependent Chromatin Remodeling Motors. Annu. Rev. Biophys. 45, 153–181 (2016).

Zofall, M., Persinger, J., Kassabov, S. R. & Bartholomew, B. Chromatin remodeling by ISW2 and SWI/SNF requires DNA translocation inside the nucleosome. Nat. Struct. Mol. Biol. 13, 339—346 (2006).

Zraly, C. B. et al. SNR1 is an essential subunit in a subset of Drosophila brm complexes, targeting specific functions during development. Dev. Biol. 253, 291—308 (2003).

7. Appendix

List of abbreviations and acronyms

Å	Ångstrom
ac	acetylation
ACF	ATP-utilising chromatin remodelling and assembly Factor
ADP	adenosine diphosphate
APS	ammonium persulfate
Arg	arginine
ARP	actin related protein
Asf1	histone chaperone asf1
ATP	adenosine triphosphate
ATR	ataxia telangiectasia and Rad3 related
attB	bacterial attachment site
attP	phage attachment site
BAF	BRG1-associated factors
BMP	bone morphogenetic protein
bp	base pair
BRCA1	breast cancer type 1 susceptibility protein
BRG1	Brahma-associated gene 1
BRK	Brahma and Kismet domain
BRM	brahma
Bromo	Bromodomains
BSA	bovine serum albumine
c-MyB	transcriptional activator MyB
C-terminal	carboxy terminal
CATD domain	CENP-A Targeting Domain
CenH3.3	centromere-specific histone 3 variant

CENP-A	Centromere protein A
CHD	chromo-helicase-DNA- binding
CHRAC	chromatin remodeling and assembly complex
Chromo	Chromodomain
Ci	Curie
CoREST	corepressor for REST
cryo-EM	cryo-electron microscopy
Cys	cysteine
DBD	DNA binding domain
dCTP	Deoxycytidine triphosphate
DDR	DNA damage response
dMec	*Drosophila* MEP-1-containing complex
dMEP-1	mog interacting ectopic P granulocytes 1
DMSO	Dimethyl sulfoxide
DNA	deoxyribonucleic acid
dNTP	desoxyribonucleotidetriphosphate
DOC1	deleted in oral cancer 1
Dpp	Decapentaplegic
dsDNA	double stranded
DTT	Dithiothreitol
E. coli	Escherichia coli
EcR	ecdysone receptor
EDTA	ethylenedioxy-diethylene-dinitrilo-tetraacetic acid
EGTA	ethylene glycol-bis-(2-aminoethyl)-N,N,N', N'-tetraacetic acid
EMT	epithelial-mesenchymal transition
en	engrailed
EtBR	ethidium bromide
F	phenylalanine

FBS	fetal bovine serum
fwd	forward
Gln	glutamine
H	histone
HAT’s	histone acetyltransferases
HDAC	histone deacetylases
HDAC	histone deacetylase
His	histidine
HMT’s	histone methyltransferases
HP1	heterochromatin protein 1
HRP	horseradish peroxidase
HSA	helicase sant domain
HSP90	heat shock protein 90
HSS	Hand sant domain
IgG	immunoglobuline G
INO80	inositol requiring 80
ISWI	imitation switch
K	lysine
KDM	lysine demethylases
L	leucine
LB	Luria Bertani
Leu	leucine
LSD1	Lysine-specific histone demethylase 1A
M	molar
MBD2	methylated DNA binding domains 2
MBT	malignant brain tumour
MDC1	Mediator of DNA damage Checkpoint 1
me	methylation
ml	mililiter

MTA	metastasis-associated protein
N-terminal	amino terminal
Nap1	Nucleosome assembly protein
NASP	Nuclear autoantigenic sperm protein
NuRD	nucleosome remodelling and deacetylation
NURF	nucleosome remodeling factor
P	proline
p53	Cellular tumor antigen p53
PAA	polyacrylamide
PAGE	polyacrylamide gel electrophoresis
PAR	poly(ADP-ribose)
PARP	Poly (ADP-ribose) polymerase
PBAF	polybromo-associated BAF
PBS	Phosphate Buffered Saline
Pc	Polycomb
PCR	polymerase chain reaction
PCV	posterior cross vein
PHD	plant homeodomain
Phe	phenylalanine
postHSA	post helicase sant domain
PP1	protein phosphatase 1
PRC2	Polycomb repressive complex 2
PRMT’s	protein arginine methyltransferases
PVDF	polyvinylidene difluoride membrane
Q	glutamine
R	arginine
REA	restriction enzyme accessibility
rev	reverse
RNA	ribonucleic acid

RNA Pol II	RNA polymerase II
RNAi	RNA interference
RSC	Remodelling the structure of chromatin
RT	room temperature
S	serine
SDS	sodium dodecyl sulphate
SEM	standard error of mean
SET-domain	Su(var)3-9, Enhancer-of-zeste and Trithorax
SF2	helicase superfamily 2
SHL	superhelical location
SMAD4	Mothers against decapentaplegic homolog 4
SMAD4	Mothers against decapentaplegic homolog 4
SnAC	Snf2 ATP coupling
SNF	sucrose non-fermentation
ssDNA	single stranded DNA
Sth1	SNF2 (Two) homolog 1
SWI	mating type switch
SWI/SNF	switch/sucrose non-fermenting
Swr1	Swi2/Snf2-related 1
T	threonine
TE	Tris-EDTA
TEMED	tetramethyl-ethylene diamine
TGF-β	transforming growth factor β
TGFβRII	transforming growth factor beta receptor II
TSG	tumour suppressor genes
Tyr	tyrosine
UAS	Upstream activation sequence
ub	ubiquitination
UV	Ultra violet

V	valine
Val	valine
WT	wild type
Y	tyrosine
Zeb2	zinc-finger E-box-binding homeobox 2
ZNF521	Zinc finger protein 521

Curriculum Vitae

Publications

1) Kreher J*, **Kovač K***, Bouazoune K, Mačinković I, Ernst AL, Engelen E, Pahl R, Finkernagel F, Murawska M, Ullah I, Brehm A, EcR recruits dMi-2 and increases efficiency od dMi-2-mediated remodelling to constrain transcription of hormone-regulated genes, Nature Communications (2017), Apr 5; 8:14806 (*equal contribution)
2) **Kovač K** et al. - Tumour-associated missense mutations in CHD4 ATPases alter their nucleosome remodelling properties (Nature Communications, in press)

List of academic teachers

My academic teachers at the University of Zagreb were: Bajraktarević, Bakran-Petricioli, Balabanić, Dolenec, Erben, Franjević, Goldstein, Habdija, Hršak, Jalšovec, Jelenić, Kalafatić, Krajačić, Krsnik-Rasol, Kučinić, Lacković-Venturin, Liber, Marinković, Marušić, Miljković, Mišetić, Mitić, Mrakovčić, Mrvoš-Sermek, Oršolić, Pavlina, Pavlica, Pevalek-Kozlina, Plenkovic-Moraj, Rudan, Sremac, Stilinović, Tadić, Ternjej, Tomić

At AgroParisTech: Mijaković

Acknowledgements

Here, I would like to thank everyone that supported me during my PhD thesis. First and foremost, to my supervisor Alexander for giving me the opportunity to do my PhD work in his lab. Alex, thank you for your guidance and endless amounts of patience. May the Force be with you!

I would like to thank my lab colleagues - Igor, Jonathan, Stephan and Ulla for all the help and support, as well as the other members of the Brehm lab. I would like to thank former lab member - Judith Kreher, for much needed help and advice at the beginning of my work. Special thanks goes to my lab and flatmate Igor for all the conversations and, of course, endless supply of 8% SDS gels. :) Thanks to other colleagues and friends - Sara, Satis, Peeyush and Joanna, for making me laugh so many times.

Additionally, I would like to express my gratitude to prof. dr. Uta-Maria Bauer and prof. dr. Rainer Renkawitz for being part of my thesis committee throughout the years. Thank you for your suggestions and helpful comments.

Last, but definitely, not least, I want to thank my family for understanding my love for science and supporting my curiosity since childhood.

Hvala mami i tati, evo i ovo ste preživjeli. :)

Ehrenwörtliche Erklärung